MECHANICAL BEHAVIOUR OF POROUS Ti-6Al-4V SCAFFOLDS USING ADDITIVE MANUFACTURING IN BIO-MEDICAL APPLICATIONS: FABRICATION, MECHANICAL PROPERTIES AND ANALYSIS

A Thesis Submitted By

PALASH MONDAL

For the award of the degree of

Doctor of Philosophy (Engineering)

DEPARTMENT OF MECHANICAL ENGINEERING
FACULTY COUNCIL OF ENGINEERING & TECHNOLOGY
JADAVPUR UNIVERSITY
KOLKATA, INDIA-700 032
2023

JADAVPUR UNIVERSITY

KOLKATA – 700 032

INDEX NO. 163/19/E

1. Title of Thesis:

Mechanical Behaviour of Porous Ti-6Al-4V Scaffolds using Additive Manufacturing in Bio-Medical Applications: Fabrication, Mechanical Properties and Analysis

2. Name, Designation & Institution of the Supervisors:

Dr. Amit Karmakar,
Professor,
Mechanical Engineering Department,
Jadavpur University, Kolkata -700032, India.

&

Dr. Apurba Das,
Assistant Professor,
Department of Mechanical Engineering,
IIEST, Shibpur, Howrah -711103, India.

3. List of Publications

i. Mondal P, Das A, Mondal A, Chowdhury AR, Karmakar A. Fabrication of Ti-6Al-4V Porous Scaffolds Using Selective Laser Melting (SLM) and Mechanical Compression Test for Biomedical Applications. **Journal of The Institution of Engineers (India): Series D. 2022 Feb 7:1-0.** doi.org/10.1007/s40033-022-00333-1.

ii. Mondal P, Das A, Wazeer A, Karmakar A. Biomedical Porous Scaffold Fabrication Using Additive Manufacturing Technique: Porosity, Surface Roughness and Process Parameters Optimization. **International Journal of Lightweight Materials and Manufacture. 2022 Apr 29.** doi.org/10.1016/j.ijlmm.2022.04.005.

iii. Mondal P, Wazeer A, Das A, Chowdhury AR, Karmakar A. Effect of Heat Treatment on Compressive Behavior of Selectively Laser Melted Ti64 Scaffolds. **Journal of The Institution of Engineers (India): Series D. 2022 May 23:1-9.** doi.org/10.1007/s40033-022-00362-w.

iv. Mondal P, Dey H, Paul S, Sarkar S, Das A, Karmakar A. Additively manufactured porous titanium alloy scaffolds for orthopaedics: An effect of process parameters on porosity. **International Research Journal on Advanced Science Hub, 2022.** http://dx.doi.org/10.47392/irjash.2022.023.

v. Mondal P, Wazeer A, Das A, Karmakar A. Low cost porous Ti-6Al-4V structures by additive manufacturing for orthopaedic applications. **Materials Today: Proceedings. 2022 Jan 1;67:398-403.** https://doi.org/10.1016/j.matpr.2022.07.349.

vi. Mondal P, Wazeer A, Das A, Karmakar A. Selective Laser Melted Porous Ti-6Al-4V Scaffolds: Modelling, Manufacturing, and Effect of Microstructure on Mechanical Properties. Transactions of the Indian Institute of Metals. [MANUSCRIPT #: TIIM-D-23-01211, under review]

4. List of Patents: Nil

5. List of Presentations in National/International/Conferences/Workshops:

i. Mondal P, Dey H, Paul S, Sarkar S, Das A, Karmakar A. "Additively manufactured porous titanium alloy scaffolds for orthopaedics: An effect of process parameters on porosity." Third International Conference on Innovation in Engineering Sciences (ICIES-2022), March 26 – 27, **2022**, Techno Engineering College Banipur, West Bengal, India & RSP Conference Hub, Coimbatore, Tamil Nadu, India, pp-88-93.

ii. Mondal P, Wazeer A, Das A, Karmakar A. "Low cost porous Ti-6Al-4V structures by additive manufacturing for orthopaedic applications" International Conference on Powder Metallurgy and 47 Annual Technical Meeting of PMAI (PM-22), April 18 – 20, **2022**, pp-398-403.

iii. Mondal P, Wazeer A, Das A, Karmakar A. "Functional Porous Scaffold of Titanium (Ti64) Alloy for Bio-medical Applications: Challenges and Scope using Additive Manufacturing Route" 1st International Conference on Mechanical Design and Manufacturing (ICMDM 2023), April 27-28, **2023**, pp-31. Indian Institute of Engineering Science and Technology (IIEST), Shibpur, Howrah, India.

PROFORMA - 1

STATEMENT OF ORIGINALITY

I, Palash Mondal registered on 19/06/2019 do hereby declare that this thesis entitled "Mechanical Behaviour of Porous Ti-6Al-4V Scaffolds using Additive Manufacturing in Bio-Medical Applications: Fabrication, Mechanical Properties and Analysis" contains literature survey and original research work done by the undersigned candidate as part of Doctoral studies.

All information in this thesis have been obtained and presented in accordance with existing academic rules and ethical conduct. I declare that, as required by these rules and conduct, I have fully cited and referred all materials and results that are not original to this work.

I also declare that I have checked this thesis as per the "Policy on Anti Plagiarism, Jadavpur University, 2019", and the level of similarity as checked by iThenticate software is 9%.

Palash Mondal

Signature of Candidate:

Date: 22/04/24

Certified by Supervisor(s):

(Signature with date, seal)

1. Amit Karmakar

Professor
Dept. of Mechanical Engineering
Jadavpur University, Kolkata-32

2. Apurba Das.

Assistant Professor
Mechanical Engg. Deptt.
Indian Institute of Engineering
Science and Technology, Shibpur
Howrah-711 103.

PROFORMA - 2

CERTIFICATE FROM THE SUPERVISOR(S)

This is to certify that the thesis entitled "Mechanical Behaviour of Porous Ti-6Al-4V Scaffolds using Additive Manufacturing in Bio-medical Applications: Fabrication, Mechanical Properties and Analysis", submitted by Mr. Palash Mondal, who got his name registered on 19/06/2019 for the award of Ph.D. (Engineering & Technology) degree of Jadavpur University is absolutely based upon his own work under our guidance and supervision. Neither the results obtained from this work nor any part of this thesis has been submitted for any degree / diploma or any other academic award anywhere before.

Amit Karmakar

(Dr. Amit Karmakar)
Professor,
Mechanical Engineering Department,
Jadavpur University,
Kolkata-700032,
India.

Professor
Dept. of Mechanical Engineering
Jadavpur University, Kolkata-32

Apurba Das.

(Dr. Apurba Das)
Assistant Professor,
Department of Mechanical Engineering,
IIEST, Shibpur,
Howrah -711103,
India.

Assistant Professor
Mechanical Engg. Deptt.
Indian Institute of Engineering
Science and Technology, Shibpur
Howrah-711 103.

ACKNOWLEDGEMENT

The author expresses his deep sense of gratitude to his supervisors, Dr. Amit Karmakar & Dr. Apurba Das for their keen interest, cherished guidance and constant inspiration during the research work. The author is grateful to him for his guidance to enter a new field of additive manufacturing of Ti-6Al-4V alloy in bio-medicals. Above all, without his moral support and constant guidance the author would have not been completed the work.

The author is thankful to Dr. A. R. Chowdhury (IIEST, Shibpur), Dr. B. Pal (IIEST, Shibpur), Dr. S. K. Acharyya (JU), Dr. K. Inaba (TIT, Japan) and Dr. T. Bandopadhyay (JU) for their encouragement and advice. The author acknowledges to the reviewers of journals and conference papers and from the audience, while presenting papers in conferences. The author extends specials thanks to the Applied Mechanics Laboratory of Jadavpur University, Kolkata, Kishimoto-Inaba Laboratory of Tokyo Institute of Technology, Japan and CTTC Laboratory, Bhubaneswar for providing facility and support during this research work.

The author takes great pleasure to thank Mr. Adil Wazeer, Masud Rana, Bivas Mandal from whom he received immense support and assistance. The author expresses extreme gratefulness to his wife (Priyanka) and daughter (Samanwita) for their constant support and motivation, without that he would not have come to this stage.

Above all, it is the wish of The Almighty that the author has been able to complete this work.

Date: 22/04/24

Palash Mondal
Signature of Candidate:

LIST OF PUBLICATIONS

The below technical papers are prepared based on the present research work which have been published/accepted or submitted in the International Journals and International/National conferences:

INTERNATIONAL JOURNAL:

1. Mondal P, Das A, Mondal A, Chowdhury AR, Karmakar A. Fabrication of Ti-6Al-4V Porous Scaffolds Using Selective Laser Melting (SLM) and Mechanical Compression Test for Biomedical Applications. **Journal of The Institution of Engineers (India): Series D. 2022 Feb 7:1-0.** doi.org/10.1007/s40033-022-00333-1.

2. Mondal P, Das A, Wazeer A, Karmakar A. Biomedical Porous Scaffold Fabrication Using Additive Manufacturing Technique: Porosity, Surface Roughness and Process Parameters Optimization. **International Journal of Lightweight Materials and Manufacture. 2022 Apr 29.** doi.org/10.1016/j.ijlmm.2022.04.005.

3. Mondal P, Wazeer A, Das A, Chowdhury AR, Karmakar A. Effect of Heat Treatment on Compressive Behavior of Selectively Laser Melted Ti64 Scaffolds. **Journal of The Institution of Engineers (India): Series D. 2022 May 23:1-9.** doi.org/10.1007/s40033-022-00362-w.

4. Mondal P, Dey H, Paul S, Sarkar S, Das A, Karmakar A. Additively manufactured porous titanium alloy scaffolds for orthopaedics: An effect of process parameters on porosity. **International Research Journal on Advanced Science Hub, 2022.** http://dx.doi.org/10.47392/irjash.2022.023.

5. Mondal P, Wazeer A, Das A, Karmakar A. Low cost porous Ti-6Al-4V structures by additive manufacturing for orthopaedic applications. **Materials Today: Proceedings. 2022 Jan 1;67:398-403.** https://doi.org/10.1016/j.matpr.2022.07.349.

6. Mondal P, Wazeer A, Das A, Karmakar A. Selective Laser Melted Porous Ti-6Al-4V Scaffolds: Modelling, Manufacturing, and Effect of Microstructure on Mechanical Properties. Transactions of the Indian Institute of Metals. [MANUSCRIPT #: TIIM-D-23-01211, under review]

INTERNATIONAL/ NATIONAL CONFERENCE:

1. Mondal P, Dey H, Paul S, Sarkar S, Das A, Karmakar A. "Additively manufactured porous titanium alloy scaffolds for orthopaedics: An effect of process parameters on porosity." Third International Conference on Innovation in Engineering Sciences (ICIES-2022), March 26 – 27, **2022**, Techno Engineering College Banipur, West Bengal, India & RSP Conference Hub, Coimbatore, Tamil Nādu, India, pp-88-93.

2. Mondal P, Wazeer A, Das A, Karmakar A. "Low cost porous Ti-6Al-4V structures by additive manufacturing for orthopaedic applications" International Conference on Powder Metallurgy and 47 Annual Technical Meeting of PMAI (PM-22), April 18 – 20, **2022**, pp-398-403.

3. Mondal P, Wazeer A, Das A, Karmakar A. "Functional Porous Scaffold of Titanium (Ti64) Alloy for Bio-medical Applications: Challenges and Scope using Additive Manufacturing Route" 1st International Conference on Mechanical Design and Manufacturing (ICMDM 2023), April 27-28, **2023**, pp-31. Indian Institute of Engineering Science and Technology (IIEST), Shibpur, Howrah, India.

ABSTRACT

Bone implants are commonly used to replace bones and joint defects; nevertheless, mechanical, biological, and structural incompatibilities between bones and implants can cause serious complications. Traditional bone implants used in orthopedic bone and joint replacements have solid and stiff components that shield the peri-implant bone stress and cause the implants to loosen prematurely. New porous materials are necessary to enable an implant to imitate the host bones, and this is the main focus of this research work.

In biomedical sectors, using additive manufacturing techniques has shown massive benefits such as flexibility in building micro and macro-scale structures based on computer models and analyses. Despite the fact that porous structures bring mechanical and biological environments closer to the host bone, poor internal architectural designs may compromise mechanical characteristics and structural integrity. As a result, the mechanical and biological performances of small-scale units of porous structure deserve additional investigation.

Titanium is one of the most prevalent and biocompatible metals (*Niinomi, 2008a and 2008b*). In orthopedics, the demand for Ti alloys and its use in clinical surgeries are constantly increasing. Because of its moderate Young's modulus, outstanding compressive strength, biocompatibility, and sufficient space for cell accommodation, the porous structures have been modeled for bone tissue engineering or orthopedic applications. Additive manufacturing (AM) technologies, particularly selective laser melting (SLM), can be used to create porous scaffolds with complicated internal and external shapes and both of these are most important for the repair of large sectional bone defects (As a result of this advantage, the SLM method is one of the most competitive AM technologies employed in biomedical applications. In this research, seven different Ti-6Al-4V porous scaffolds (Diamond, Grid, Cross, Vinties, Tesseract, Star, and Octet) of 15 mm cube with 65% porosity are designed using Rhino 6 software and manufactured using Ti-6Al-4V powders by SLM. Because of its high heating rate and low holding time, SLM can build nanoscale grain scaffolds. However, in most cases, this method results in insufficient compaction where desired functions are not achieved.

Compression test of all the seven scaffolds is performed on an INSTRON compressive testing machine with a maximum load cell capacity of ±25 kN to measure its mechanical

properties. Actual porosity and surface roughness of the fabricated scaffolds are measured. Then all the scaffolds are analyzed by Ansys 2020 R2. The elastic modulus of fabricated samples is very similar to that of human bones (E=3-30 GPa), but compressive strength is higher than that of human bone, which will minimize the stress-shielding effect and extend the implant's longevity. The Gibson-Ashby Correlation Model is used to investigate the samples relative elastic modulus. Ti-6Al-4V porous scaffolds have a low effective Young's modulus, high compressive strength, and enough cell accommodation space to meet medical needs for clinical demands. Porous Ti-6Al-4V scaffolds (Diamond, Grid, Cross, Vinties, Tesseract, Star, and Octet) have shown the relative elastic moduli and compressive mechanical strength are 6.5 GPa, 11.15 GPa, 10.33 GPa, 7.16 GPa, 5.87 GPa, 7.9 GPa & 11.16 GPa and 96.41 MPa, 98.42 MPa, 101.39 MPa, 95.63 MPa, 94.02 MPa, 88.71 MPa & 90.49 MPa respectively, which are comparable to human bone. The scaffolds made by SLM have a reasonably good pore structural accuracy and excellent mechanical strength. Grid type structure exhibits lower surface roughness value and better manufacturing ability whereas error percentage of porosity is lower than the other scaffolds.

It is found that using porous Ti-6Al-4V structures in orthopedic bone implants could be a better option for load-sharing implants because it balances stability, maintains bone matching stiffness, decreases bone stress shielding, and possibly extends implant longevity.

KEYWORDS

Bone, Stress shielding, Ti-6Al-4V, Porous scaffolds, Additive manufacturing, Selective laser melting, 3D printing, Biomedical implant, Mechanical testing, Ansys 2020 R2 analysis.

NOMENCLATURE

Ti	Titanium
Al	Aluminium
V	Vanadium
AM	Additive manufacturing.
SLM	Selective laser melting
THR	Total hip replacements
E	Effective elastic modulus
FCC	Face centred cubic
MIM	Metal injection moulding
CP	Commercially Pure
HA	Hydroxyapatite
HCP	Hexagonal closed packed
BCC	Body centred cubic
2D	Two dimension
3D	Three dimension
EBM	Electron beam melting
SLS	Selective laser sintering
DED	Directed energy deposition
LENS	Laser engineered net shaping
DLD	Direct laser deposition
PBF	Powder bed fusion
DMLS	Direct metal laser sintering
LC	Laser cladding

LOM	Laminated object manufacturing
SMD	Shape metal deposition
LS	Lattice structure
UTS	Ultimate tensile strength
STL	Standard tessellation language
CAD	Computer-aided design
CGS	Constructive solid geometry
B-Rep	Boundary representation
CASPS	Computer-aided system for porous scaffold
UCS	Ultimate compressive strength
SLA	Stereolithography
UV	Ultraviolet
PCL	Polycaprolactone
E_d	Energy density
h	Hatch distancing
v_s	Scan speed
t	Layer thickness
P_l	Laser power
E_i	Energy input
d_l	Diameter of laser beam
LED	Linear energy density
P	Laser power
V_b	Building rate
PLS	Porous lattice structure
SEM	Scanning electron microscope

R_a	Surface roughness
W_p	Weight of the porous scaffold
W_d	Weight of the dense scaffold
LMD	Laser metal deposition
E_p	Effective Young's modulus of porous scaffolds
E_s	Effective Young's modulus of dense scaffolds
σ_p	Compressive strength of porous scaffolds
σ_d	Compressive strength of dense scaffolds
SS	Scan speed
PD	Particle diameter
HD	Hatch distance
LP	Laser Power
LD	Laser diameter
ρ	Density
LT	Layer thickness
T_i	Initial Bed Temperature
VED	Volume energy density
a, b, C_1 and C_2	Constants
RD	Relative density
RH	Room humidity
HA	Hydroxyapatite
DOE	Design of experiments
S/N	Signal-to-noise
FE	Finite element
FEA	Finite element analysis

Numbering of Figures, Tables and Equations

Figures, tables, and equations have been numbered in accordance with the chapters in which they appear in the thesis. Each table, figure and equation has two distinct numbers. The first number specifies the number of the chapter, and the second number denotes to the actual number of the figure, table, and equation in that chapter.

Representation of References

The list of references has been furnished at the end of the thesis. These references have been represented by the respective name of the author(s) along with the year of publication.

CONTENTS

LIST OF TABLES

LIST OF FIGURES

CHAPTER 1 INTRODUCTION

This portion of the chapter explains the history of research and problems, as well as its aims and objectives. The research scope and significance are described in the following section. The last portion of the thesis describes the remaining chapters.

1.1 BACKGROUND

In orthopedic surgery, it is very desirable to develop artificial organs and implants to replace damaged and sick hard tissues including bones, teeth, and joints. Orthopedic prosthesis has shown to be incredibly effective in restoring function and providing great quality of life to millions of people each year. To restore the normal function of damaged hard tissues, it is important for an engineer to devise innovative methods. Since 17th century, metals have been employed as bio-implants. A huge number of metals and applied materials have been produced during the past several decades with notable improvements in different characteristics for a variety of medical applications. Traditional metallic bone implants, on the other hand, are dense and frequently plagued by issues including adverse reactivity, bio-mechanical incompatibility (*Asaoka et al., 1985*), and a lack of sufficient area for new bone tissue to develop within the implant. The construction of porous scaffolds that resemble the structure and mechanical characteristics of genuine bone has been made possible. Osteointegration is the process of bone cells growing into and integrating with a porous material. The stress-shielding issue may be reduced or resolved if the necessary mechanical characteristics are present, a low elastic modulus like that of bone. To reduce or eliminate undesirable bodily reactions, it is necessary to produce biocompatible and corrosion-resistant metallic materials. Even though a broad variety of materials may be employed in this rapidly expanding industry, certain of them are more frequently used in medical applications. For dental and orthopaedic implants, titanium and its alloys provide several benefits, including great biocompatibility, a high strength-to-weight ratio, a reduced elastic modulus, and improved corrosion resistance (*Bai et al., 2017*). Zr, Nb, Ta, Sn, Mo, and Si are alloying elements that would significantly improve the characteristics of titanium for biomedical applications.

Metals have strong elastic modulus and tolerable yield points, allowing structures to be built that can withstand enormous loads without major elastic deformations. Since they are ductile, indicating that crossing the yield point results in plastic deformation instead of an abrupt brittle fracture, enabling for repair treatment such as surgical therapy to restore components before major damage occurs. Metals have considerable flexibility and, as a result, fatigue endurance limitations, making them the most preferred biomaterial for applications such as bone plates that must resist a significant number of load-unload cycles. Metal devices provide great durability to the diversity of both external and internal conditions found in orthopedic treatment if appropriate thought is given to production, surface polishing, and handling.

The material selection of the implants fabrication for bone support and replacement is purely dependent on number of properties. With the advancement of technology, additive manufacturing (AM) has opened up a new route for metal implants. Additive manufacturing has a number of benefits over traditional approaches, including complex forms, patient specific designs, and custom porosity. AM has about 50 process parameters that must be optimized in order to get the desired implant characteristics for long-term functionality. In addition to the treatment parameters, lattice structures are used to promote porosity and improve osseointegration and tissue ingrowth (*Bandyopadhyay et al., 2010*).

Joint replacement surgeries are most typical and major surgical treatment that have high success rate in relieving of pain and dysfunction in patients over the age of 60. In Australia, four lakh ninety-eight thousand six hundred sixty (498,660) total hip replacements (THRs) were conducted in 2015, a 64.9% rise over the previous 12 years (*Huang et al, 2017*). These procedure's outstanding success broadens its application to younger adults. Porous coated surfaces, which were first introduced on femoral prosthesis in the 1980s, make bone implant attachment easier by permitting bone regeneration (*Abbasi et al., 2020*) into pores with no need of cement bonding. A "cementless femoral stem" is the name of this type of implant. The cementless femoral stem is the best alternative for pediatric patients and those who lead healthy lifestyle (*Khanuja et al., 2011*).

Cementless prosthesis has increased in popularity of all total hip replacements from 51.3% (in 2003) to 63.3% (in 2015), and this trend has maintained (*Huang et al, 2017*). The cumulative

percentage revision rate for this prosthesis over a 15-years period is 4.3-12.4%, with aseptic loosening of the proximal femur becoming the most prevalent cause of implant failure (*Huang et al, 2017*). Because of the predicted trend of younger patients requiring THR, revision rates are expected to increase as average life span increases. Today's unavoidable increase in the number of revision procedures makes long-term fixation a big issue. The development of a long-term stable prosthesis is crucial for avoiding the problem of loosening implants.

Because the load that normally exerts on a femur is shielded by the metallic prosthesis, long-term fixation of the prosthesis is a big issue. This phenomenon is known as the "stress-shielding effect," and it occurs because of the prosthesis being stiffer than the bone it replaces. As a result of the absence of load on the implanted femur, it fails within 10 years of implantation. Both orthopedic bone implants and dental implants have a stress-shielding effect. The stress-shielding effect for hip implants is particularly aggressive due to the increased load demand and brittle bones caused by osteoporosis of the hip bone. Stress shielding causes three major issues: (1) periprosthetic fracture or avulsion of bony prominences such as the greater or lesser trochanter; (2) less bone support for a revision implant after removal of a well-fixed implant from the stress-shielded bone; and (3) increased intracortical porosity of the stress-shielded bone. As shown in *Fig. 1.1*, one aetiology of implant loosening because of periprosthetic bone resorption is stress shielding, which leads to the premature failure of a THR via mechanisms that include aseptic loosening, implant migration, and periprosthetic bone fracture. As a result, it would be advantageous if femoral implants could be produced with features that reduce stress shielding.

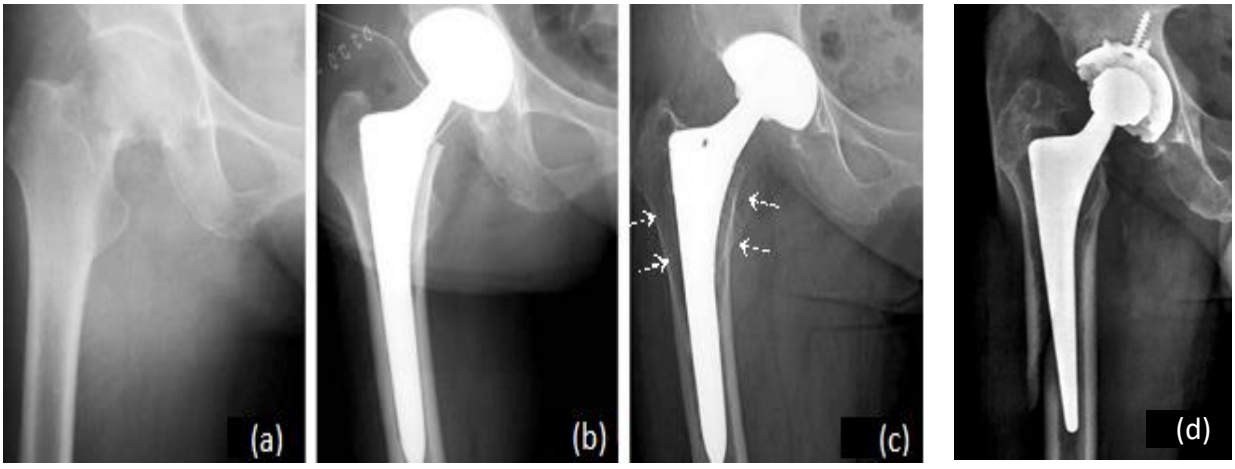

Fig.1.1: Natural progression of a hip replacement: (a) pretreatment x-ray; (b) immediate postoperation; (c) post-operative bone resorption occurs after 8 years; and (d) stem migration and post-operative fracture (*Yamada et al., 2009*).

Because of their high stiffness, modern cementless femoral prostheses cannot avoid the problem of stress shielding. Even metal implants with low-stiffness like titanium (E = 112 GPa), which are generally employed as the best implant choice, are stiffer than cortical bone (E = 30 GPa). The present model of these femoral implants favours a modular stem that consists of a titanium alloy femoral stem which is connected to a cobalt–chromium femoral head by a taper junction. The advantages of this modular stem allow the surgeon to remedy irregularities in leg length, offset, and version. Because of its superior mechanical strength, abrasion resistance, and corrosion resistance titanium alloys are employed as joint prosthesis. When a cobalt–chromium femoral head is used with a titanium femoral stem, however, crevice corrosion is accelerated galvanically. The wear particles generated by metal corrosion because bone lysis and inflammatory reactions in the soft tissue, resulting in implant loosening. One option is to employ a modular cobalt-on-cobalt prosthesis. The cobalt–chromium femoral stem is significantly stiffer than titanium, which can accentuate the early aseptic loosening from stress shielding and increase the risk of implant loosening. As a result, there is no such a suitable material for metallic implants that can provide the same stiffness as human bone.

1.2 METALLIC BIOMATERIALS

A perfect biomaterial should have qualities such as excellent biocompatibility and no unfavorable tissue reaction. It must also have a bone-like density, strong mechanical strength and fatigue resistance, low elastic modulus, and excellent wear & corrosion resistance (*Attar et al., 2019*). Even though combining all these properties in a single material are extremely challenging. Because of their superior mechanical qualities and biocompatibility, several metals are employed as biomaterials. A few are utilized as quiet alternatives for hard tissue repairs including total hip and knee joints, broken healing devices like bone plates and screws, spinal fixation apparatus, and dental implants. Various metallic alloys are utilized as actuators in more active devices like vascular stents and orthodontic arch wires.

Implants in bio-medicals must have precise mechanical properties that harmonise with human bones to ensure long-term effectiveness (*Fig. 1.2*). Young modulus, tensile strength, compressive strength, and toughness are mechanical properties of human bone that are affected by age, gender, location in the body, water content, and illness history. Bone is a natural composite substance made up mostly of collagen fibres and an inorganic bone mineral matrix called apatite, which is a tiny crystal. Cartiligen is a collagen-based tissue that comprises big protein saccharit molecules that bind collagen fibres together in a gel. The baring surfaces of the body's movable joints are formed by articular cartillery, which has a linear visco-elastic behaviour. It also has an extremely low coefficient of friction, which is due to the existence of senovial fluid, which may be squeezed when compressed.

The most important step to examine before using implants is in-vitro characterization. The outcomes of in-vitro research are critical in providing the required proof of concept. Implant into animals such as a rat, rabbit, sheep, even directly in the human body, would be used in the in-vivo investigation. Pure titanium, titanium alloys, surgical grade stainless steel, and cobalt–chromium alloys are the most commercially available biocompatible metals.

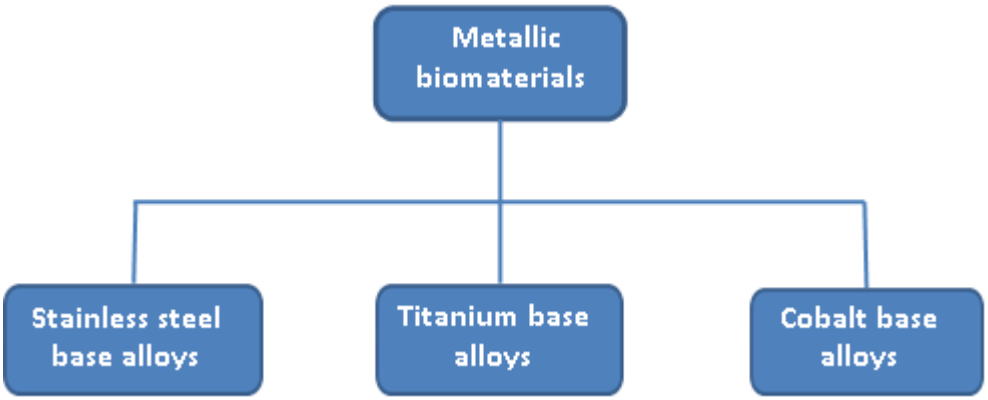

Fig. 1.2: Classification of metallic Biomaterials.

1.2.1 Stainless steel and its alloys

Stainless steel is the first metal to be employed as a biomedical implant due to its excellent mechanical properties, but it was not a long-term success because of its poor biocompatibility with living tissues. Despite its greater vulnerability to crevice corrosion than other prevalent

metallic biomaterials, 316L austenitic stainless steel (ASTM-F-138/139) has proven acceptable and the metal of choice for fracture healing devices throughout decades of usage. It's also been utilized to create certain joint replacement parts.

From forging temperature (1050^0C) to room temperature, it forms a single phase (FCC austenite phase) and achieves its excellent strength and fatigue resistance by strain hardening and solid solution strengthening processes, as well as a fine grain size. Implants are typically forged at temperatures beginning at 1050^0C and progressing through a succession of forging and re-annealing processes until they reach a near-final form.

1.2.2 Cobalt and its alloys

Cobalt alloys have been employed for a long time because of their superior corrosion resistance in physiological environments. Casting or forging can be used to make Co-based alloy implants (*Bahrami et al., 2015*), with the latter employing bar stock created by traditional forming of cast billets (rolling, extrusion) or hot isostatic pressing of Co alloy powders. Novel technologies for near net-shape creation of objects from metal powders (metal injection moulding) are also being investigated.

All Co-Cr-Mo implant alloys comprise Cr (26–30 wt%), Mo (5–7 wt%), some Ni (1 wt%), additional residual trace elements (Mn, Fe, Si, N), and C (low-C~0.05 wt%) or high-C~0.25 wt%).

1.2.3 Titanium and its alloys

Since the late 1960s, titanium and its alloys have been employed progressively in the manufacture of orthopedic implants (for fracture repair and joint replacement). Titanium and its alloys are thought to be the most suitable biomaterials. Titanium-based biomaterials have demonstrated good biocompatibility as well as fatigue & corrosion resistance and comparatively low cost (shown in *Table 1.1*). Their high strength-to-weight ratio also makes them lightweight (*Fig. 1.3*). Surface modification is necessary to improve the osseointegration of Ti-implants,

which may be accomplished using the AM method. Titanium implants are made by casting and contain a variety of refractive components with much higher melting temperatures than titanium, causing mechanical problems. Further efforts were undertaken to develop a material that would be both biocompatible and strong enough to be used in a medical setting. Titanium may be employed as a biomaterial in two forms: pure Ti CP (Commercially Pure) and Ti-6Al-4V ELI (Al: 5.5-6.5 %, V: 3.5-5.5 %, Impurities of C, Fe, O, N, H: 0.5-0.6 %, 89-98% Titanium). Approximately 45% of titanium production is attributed to the use of Ti-6Al-4V as a biomaterial.

Table 1.1 - The melting temperatures, densities, and estimated elemental cost commonly employed in titanium alloy.

Element	Melting Point Temperature (^{0}C)	Density (g/cm^3)	Price (Rs./Kg)
Ti	1678	4.5	2000
Al	660	2.7	208
V	1910	5.8	2500
Ta	3020	16.6	10810
Nb	2477	8.5	20000
Zr	1855	6.5	3000
Mo	2623	10.2	3500
Fe	1538	7.8	100
Ni	1455	8.9	1100
Co	1495	8.9	4500
Mn	1246	7.4	390
W	3422	19.3	6000
Cr	1907	7.2	1000

Fig.1.3: Uses of Titanium scaffolds for in orthopedics bone replacement and supports: (a) Compression plate for distal femoral locking; (b) Internal locking plate for proximal humerus fractures; (c) Titanium elastic nails for pediatric long bone fractures; (d) Locking and non-locking screws; (e) Titanium acetabular cup with HA coating for THR; (f) Polyethylene liner with a titanium lining on its rim (the polyethylene liner is fitted into the acetabular cup and represents as a acetabular component togetherly of THR (*Ghosh et al., 2018*) & (g) screws and main rod for broken bone surgery (collected from Dishari Hospital, Malda).

The most prevalent Ti alloy used in biomedical applications is Ti-6wt% Al-4wt% V (Ti64) (*Niinomi, 2003*). The microstructure of Ti-6Al-4V alloy has a combination of α and β phases with hexagonal closed packed (HCP) and body centred cubic (BCC) crystal structures, respectively (*Chlebus et al., 2011*). Al serves as an α stabiliser in the Ti-6Al-4V alloy, whereas V serves as a β stabiliser. *Figure 1.5* shows the Ti-6Al-4V beta-transus temperature. The key properties of (α +β) titanium are its high strength, great fatigue and corrosion resistance, and comparably low density. The mechanical properties associated with phase transitions, which are determined by previous processing and heat treatment operations, have a significant impact on the microstructure of Ti64. At temperatures over 883°C (β-transus temperature), pure Ti is BCC (β-phase), and HCP (α-phase) at lower temperatures. The addition of other components stabilizes one of the two phases. Al, O, N, and C are the α-stabilizers, where β-stabilizers are divided into two types: β-isomorphous (Mo, V, Nb, and Ta) and β-eutectoid (Fe, W, Cr, Si, Ni, Co, Mn, and H). Recently, isomorphous Ti alloys have piqued attention for implant applications due to the low elastic moduli that these alloys may achieve when properly treated. Some Ti alloys contain the elements Zr and Sn, which are termed 'neutral' alloying elements since they have no influence on either α or β-phase stabilization. This alloy works best when direct contact is necessary with tissues or bones as shown in *Fig. 1.4.*

Because vanadium works as a beta-stabilizer, the beta-increased phase's strength persists below the transition temperature, resulting in a two-phase system. Although vanadium has been shown to be hazardous in a few studies over the years, aluminium ions have been linked to Alzheimer's disease. As a result, advance biomaterials with less harmful for long-term effects are being developed. Toxic components should also be avoided or utilized in a reasonable proportion for broader application. Furthermore, elements such as chromium and nickel can be used to replace them.

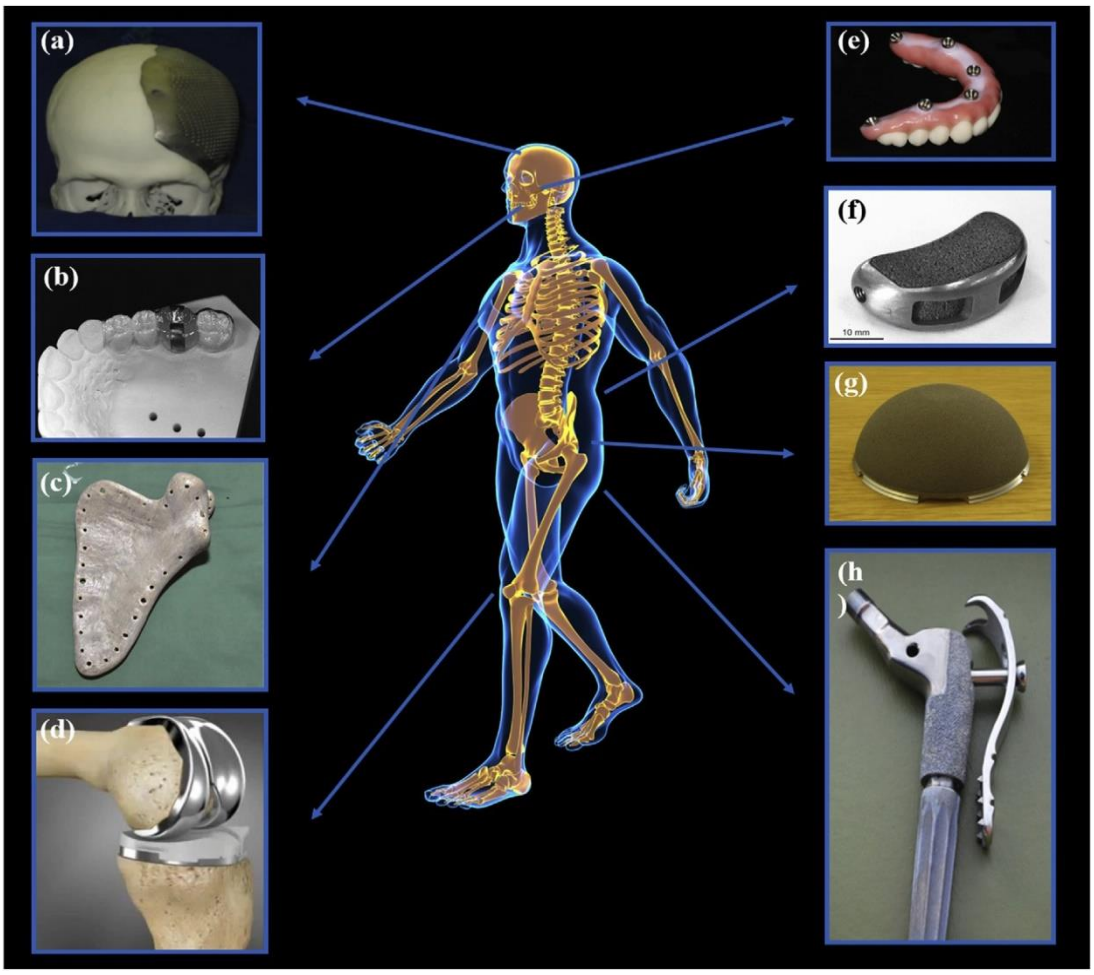

Fig. 1.4: The applications of Ti alloy biometals in biomedical by 3D printing: (a) cranial prosthesis (b) surgical guide (c) scapula prosthesis (d) knee prosthesis (e) dental implants (f) interbody fusion cage (g) acetabular cup and (h) hip prosthesis (*Ni et al., 2019*).

In general, most Ti alloys have suitable mechanical characteristics for orthopedic applications. Ti alloys have higher torsional and axial stiffness (modulus) than stainless steel and Co-Cr alloys and, as a result, provide less stress shielding. As compared to Co-Cr-Mo alloys, the most undesirable mechanical properties of Ti alloys are susceptibility to crack propagation, comparative softness, and relatively low wearing and frictional qualities. The existence of a passive oxide layer on the surface of Ti and its alloys is responsible for their clinical success in terms of biocompatibility. TiO_2 is a naturally occurring titanium oxide with 5 to 29 nm thickness that may be repaired fast after injury (*Breme and Biehl, 2016; Bram et al., 2000*). Nonetheless,

there is significant debate over the precise chemistry of pure titanium vs alloyed titanium oxides (*Brunski, 2004*). Some Ti alloys created for biomedical applications are listed in *Table 1.2*. *Table 1.3* shows a comparison of the characteristics of Ti with their metallic biomaterial analogues.

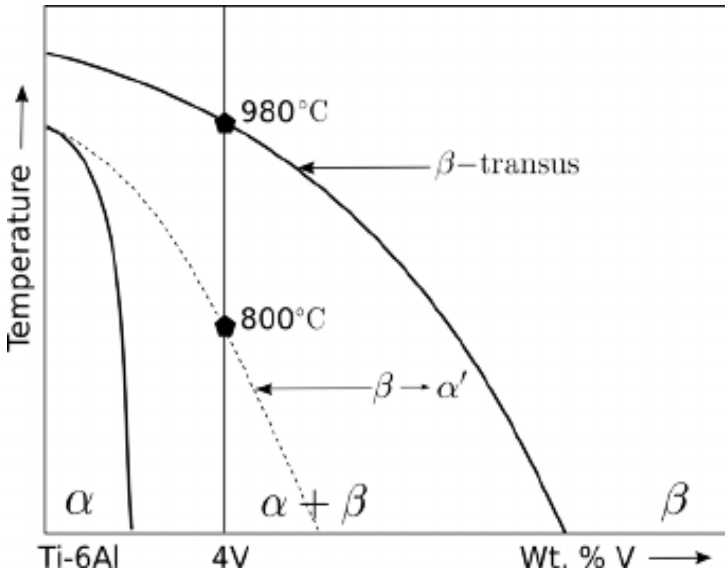

Fig.1.5: The beta transus of Ti-6Al-4V.

Table 1.2 - Titanium alloys for bio-medical applications (*Niinomi et al., 2004*).

Composition	**Type**
Pure Ti	A
Ti-6Al-4V ELI (ASTM F136084, F620-87)	α+β
Ti-6Al-7Nb	α+β
Ti-6Al-4V (ASTM F1108-88)	α+β
Ti-5Al-2.5Fe	α+β
Ti-5Al-3Mo-4Zr	α+β
Ti-15Sn-4Nb-2Ta-0.2Pd	α+β
Ti-15Zr-4Nb-2Ta-0.2Pd	α+β
Ti-13Nb-13Zr	near β (low modulus)
Ti-12Mo-6Zr-2Fe	β (low modulus)
Ti-15Mo	β (low modulus)

Ti-16Nb-10Hf	β (low modulus)
Ti-15Mo-5Zr-3Al	β (low modulus)
Ti-15Mo-2.8Nb-0.2Si-0.26O	β (low modulus)
Ti-35Nb-7Zr-5Ta	β (low modulus)
Ti-29Nb-13Ta-4.6Zr	β (low modulus)
Ti-40Ta, Ti-50Ta	β (high corrosion resistance)

Table 1.3 - Comparison between the properties of three major metallic biomaterials.

Characteristics	Stainless Steel	Cobalt-Chromium	Titanium
Stiffness	High	Medium	Low
Strength	Medium	Medium	High
Corrosion resistance	Low	Medium	High
Biocompatibility	Low	Medium	High

1.2.3.1 Ti-6Al-4V

Because of its biocompatibility, most of the Ti-6Al-4V research is motivated by its prospectiveuses as body prosthesis and implants. Ti-6Al-4V is of relevance due to its uses in the biomedical industry (*Marin et al., 2013*). Because of its superb biocompatibility, exceptional corrosion resilience, and superior mechanical durability, Ti-6Al-4V has indeed been extensively employed for different orthopedic implants (*Pattanayak et al., 2011*). Furthermore, Ti-6Al-4V has a higher specific strength and elastic modulus over cobalt chromium alloys and stainless steel (*Abe et al., 2003*). ASTM standards, ISO standards, and the US FDA all specify functional standards for Ti-6Al-4V implants. Regardless of how the alloy is processed, Ti-6Al-4V components could have a variety of microstructures. Casting, wrought ingots, and powder metallurgy; for instance, provide three distinct microstructures for Ti-6Al-4V. It is due to the microstructure of pure titanium is entirely α. β Phase occurs along grainboundary whenever pure

titanium is alloyed with stabilizers (*Attar et al., 2015*). The proportion of α and β phases can vary depending on treatment factors such as temperature, cooling rates, and mechanical stress levels.

The price of titanium alloys originates primarily from two factors: (i) the expenses associated to its extraction technique (presently utilized Kroll's reduction procedure is energy-intensive and not so far robust) and (ii) the pay of current manufacturing techniques which needs preventive habitats, greater energy intake and usually entails substantial waste production (*Imam et al., 2010*). To reduce the aggregate expense of manufacturing, study has thus centred on unconventional effectual manufacturing methods (*Lütjering et al., 2007a*). In recent times, additive manufacturing (AM) has sparked considerable interest in addressing a few of these difficulties. In theory, additive manufacturing permits one to create an object of practically any desirable shape via a digital model using sequential material layers placed and fused together.

Aside from the ability to build components with unique functional geometries those are hard to obtain with traditional processing, additive manufacturing processes are employed (*Gibson et al., 2010*). For instance, excluding support structures in certain circumstances, AM employs only the raw material required to build a component, regardless of its form, minimizing material waste dramatically. Selective Laser Melting is among the most intriguing AM methods for the manufacturing of titanium alloys (SLM). Following precise adjustment of the SLM system, literatures have revealed that exceptionally dense (99.7% or higher) SLM titanium alloy may be created. As a result, super dense SLM titanium alloys have mechanical qualities equivalent to those of traditionally made alloys. The preponderance of titanium alloy SLM research has, though, concentrated on selecting processing parameters which could enhance sample density and construct rate with minimal respect for component microstructure. As a result, whenever multiple SLM systems are employed, component grade, consistency, and mechanical characteristics of SLM specimens are frequently uneven.

1.3 ADDITIVE MANUFACTURING (AM) PROCESSES FOR METALLIC BIOMATERIALS

Acellular and cellular AM approaches for biomaterials are the two primary kinds of AM techniques. Cellular processing uses both living cells and biomaterials, as opposed to acellular

processing, which involves the processing of biomaterials without the need of living cells. According to the ASTM standard, acellular additive manufacturing technologies may be categorized into following seven groups: (1) binder jetting, (2) directed energy deposition, (3) material extrusion, (4) material jetting, (5) powder bed fusion, (6) sheet lamination, and (7) vat photopolymerisation (*Fig. 1.6).* Individual AM procedures vary based on the material used and the machine technology used. In AM methods like as powder bed fusion and directed energy deposition, there are a few metal-AM procedures for powder-based metallic feedstock systems. A procedure called "powder bed fusion" uses heat energy, such as a laser or an electron beam, to fuse powdered material in specified locations on a powder bed. A few of the advantages of this method are the ability to create intricate, small-scale items with high dimensional accuracy, construct without the need for support, and employ a variety of powders. Powder bed fusion is one of the earliest AM techniques to be commercialised, and it has made a significant contribution. Selective laser melting (SLM), electron beam melting (EBM), and selective laser sintering (SLS) are three types of powder bed fusion processes capable of processing biocompatible powder metal.

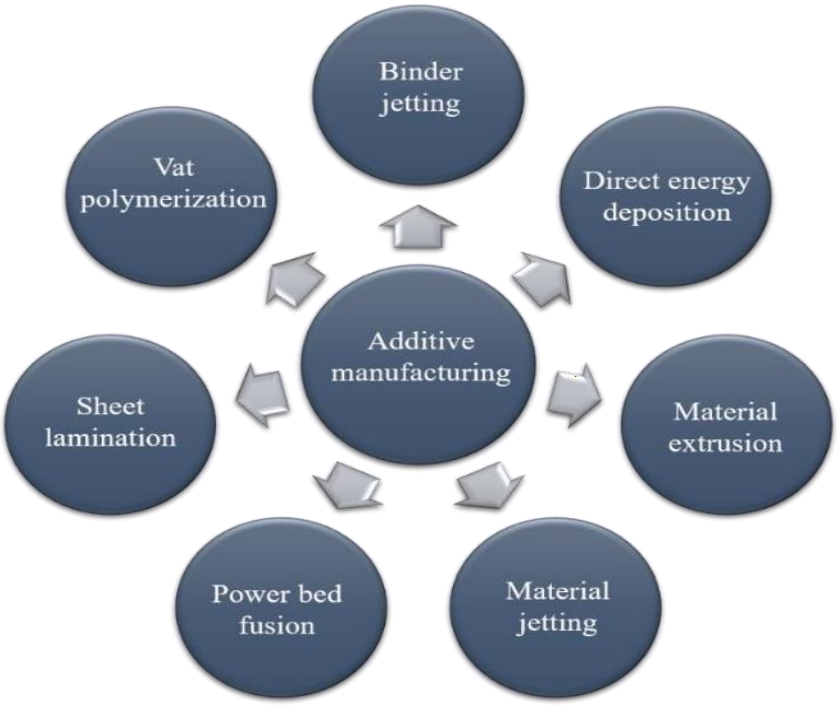

Fig. 1.6: Classification of Additive Manufacturing (AM) techniques (*Guo et al., 2013*).

Direct energy-based approaches used a direct source of energy, which was often a laser, electron beam, or plasma arc. Directed energy deposition (DED), as described by ASTM F2792-12a, is an AM technique "in which concentrated thermal energy is employed to fuse materials by melting as they are deposited. Powder, filament, or wires are all employed to feed the fused material. The starting material was continuously fed into these processes before the heat energy melted it and deposited it in a layer-by-layer manner. A computer controls the geometry and pattern creation in these operations using the XYZ system. These processes can be used on ceramic, composite, and polymeric materials, but they are most commonly used on metals. LENS (laser engineered net shaping) is an AM technology that uses powder-based metallic biomaterials and is classified as a direct laser deposition (DLD) technique. An overview of several AM methods is shown in *Table 1.4.*

Table 1.4 - Outline of additive manufacturing approaches.

	Process	Layout	Layer creation method	Phase change	Materials
LIQUID	**Stereolithography (SLA)**	Liquid resin in a vat	Liquid layer deposition	Photo-polymerisation	Acrylates, epoxies, filled resins
	Fused deposition modelling (FDM)	Material melted in a nozzle	Continuous extrusion and deposition	Solidification by cooling	Polymer (ABS, PA), wax, filled polymers, metals
	Ink jet printing	Droplets of molten material	Drop on demand deposition	Solidification by cooling	Polymers, wax
POWDER	**Three-dimensional printing**	Binder and powder in bed	Layer of powder and drop on demand deposition	No phase change	Ceramics/metals/polymers with binder
	Selective laser sintering/melting (SLS/SLM)	Powder in bed	Layer of powder	Sintering/melting by laser and resolidification by cooling	(Filled) polymers, metals with binder, (pure) metals, ceramics (with binder)
	Electron Beam Melting (EBM)	Powder in bed	Layer of powder	Melting by electron beam and resolidification by cooling	Non-magnetic metals
	Laser Cladding (LC)	Powder delivery through Nozzle	Continuous injection of powder	Laser melting and solidification by cooling	Metals
SOLID	**Laminated object manufacturing (LOM) and variants**	Feeding, cutting and binding of sheets	Deposition of sheet material	No phase change	Paper, polymer (foam), composites, metals, ceramics
	Shape Metal Deposition (SMD)	Metal wire delivery through Nozzle	Continuous injection of powder	Laser melting and solidification by cooling	Metals
VAPOUR	**Selective Laser Chemical Vapour Deposition**	Gas flow in laser	Condensation of gas	Forming solid material from gas by chemical decomposition	Metals, ceramics

1.3.1 Powder bed fusion (PBF)

Powder Bed Fusion (PBF) methods create solid parts by inducing fusion (sintering or melting) between the particles of a plastic or metal powder one layer at a time using a heat source. The majority of PBF technologies use mechanisms to distribute and smooth thin layers of powder while a part is formed, resulting in the final component being encased in powder when the build is finished.

Different energy sources (i.e. lasers or electron beams) and powders utilized in the process are the key differences in PBF technology (plastics or metals). Power bed fusion technology is further divided into following technologies as shown in *Fig. 1.7*.

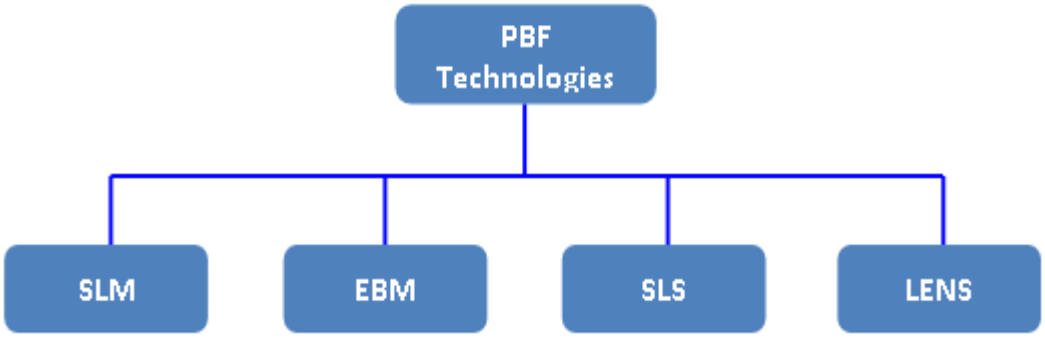

Fig. 1.7: Classification of Power Bed Fusion (PBF) technology.

1.3.2 Selective laser melting (SLM)

SLM is a kind of laser-based powder bed fusion which is also known as an improved form of selective laser sintering (SLS) (*Amado et al., 2011*), because it permits complete melting of metal particles and generates a homogeneous SLM product. Only pure and alloyed metal powders are used in SLM. Direct metal laser sintering (DMLS) is almost synonymous with SLM. The original DMLS technique is similar to the SLM in that it uses high-powered lasers to melt tiny metallic particles completely. In the year 2002, SLM was created. This technology has been employed for the biomedical sector as one of the 'non-traditional' manufacturing complicated part ways under metal- AM. The manufacturing of jaw and bone implants for dentistry and orthopedic purposes is one of the first investigations.

In comparison to other metal-AM techniques, SLM is the most widely used metal powder bed fusion process in the production of metallic biomaterials today. This situation corresponds

to the expansion of the SLM system in terms of new machine development and innovation in order to make it more productive and profitable. As the increase reached the year 2012, the importance of new technology development and well-developed innovation for machine usage grew. It involved the fabrication of SLM systems in-house for research including in vitro studies for bone scaffolds and biomedical implants made of a variety of titanium alloys.

1.3.3 Electron beam melting (EBM)

The Electron Beam Melting (EBM) technique is named after a commercial equipment created by a Sweden company Arcam in 2015. The process is one of the most well-known powder bed fusion methods for metal. The system has a rake, build platform, powder hoppers, and an energy supply, similar to SLM. In the processing approach, however, the device employs electron beam energy rather than a laser. EBM must operate in a high vacuum due to several fundamental features of electron beams. Furthermore, some metals and alloys with a highly reactive state are prone to absorbing contaminants when exposed in air. The vacuum chamber is utilized to maintain the integrity of the EBM created object by creating a vacuum atmosphere during the process. The intrinsic capacity of technological maturity provides benefits such as high build resolution, good dimensional precision, a clean build environment, reduced surplus materials, and near-net- form capabilities. These studies demonstrated the ability of SLM and EBM to directly construct tailored metallic cellular scaffolds for orthopedic implants.

1.3.4 Selective laser sintering (SLS)

Selective laser sintering was the one and only powder bed fusion technique to be formed and commercialized. The material choices and powder fusing process are the main distinctions between SLS and other powder bed fusion procedures. SLS is a laser-based powder bed fusion technology similar to SLM. Unlike SLM, however, the raw powder is partly molten or heated to the sintering point during the SLS process. SLS can manufacture thermoplastic polymer/ceramic or metal composite powders as material alternatives. Polymer is employed as a binder in powder-based metallic material technology to hold fused metal particles together at low temperatures. Depolymerisation is used to remove the polymer from the green body afterwards. As a result, the portion created has porous features by nature.

Previous biomedical research has focused on using a mix of SLS and post-processing to reduce porosity and quickly produce near-full-density components. The production of metallic foams for bone implants is the most common use for porous structural materials.

Metallic foam's cellular structure may be created to mimic cancellous bone's structure while still fulfilling design requirements for porosity, form, size, strength, and biocompatibility. Metallic foam should allow for greater bone contact. The porous structure is thought to aid bone formation by allowing bodily fluid to pass through the open cell foam's linked network of holes. As a result, the implant and bone have a better interlock, which helps to prevent or eliminate implant loosening faults.

1.3.5 Laser engineered net shaping (LENS)

Sandia National Laboratory (a renowned research institution in the United States) pioneered LENS technology (a type of additive manufacturing) by developing the fundamental principles and initial applications, while Optomec Inc. played a crucial role in commercializing and advancing the technology for widespread industrial use. It is recognized as a widely utilized AM method that employs biocompatible metal powders and falls under the category of direct laser deposition techniques. This technology may be used to modify the surface of a part as well as fabricate near net-shaped functional components. It is a method in which a pool of molten material isn't surrounded by a bed of powdered material during the process. LENS has a 4 kW high-power laser (solid state or fibre optic laser). A combination of particles is fed through argon pressured nozzles in the LENS process. It is directed to a point of convergence that also acts as the laser's focal point.

A micro-melt pool is then created once the powder has melted. The melt pool sticks to the surface. The substrate of the LENS is stationary, but the above laser system travels upward as each layer is deposited. To prevent oxidation of the build material during deposition, the entire build assembly of LENS system is contained in a controlled environment. LENS is anticipated to provide higher benefits over powder bed fusion in terms of fabrication effectiveness, improved cooling effect, and the ability to re-fabricate parts. The molten pool is not enclosed by a powder bed in the LENS process.

1.4 LATTICE STRUCTURED (LS) POROUS BIOMATERIALS

Compared to porous biomaterials made using traditional manufacturing processes, additive manufacturing has three significant benefits. First, the micro-architecture of porous biomaterials can be minutely controlled (*Fig. 1.8*). Because the mechanical characteristics of porous biomaterials are based on their micro-architecture, this is a significant benefit. Porous biomaterials' mechanical characteristics can thus be altered by altering their micro-architecture. The ability to combine solid materials with porous materials or porous materials with diverse micro-architectures in one single construction is the second benefit. Because each micro-architecture produces a different set of mechanical characteristics, the distribution of mechanical qualities inside the implant may be tuned to reduce stress shielding. Third, additive manufacturing methods may be used to create patient-specific implants. There are two major benefits to increasing the porosity of porous metallic biomaterials. Initially, the stiffness of the metallic biomaterial decreases to the level of stiffness values generally determined for bone. Second, extremely porous biomaterials allow for sufficient bone growth and implant fixation. High degrees of porosity may compromise the fatigue properties of highly porous biomaterials.

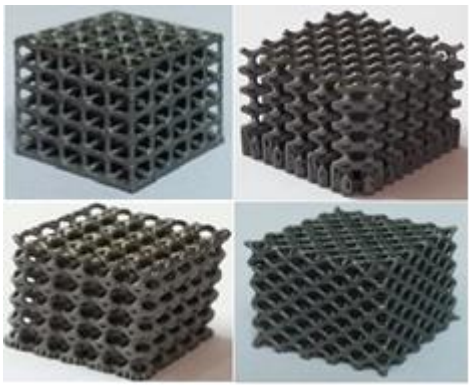

(a)

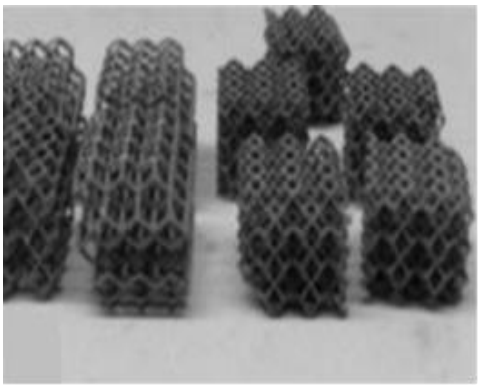

(b)

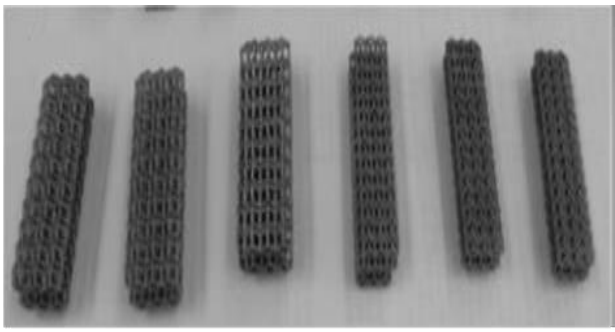

(c)

(d)

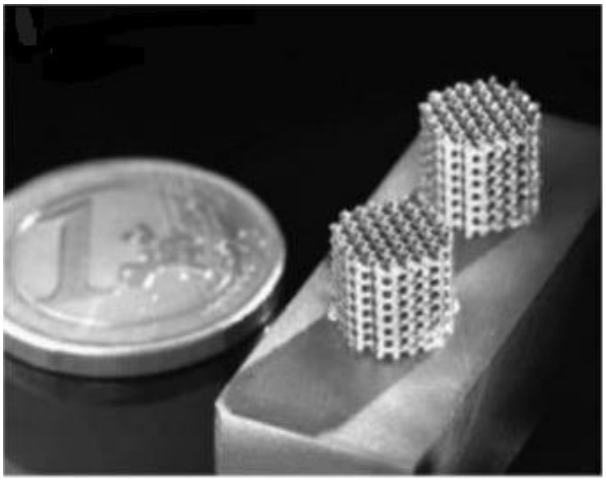

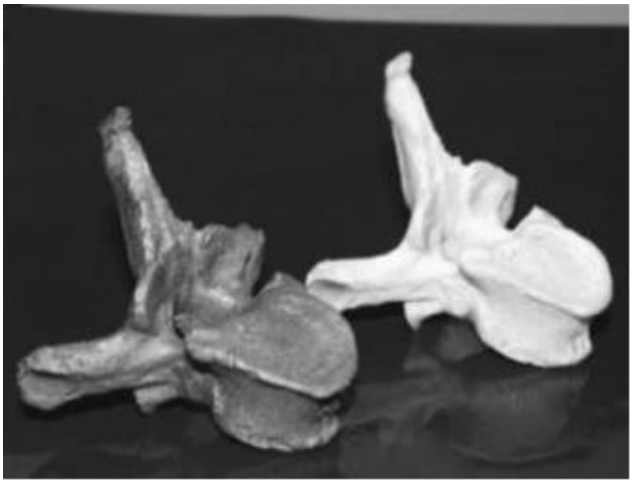

(e) (f)

Fig. 1.8: (a-d) Different types of Ti-6Al-4V structures (e) Mesh Ti-6Al-4V alloy structures and (f) Replica of human vertebrae fabricated by SLM technique (*Bose et al., 2018*).

1.5 A COMPARISON OF METALLIC BIOMATERIALS IN THE FIELDS OF ADDITIVE MANUFACTURING

Metal-AM technologies are expected to expand in popularity in the next years. In 2012, 16.4% of the AM's entire system-related revenue came from biomedical applications. The ability of metal-AM to correlate with the in-demand of medical device components and technology is the primary reason for this (*Fig. 1.9*). Most medical equipment, including as dental crowns and surgical implants, require miniaturizations and so benefit from metal-AM technologies envelope size fabrication.

Furthermore, the technologies are capable of satisfying clinical efficacy, as evidenced by the successful matching of particular patients with good features by customized solutions. In the biomedical domain in 2017, the majority of metal-AM procedures were quite competitive. Nonetheless, due to their capacity to give precise control over interior pore patterns and complicated forms as required in biomedical applications, SLM and EBM technologies are likely to lead the potential.

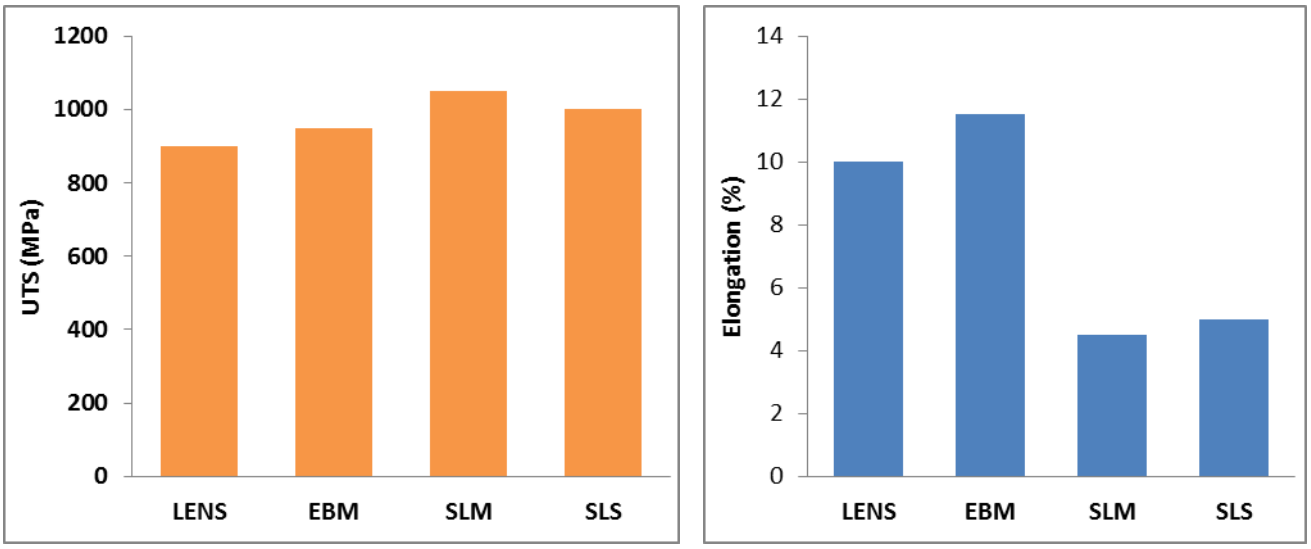

Fig. 1.9: (a) Ultimate tensile strength (UTS), and (b) elongation of Ti-6Al-4V processed by metal-AM processes.

On the other hand, metal-AM companies are competing to offer new equipment that let manufacturers to process metal goods efficiently and affordably. Because of their outstanding characteristics, titanium and its alloys have remained the preferred biomaterial employed by metal-AM techniques and have maintained their dominance. For the production of metal-AM, electron and laser melting technologies provide appealing alternatives, especially for orthopedic and dental implants that need to match the body while being speedier and less costly. In the areas of implant structural design and process development, further work will be done in the future.

1.6 PROBLEM STATEMENT

The metallic orthopedic implant loosens prematurely due to a stiffness mismatch between it and the surrounding bone. Porous metals have been offered as a way to reduce metal stiffness and more nearly mimic bone stiffness. Porous implants are commonly made using traditional methods such freeze drying, solvent casting, and salt leaching. Non uniform pore distribution, lack of adjustable strength, toxic material residue, and unregulated internal architecture are all shortcomings of these procedures, resulting in unsatisfactory bone implant production. To design and create a perfectly controlled internal architecture of porous metals, advanced additive manufacturing (AM) techniques integrate diverse computer-aided

capabilities. Using selective laser melting (SLM) processes, the complicated porous patterns are produced layer by layer. This form of well-defined porous metal is called cellular structure. The construction of a correct internal architecture of the cellular structure remains a difficult trial-and-error process, even though the pores of the cellular structure enhance the biological environment required for bone tissue and decrease the mechanical stiffness of solid metal alloys.

The biomechanics of human bone should be reflected by the internal design of metallic bone implants. From a morphological standpoint, bone is a complex structure with optimized functions spanning nano, micro and macro-scales (*Kumar et al., 2018*). The multi-scale bone formations stimulate the question of whether a graded cellular method may be employed to manufacture a bonelike material for tissue regeneration and replacement technologies. Successfully constructing implants with porous structures should mimic bone characteristics, avoid, or eliminate peri-implant bone stress shielding, and increase hip implant longevity.

1.7 RESEARCH AIM

The focus of this research is to come up with alternative designs of porous structures that are biocompatible with bone and to resist bone stress. Prosthetic devices for joint replacements and other bone replacement applications can be made using Ti alloy powders by AM methods.

The main aim of this research is that porous Ti alloy implants might be created using SLM methods to mimic human bone and avoid or minimize proximal bone stress shielding after insertion.

1.8 RESEARCH OBJECTIVES

Stress shielding reduces the durability of cementless implants and orthopedic bone implants, resulting in increased revision surgery morbidity and mortality. The primary objective of this study is to investigate the mechanical properties and manufacturing feasibility of laser melted porous Ti alloy structures to minimize peri-implant bone stress shielding. These objectives are:

- To investigate the internal architecture of porous structures and to see how they might provide mechanical and biological performance for bone implants.
- To investigate the production feasibility of laser melted porous titanium structures and their potential as osseointegration implants.
- To investigate the effects of graded orientations on the mechanical properties and stress-transfer properties of titanium porous structures.

1.9 RESEARCH SIGNIFICANCE

Human bones are formed of biological composite material with a porous structure, whereas implants are normally constructed of solid metal. By merging porous structures with the implant, this study attempted to build a bone biomimetic implant that might minimize the stress shielding effect. These porous structures should give a light weight structure with bone-like biomechanics and support a biological environment for bone cell processes, which should help the implanted prosthesis last longer.

The findings of this thesis will help to advance material synthesis for bioengineering and medicinal applications. This thesis is mostly concerned with mechanical and biological performances of porous titanium implants. Novel applications for manufacturing weight bearing orthopedic bone implants that perform more nearly to human bone will be found by establishing new internal architectural patterns and graded orientation.

The significance of this research is that it will be used to create a new cementless implant that will eliminate periprosthetic bone stress shielding and hence increase implant longevity. SLM methods can minimize the cost of graded cellular prosthesis by employing less material. Furthermore, lowering the rates of revision surgery morbidity and death will save lives, money, and limited health resources.

1.10 SCOPE OF CURRENT RESEARCH WORK

Metal AM creates implants that are very patient-specific, stronger, have lower impurity content, have a superior osseointegration surface, and many other benefits. Metal AM has about 50 parameters that must be optimised for the manufacture of porous implant lattice

structures, which are distinct from the parameters utilised for the fabrication of bulk materials. The optimal AM parameters for fabricating lattice structure (LS) porous implants are investigated in this research. Furthermore, this research identifies the optimal combination of porosity percentage and lattice unit cell strut thickness for reducing implant volume and eliminating stress shielding. This study will aid in determining the most appropriate AM settings and lattice geometrical considerations for the commercialization of LS porous medical implants.

1.11 ORGANISATION OF THE THESIS

This thesis is divided into the following five chapters.

Chapter 1: Introduction

This part discusses the background, metallic biomaterials, manufacturing processes, problem statement, research aim, objectives, significance, and scope of this research.

Chapter 2: Literature review

The properties that distinguish bone as a distinct structure are investigated. The evolution of osseointegrated implants is examined in order to identify research gaps that may be investigated in order to increase bone implant efficiency by bringing it closer to bone properties. Finally, methods of additive manufacturing procedures that may be utilized to construct complicated three-dimensional porous structures are discussed.

Chapter 3: Problem formulation, objectives, and methodology.

The porous Ti-6Al-4V alloy structures are designed through Rhino 6 software. This chapter examines the capability of fabricating a porous structure using AM techniques particularly SLM and different methodologies used in this work.

Chapter 4: Results and discussion

Microstructure observation, porosity measurement, surface roughness measurement and compression test are performed physically on different Ti porous scaffolds and mechanical properties are compared between them. The mechanical, biological and chemical

characteristics of the porous titanium alloy implants are compared in graphical representations with human bones whether the metallic implants are suitable or not to meet the biomedical needs.

Chapter 5: Conclusions and recommendations for future study.

This chapter summarizes the thesis key results and offers knowledge gaps that could be worth investigating further.

CHAPTER 2 LITERATURE REVIEW

2.1 INTRODUCTION

Bone replacement is a popular and significant surgical technique used to cure pain and disability in biomedical surgery. Porous surfaces for femoral prosthesis have recently been effectively introduced in the fixation of bone-implant by permitting bone development through the pores. However, with time, body pressure focuses on the bone site, resulting in stress-shielding phenomena. According to *Hussaini et al.* (2015), this stress-shielding effect was discovered in post-implant instances. To counteract this impact, porous metals were developed to reduce the stress-shielding effect by lowering the effective elastic modulus closer to that of natural bones. Interconnected porous structures are also effective for adhesion, proliferation, and differentiation of bone tissues (*Chen et al., 2020*). Porous scaffolds can avoid osteonecrosis and osteogenesis abnormalities surrounding the implant.

The capacity of mature bone tissue to renew via osteoclasts and form new bone via osteoblasts has been extensively established (*Gao et al., 2017 and Currey, 2012*). Although self-repair potential is restricted for bone lesions less than 10 mm (*Heuijerjans et al., 2017*). Autografts are taken from patients for smaller transplants, however the size of the graft is rigorously regulated, and the patient's health are also a consideration. When a bone defect or damage reaches this essential size, medical practitioners can employ bone grafts to effectively implant in the afflicted area once the healing process is completed. According to the disease control centre, more than two million bone procedures are performed each year (*Hoover et al., 2017*).

Because of its good biocompatibility, improved corrosion resistance, high strength-to-weight ratio, and higher stiffness, titanium alloy (Ti-6Al-4V) is extensively employed as a potential implant material in orthopedic areas for the replacement of knee and hip prostheses. Young's modulus of dense Ti-6Al-4V is significantly greater than that of human bone (*Liu et al., 2017*). The Young's modulus of dense Ti-6Al-4V is 112 GPa (*Geetha et al., 2009*), but it is 3 to 30 GPa in human bone (*Martens et al., 1983*). Because of the large elastic modulus mismatch, employing such material for bone grafting is limited. To solve this difficulty and match the human bone, Ti-6Al-4V scaffolds with porous structures are designed in such a way that the effective Young's modulus of the porous scaffolds closer that of the human bone.

Furthermore, the porous nature of the scaffold will aid in the development of new bone by the osteoblast method through this porous route. An ideal solution for application-specific scaffold printing for a bone replacement application is advanced additive manufacturing, such as the three-dimensional printing technique. 3D printing is a method of creating items from 3D model data by depositing material layer by layer. Selective laser melting (SLM) is a technology that may be used to make patient-specific porous scaffolds with a high degree of external form control (*Bose et al., 2018*). Using Rhino 6 software, a 3D scaffold model with proper dimensions is first created, and then the model is sliced into multiple 2D components and saved as standard tessellation language (STL) files. The AM machine setup executes layer by layer deposition along the defined tool path to construct the 3D porous scaffold after receiving the files. This approach of creating porous bone implants is gaining popularity among researchers since bone implants are needed to treat a variety of patient-specific bone fractures. *Jardini et al.* (2014) used AM methods to effectively produce porous scaffolds for a mandibular implant and a big cranical defect. Due to its capacity to construct complex, light-weight structures, AM technologies are widely applied in the biomedical field (*Melchels et al., 2010*). AM technologies have been embraced by the automotive, aerospace, jewellery, and other biological uses industries (*Petrovic et al., 2011*). A comparison of trabecular implant surfaces manufactured by SLM and EBM was published by *Biemond et al.* (2013). They demonstrated the differences in morphological properties and surface roughness between specimens fabricated using two different techniques: individual granules can be seen clearly in specimens fabricated using the EBM process, whereas specimens fabricated using the SLM process have a comparatively smoother surface with almost no grain visibility. Surface roughness of manufactured components improved by EBM implants is unsatisfactory, and osteoblasts are required to enhance surface roughness (*Ponader et al., 2008*).

2.2 GAP ANALYSIS

The following gaps are listed from review of open literatures:

- During fabrication via SLM, the porosity of porous scaffolds may differ than the designed porosity that was not considered earlier.
- Optimisation of process parameters was not addressed to get the suitable results.

- Surface treatment, compression test and finite element simulation of porous scaffolds with Diamond, Cross, Grid, Vinties, Tesseract, Star & Octet structures was not reported.

2.3 OVERVIEW

The fundamentals of bone biomimetic implants are introduced in this chapter. Firstly, bone properties and structures are described on hierarchical scales. Finally, the use of additive manufacturing (AM) techniques, selective laser melting (SLM) and stereolithography (SLA) in the creation of a novel design of bone biomimetic implants is discussed.

2.4 METALLIC IMPLANTS

Metallic implants claim to increase the quality and sturdiness of human life through contributing to healthcare as technology advances. Biomedical implants are distinctively different in terms of their usage and application, with each type exhibiting a distinct set of characteristics. For example, femoral implants have higher tensile and compressive strengths, but dental implants have higher wear and fatigue resistance. Due to differences in the elastic modulus of metallic implants compared to human bone, stress shielding may be a concern (*Weinmann et al., 2018*). In terms of biological use, titanium alloys are more prevalent (*Oldani et al., 2012*). Due to their superior mechanical and biological qualities, Ti alloys are preferred over stainless steel and Co-alloys in the fabrication of biomedical implants (*Dallago et al., 2017*). The modulus of elastic of stainless steel and Co alloys is noticed to be 10 times that of bones, whereas titanium alloys' elastic modulus is only 0.5 times that of stainless steel, resulting in a low risk of stress shielding compared to Co alloys and stainless steel (*Li et al., 2017*).

Porosity is also added to implants with three-dimensional (3D) open cell structures called lattice structures (LS) to reduce stress shielding (*Ullah et al., 2014*). Porosities in lattice-generated structures can range from 20 to 80 percent, depending on the application and load bearing capability. The technique of Additive Manufacturing can best achieve the production of lattice produced structures with required controllability and accuracy of up to micrometre scale, as is sought for biological uses (*Yavari et al., 2013*). Osseointegration, or

the direct structural and functional connection between the organised living bone and the surface of a load-bearing implant, is made possible by lattice structures (*Koppolu et al., 2016*). As a result, modeled porosity (form and size) is critical for bone ingrowth and hence biocompatibility.

In compared to bulk material, lattice structures provide different mechanical and biological behaviour (*Ullah et al., 2014*). These materials serve as the most realistic substitute for a bone, and hence the most appropriate choice (*Taniguchi et al., 2016*). The mechanical and biological features of these porous materials have been explored by a group of authors (*Pyka et al., 2012*). It has been established that the kind of unit cell (*Campanelli et al., 2014*), pore size (*Barui et al., 2017*), porosity (*Yavari et al., 2015*), strut diameter (*Cansizoglu et al., 2008*), and build angle (*Bagheri et al., 2017*) have an impact on the implant material's intrinsic mechanical and biological qualities. Furthermore, modulating SLM process parameters and initiating post heat treatments improves implant performance (*Li et al., 2016*).

2.5 TITANIUM

Ti possesses a hexagonal closed-packed (HCP) structure at room temperature, which generally istermed as α (*Lütjering et al., 2003*). Ti undergoes an allotropic change to body-centered cubic (BCC) β structure at 883°C and remains stable in the β-phase till it achieves its melting point of 1678°C (*Lütjering et al., 2003 and Lütjering et al., 2007b*). *Fig. 2.1* depicts the body cell for these structures. Ti alloys could have α, β or mixed α/β microstructures owing to the allotropic transition that is impacted by replacement and intervening elements and is reliant on metal purity (*Lütjering et al., 2007b*).

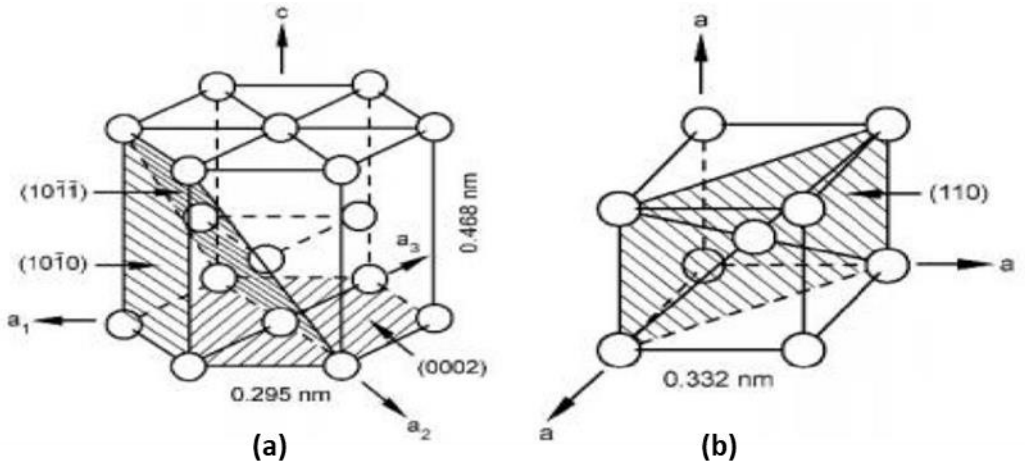

Fig. 2.1: a) HCP Structure & b) BCC Structure (*Lütjering et al., 2007b*).

Ti alloys are created by alloying elements stabilizing between the α or β phases, and the amount of bonding electrons engaged is depending on the degree of bonding electrons participating. Electron/atom ratios of alloying elements lower than 4 stabilize the phase, ratios of 4 neutralize the phase, and ratios larger than 4 stabilize the β phase (*Polmear, 2005*). The β-phase has substantial anisotropy from α, physical and mechanical characteristics, lesser ductility, elevated opposition to plastic deformation, greater creep resistance, as well as diffusion rates at least two orders of magnitude lesser than β-phase (*Polmear, 2005*).

2.5.1 Titanium as a Biomaterial

Scaffolds comprised of alloys like stainless steel, cobalt, and titanium have long being employed inside the human body (*Mengucci, 2016*). The *Table 2.1* lists the several standards which these biomaterials should fulfil in order to be employed in biological applications. *Table 2.2* lists some of the features of these metals and alloys.

Table 2.1- Scaffolding Requirements for Implants (*Long et al., 1998*).

Compatibility	**Mechanical Properties**	**Manufacturing**
Tissue reactions	Elasticity	Fabrication methods
Changes in properties- ➢ Mechanical ➢ Physical ➢ Chemical	Yield stress	Consistency and conformity to all requirements
	Ductility	Quality of raw materials
	Toughness	Superior techniques to obtain excellent surface finish or texture
	Time dependent deformation	Capability of material to get safe and efficient sterilization
Degradation leads to- ➢ Local deleterious changes ➢ Harmful systemic effects	Creep	Cost of product
	Ultimate stress	
	Fatigue strength	
	Hardness	
	Wear resistance	

Although the *Table 2.2* lists several problems connected with particular biomaterials, Ti as well as its alloys is becoming progressively highly relevant in the

market owing to its elevated qualities, which make them perfect as implant materials. Because of its great resistance to corrosion, biocompatibility, and strength, Ti and its alloys can fulfil the criteria for implants higher than anymaterial (*Lütjering et al., 2007b*).

Table 2.2 - Typical Metallic Implant Materials' Properties (*Long et al., 1998*).

	Stainless steels	**Cobalt-base alloys**	**Ti & Ti-base alloys**
Designation	ASTM F-138 (*316 LDVM*)	ASTM F-75 ASTM F-799 ASTM F-1537 (Cast and wrought)	ASTM F-67 (ISO 5832/II) ASTM F-136 (ISO 5832/II) ASTM F-1295 (Cast and wrought)
Principal alloying elements (wt%)	Fe (bal.) Cr (17-20) Ni (12-14) Mo (2-4)	Co (bal.) Cr (19-30) Ni (0-37) Mo (0-10)	Ti (bal.) Al (6) V (4) Nb(7)
Advantages	• cost, availability • processing	• wear resistance • corrosion resistance • fatigue strength	• biocompatibility • corrosion resistance • minimum modulus • fatigue strength • power rear resistance
Disadvantages	• long term behavior • high modulus	• high modulus • biocompatibility	• low shear strength
Primary utilisations	Temporary devices (fracture plates, screws, hip nails) Used for THRs stems in UK (high Nitrogen)	Dentistry castings Prostheses stems Load-bearing components in TJR (wrought alloys)	Used in THRs with modular (Co-Cr-Mo or ceramic) femoral heads Long-term, permanent devices (nails, pacemakers)

According to *Lutjering* (2007b) *and Williams* (2005), the main drawback of Ti is its high elastic modulus of roughly 112 GPa. Mechanical strength is an important consideration when employing scaffolds for bone replacement. The scaffold must be robust enough to handle acceptable loads, and not so strong that it causes stress shielding.

The modulus discrepancy among two materials causes stress shielding. Reduced stress is passed to bone linked to implant, resulting in bone resorption and, as a result, implant loosening (*Li et al., 2014*). Bone has a modulus of 3-30 GPa, that is much lower than Ti (*Choi et al., 1990; Wang et al., 2006; and Elias et al., 2008*). It reduces the implant's lifespan, frequently leading to uncomfortable and expensive modification operations. As a result, research has been carried out to identify novel strategies for improving mechanical characteristics of Ti and titanium alloys for biomedical purposes (*Li et al., 2014*).

2.5.2 Biomedical Titanium Alloys

Titanium alloys possess significantly less Young's moduli (55–110 GPa) than 316LSS (210 GPa) and Co–Cr alloys (240 GPa). The *Fig. 2.2* depicts the elastic moduli of several biomedical titanium alloys as well as bone. They do, meanwhile, contain moduli that are much greater than bone (3–30 GPa). Because of the large disparity in moduli between such implants and the surrounding bone, bone resorption occurs all around implant, causing implant loosening and, as a result, the sufferer might undergo severe reoperation. The "stress shielding effect" refers to this biomechanical mismatch. As a result, implant materials must have a modulus similar to bone they restore so as to minimize stress shielding effect. This eventually led to growth of novel forms of Ti materials for implant (containing design plus fabrication) with lower modulus similar to those of bone, thru goal of achieving reduced stiffness and sacrificing other important parameters (*Niinomi, 2003; Haghighi et al., 2015; Niinomi, 2012; Li et al., 2008 and 2016*). Several low-moduli, non-toxic β-type titanium materials for implants, like Ti–24Nb–4Zr–8Sn (Ti2448) (*Hao et al., 2005*) and Ti–29Nb–13Ta–4.6Zr (TNTZ) (*Niinomi, 2003*), have indeed been produced. Other option is utilizing porous structures rather than solid materials since porosity may lower the both modulus as well as weight of material when compared to solid alternatives. Additionally, modulus of a porous material may be conveniently adjusted, and bone cell in-growth might be enhanced over solid equivalents (*Cheng et al., 2012; Attar et al., 2014 and Challis et al., 2010*). As a result, porous materials can be used in joint replacement surgery as well as bone grafting application (*Barbas et al., 2012*).

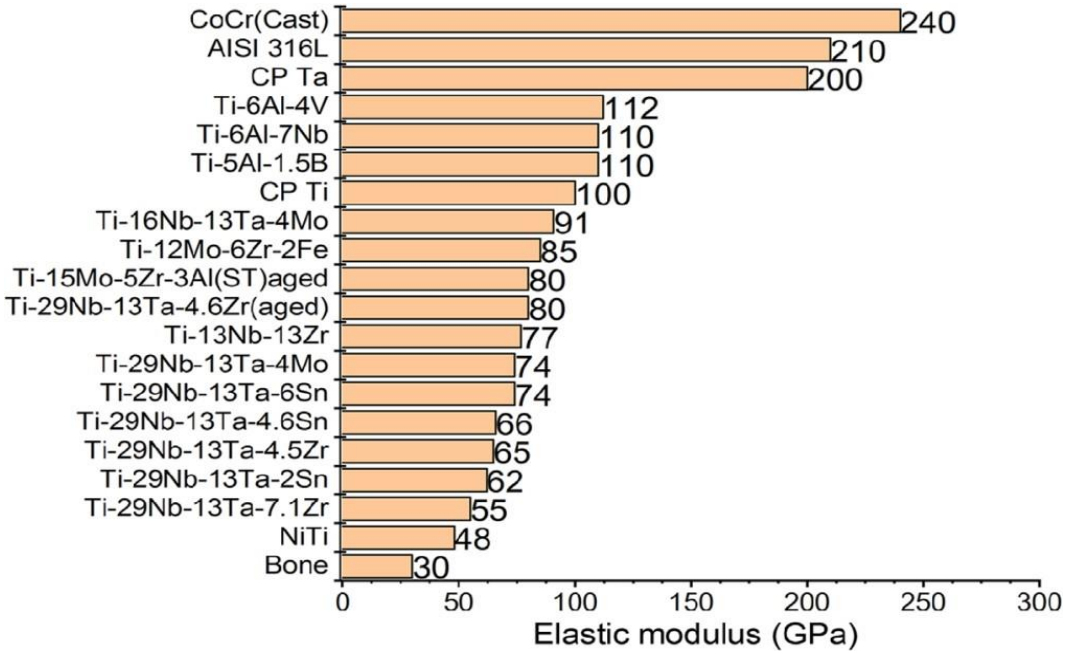

Fig. 2.2: Elastic moduli of different biomedical alloys and bone (*Geetha et al., 2009*).

2.6 POROUS SCAFFOLDS

Porous materials have recently been explored in research. *Parthasarathy et al.* (2010 and 2011) demonstrated how Ti-based biomaterials may be tailored to human bone by including a greater porous structure that is essential for cell adhesion, growth, and survival. Researchers came to the conclusion that porous structure minimizes the elastic modulus and consequences of stiffness misalignment, which are frequent in mass metallic biomaterials. This really is due to the fact thatthere is far lower material sustaining same cross-sectional area. Furthermore, porosity produces an open channel which favours tissue ingrowth and hence allows for improved tissue conduction (*Li et al., 2014*). The linked structure enables for full bone ingrowth and a steady blood supply, both of which are critical for biocompatibility and been a source of concern in previous biomaterials (*Long et al., 1998*). *Fig. 2.3* depicts the microstructure of a porous Ti scaffold (*Ryan et al., 2006*).

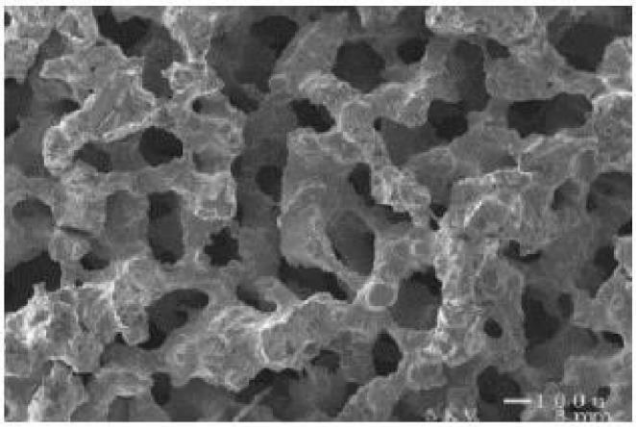

Fig. 2.3: SEM micrograph of Porous Ti (*Ryan et al., 2006*).

For scaffolds, significant porosity is needed to permit for tissue conduction; nevertheless, a combination with mechanical strength should be established.

2.7 BONE STRUCTURE

Bone is an open cell composite material that has a complicated vascular system as well as a considerable number of protein-related components. Bone is composed of two different types of tissues that are firmly packed together at the architectural level: cortical bone and trabecular bone. The outer shell of bone, called cortical bone, is a dense compact structure that covers the inner 3D lattice structures or trabecular bone. Cortical bone, also known as the Haversian system, is extremely dense and has cylindrically arranged osteons that range in size from 10 to 500 µm. It is noteworthy that the blood veins in the Haversian canal run parallel to the long axis of bone. Through perforating canals, blood arteries are linked to vessels on the bone's surface. The inner surface of cortical bone, referred to as trabecular bone, is connected by rod and plate-shaped structures. Furthest from to cortical bone, cancellous bone is very porous and is made up of an interconnected network of trabeculae with a diameter of between 50 and 300 µm. Porosity or density variations exist between these two forms of bone tissues. Whereas the porosity of cancellous bones ranges from 75% to 90%, that of cortical bone is just 5–10% (*Burr and Martin, 1989; Choi et al., 1990 and Rho et al., 1995*).

According to *Ritchie et al.* (2005), bone is a living tissue with the capacity for self-repair and the ability to modify its physical characteristics to suit the load and environmental circumstances. The combined actions of osteoblasts (cells that make new bone) and osteoclasts (cells that break down existing bone) are what cause this adaptive remodeling process. The variety, hierarchical (*Akbarzadeh et al., 2015*) structure, and composite components that characterize bone make it a special type of material. The volume percentage of individual trabeculae, the 3D architecture of those trabeculae, and tissue characteristics are the three factors that most significantly influence bone heterogeneity (*Keaveny et al. 2001*). For the entire organ to operate well bone tissues display functional gradients throughout a spatial volume in which each layer or component serves a specific purpose. As a result, depending on the functionality needed, various bone portions may have varied bone characteristics and orientation.

Depending on how it performs, bone has to be both structurally and mechanically sound. The brain is shielded from impact stresses by the skull, whereas a femur is continually stressed by repetitive strain during routine everyday activities. Hence, a femur is stronger than the skull bone. Walking causes the femoral bones to experience cyclic loading, which encourages the laden bones to modify their characteristics in response to the mechanical stimuli. Depending on where each bone is located and what it does, the intensity and direction of mechanical impulses on those bones may vary (*Carter, 1984*).

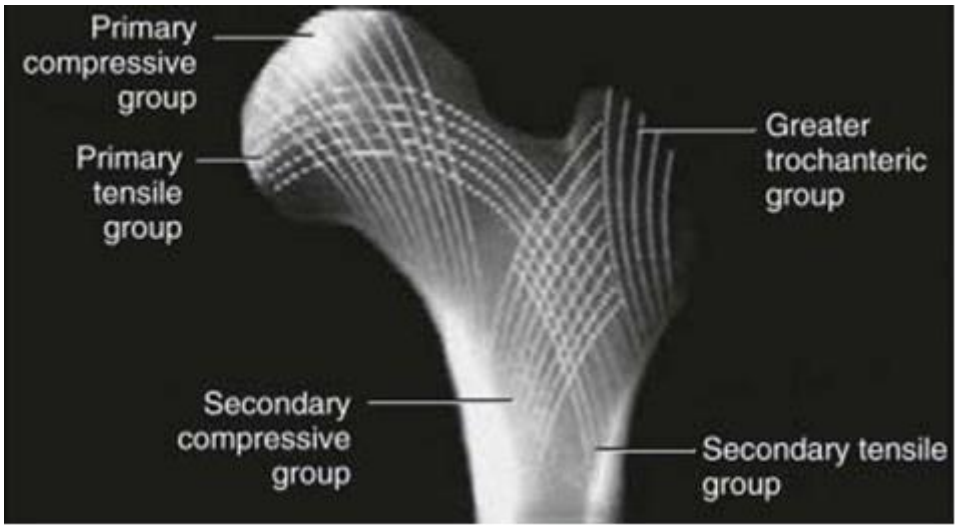

Fig. 2.4: An anteroposterior radiograph of the hip showing the trabecular orientations.

Since it resists both tensile and compressive pressures during weight bearing, the proximal femur is a superb illustration of functionally optimized structures. According to the direction of the trabecular lines, those forces optimize the internal structure of the femoral neck. The trabecular shape is seen in *Fig. 2.4* and includes both compressive and tensile groups that are oriented in certain planes. In contrast to the primary tensile group, which originates from the femoral head's foveal region and travels through the superior femoral neck and into the lateral sub-trochanteric cortex, the primary compressive group extends from the medial sub-trochanteric cortex and lines superiorly into the weight-bearing femoral head. In response to the weights applied to this bone, the trabecular orientation develops. Cortical bone density changes as well to accommodate the load needed in each place.

Bone is a special substance due to the heterogeneity of the bone tissue and the variations in density depending on location. The calcar femoral, a cortical bone in this region with the thickest cortex to accommodate the mechanical demands, is located in the medial cortex of the proximal femurs, which resists the maximum load. Analyzing bone structures and material components at hierarchical length scales spanning from the macro to nanoscale components is crucial to comprehend how bone adaptive structures relate to mechanical qualities.

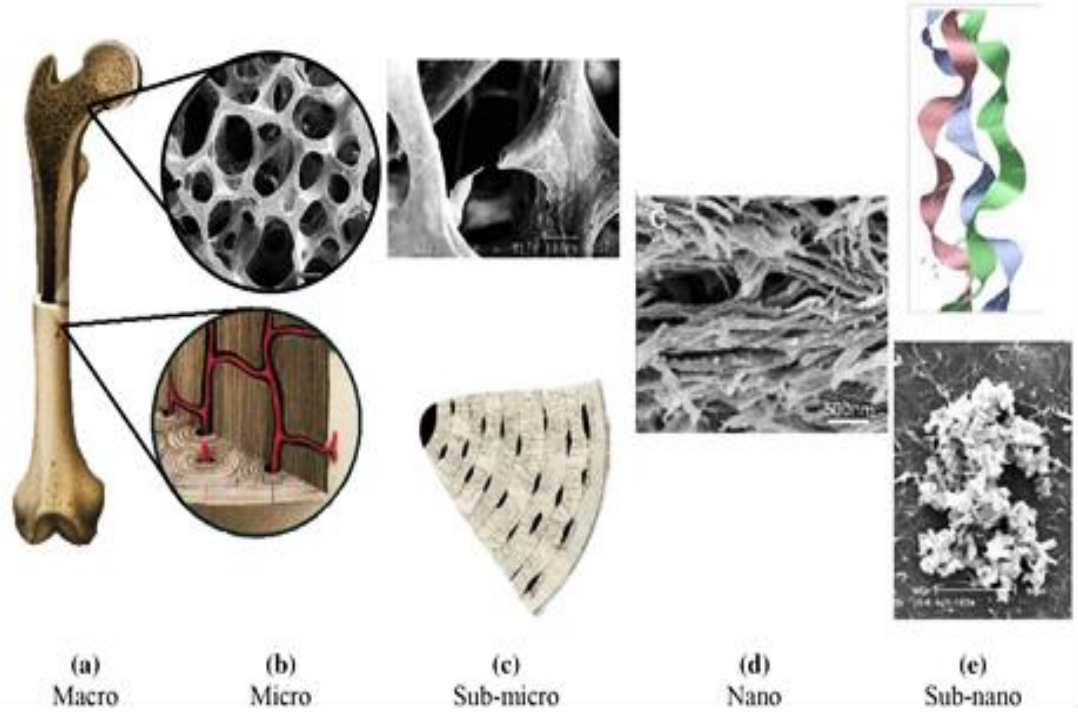

Fig. 2.5: The hierarchical structure of bone tissue (*Podshivalov et al., 2014*).

Groups of osteons and trabeculae at the microscale (10-500 µm) (*Fig. 2.5b*) are part of the hierarchical structure of bone shown in *Fig. 2.5*. Lamellae and trabecula combine to form this group structure at the sub-microscale (1-10 µm) (*Fig. 2.5c*), which is produced by fibrillary collagen, minerals, and non-collagenous organic proteins at the nanoscale (100 nm-1 µm) and sub-nanoscale (<100 nm) (*Fig. 2.5d & e*).

It is crucial to comprehend the form and characteristics of bone to build scaffolds that can replace it. Extra cellular matrix (ECM) and bone mineral make up the extremely intricate architecture of bones (*Zilberman et al., 2011*). Bones provide a variety of purposes, including as facilitating bodily movement, providing places for muscles to connect, and providing support for soft tissue (*Zilberman et al., 2011*). Bone may be characterized as a natural material composite with anisotropic properties and a seven-tiered organization (*Zilberman et al., 2011*). *Fig. 2.6* depicts a schematic representation of this organization, which is present in most body regions.

Cortical bone has an apparent density of 1.99 g/cm^3 (*Currey, 1999*), but cancellous bone has a much lower apparent density, often ranging from 0.05 to 1.0 g/cm^3 (*Keaveny, 2002*). The entire volume of cancellous bone that is not occupied by bone tissue and is generally filled with marrow is referred to as its porosity. Although the difference between the two bone tissues is difficult for porosities less than 50%, the transition from compact to cancellous bone is typically evident and occurs over a short distance. The cortical region makes up 80% of bone, whereas the remaining 20% is made up of the cancellous or spongy trabecular region (*Zilberman et al., 2011*). Due to these various locations, the elastic modulus for bone varies between 4 GPa and 30 GPa (*Choi et al., 1990; Wang et al., 2006 and Elias et al., 2008*). The cancellous area is referred to as "a porous network of connecting rods or plates," whereas the cortical region can be regarded as a thick solid (*Gibson et al., 1985*). The percentage of cancellous bone differs amongst living organisms. For example, birds flying in the sky have a higher proportion of cancellous bone than creatures crawling on the ground (*Nakajima, 2007*). Histological examination of the tissue's microstructure reveals the distinction between cortical and cancellous bone. Cortical bone is distinguished by uniform, cylindrically formed lamellae, whereas cancellous bone can be distinguished by non-uniform, wavy convolutions of lamellae. Moreover, cancellous bone tissue is metabolically active and may be reshaped more often than cortical bone tissue (*Rho et al., 1995*).

As depicted in *Fig. 2.6*, bone porosity is defined by small pores of canaliculi and smaller lacumae, as well as bigger pores of osteons and Volksmann's canals. The smaller canaliculi and vascular channels in typical cortical bone range in size from 1 to 5 μm (*Ascenzi and Bonucci, 1976*). Moreover, bone is a calcium reservoir in the body, storing 99% of the body's calcium. The majority of bone mineral is hydroxyapatite ($Ca_{10}(PO_4)_6(OH)_2$). Carbonate ions are used as replacement groups in the phosphate and hydroxyl sites of biological hydroxyapatite. The effective implantation of bone scaffolds requires not only biological criteria but also enough mechanical strength. The interaction of bone with other bones, joints, or muscles in the body defines its mechanical properties. Yet, the overall shape of the bone and tissue distribution promotes mechanical strength of the structure. Bone is primarily an anisotropic material, and its mechanical characteristics vary depending on anatomical position and loading direction. The modulus also varies greatly between the longitudinal and transverse orientations (*Rho et al., 1995*).

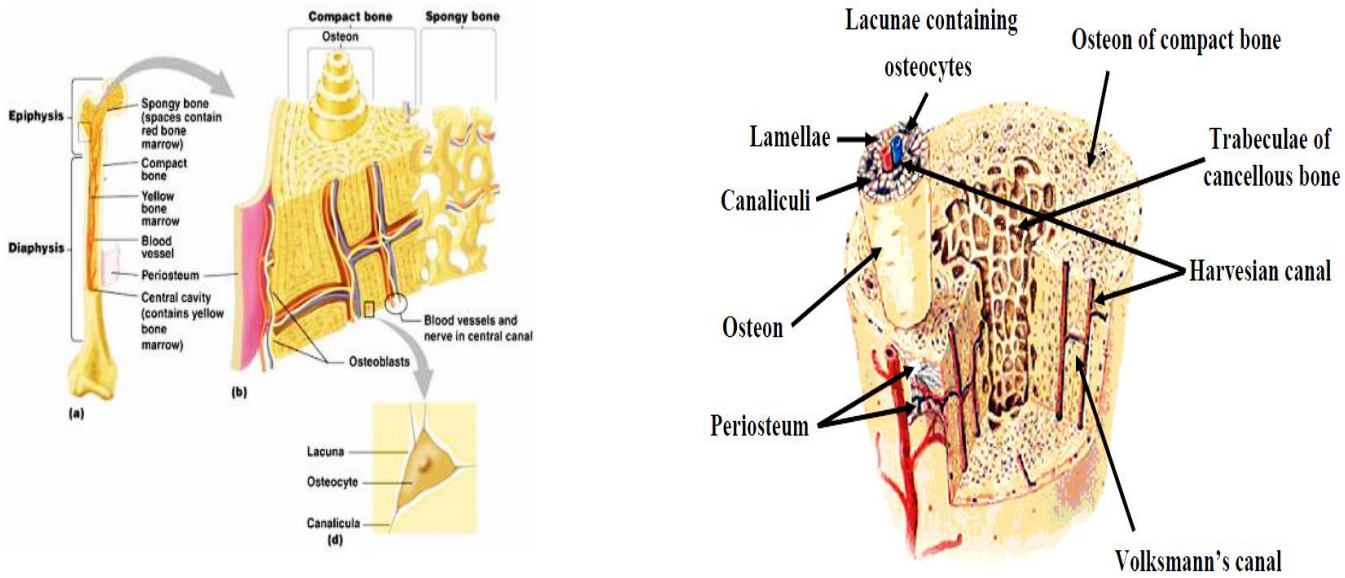

Fig. 2.6: Bone Structure (*Zilberman et al., 2011*).

As a result, cancellous bone has substantially wider mechanical characteristics than cortical bone. The trabeculae of cancellous bone follow stress lines and may be realigned by variations in stress direction. The compression strength is claimed to be between 2 and 5 MPa, while the elastic modulus is between 0.76 and 4 GPa (*Veiseh and Edmondson, 2003*).

Wang et al. (2013) measured the elastic modulus in the longitudinal and transverse directions of a dry cancellous bovine bone to be 20 ± 2 GPa and 14.7 ± 1.9 GPa respectively.

Fig. 2.7 illustrates this permeable network. Their relative densities, or the volume ratio of solids, explain the difference between these two locations. Cortical bone has a density more than 70%, while cancellous bone has a relative density of less than 70% (*Zilberman et al., 2011*).

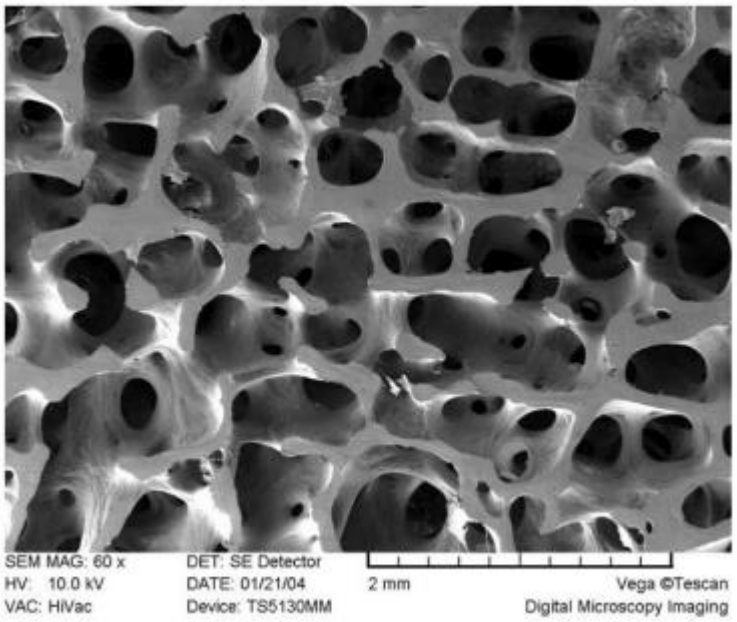

Fig. 2.7: SEM of 22-Year Old Male Human Bone (*Hansma, 2004*).

2.7.1 Macro and microstructures

2.7.1.1 Trabecular bone

Long bones like the femur and tibia have trabecular bone on both ends, as well as flat bones like the sternum, pelvis, and vertebrae. Trabecular bone resembles cortical bone in appearance, but it contains less hydroxyapatite, collagen, water, and other proteins. As a result, trabecular bone is a complex anisotropic material with different tension, compression, and shear strengths than trabecular and cortical bone. Variations in this composition as a function of age and sickness generate differences in mechanical qualities (*Keaveny et al., 2002*).

Trabeculae are thin rods and plates that create highly anisotropic and heterogenic materials at the microscale in spongy trabecular bone. These trabeculae are arranged in semiregular 3D patterns with interconnected open–porous networks, and they resemble a cellular solid material macroscopically. The porous networks inside the trabecular bones improve metabolite and nutrient transport. Bone marrow and cells within pores assist bone formation (*Keaveny et al., 2001*). Trabeculae have an average thickness of 300 μm and a pore size of 800 μm (*Hildebrand et al., 1999*).

The architecture of trabecular bone varies depending on anatomical location. The architecture of spinal bone, for example, is created by rod-like pieces, but the femoral head, as shown in *Fig. 2.8*, has a plate-like structure. The architecture of multiple locations on the same bone may change in response to the magnitude and direction of mechanical stimulation. Low-stress zones have rod-like trabecular structures, whereas high-stress areas have plate-like trabecular structures. This variability suggests that the design of the trabecular structure is compatible with its mechanical capabilities. According to *Ding et al*. (2002), the plate-like structure has higher strength than the rod-like structure.

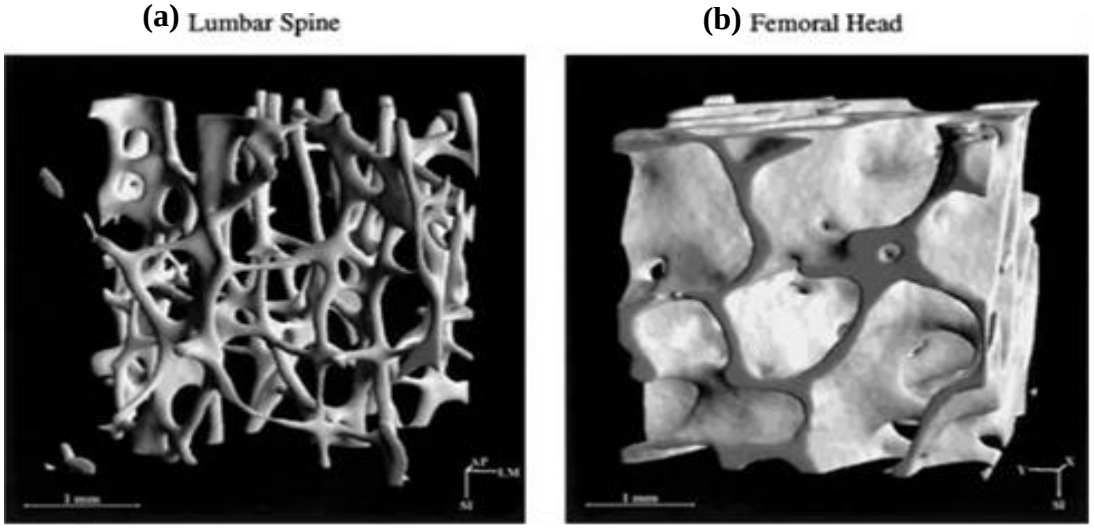

Fig. 2.8: Bone architecture fabricated with additive manufacturing techniques:
(a) rod-like specimen from lumbar spine; (b) plate-like specimen from femur (*Hildebrand et al., 1999*).

In conclusion, the mechanical characteristics of trabecular bone are determined by its volume fraction, architecture, and the material qualities of local trabecular tissue. The

trabecular bone structure is now widely acknowledged as the outcome of load adaptive bone remodeling. Understanding features like elastic modulus and failure qualities is crucial for creating novel applications and assessing the impacts of pharmacological therapy, ageing, and illnesses at the tissue level (*Bayraktar et al., 2004*).

2.7.1.2 Cortical bone

The cortex or shell of most bones is made up of cortical bone, which accounts for around 80% of the weight of the human skeleton. Cortical bone has three major functions: (a) supporting the entire body, (b) safeguarding the organs, and (c) storing and releasing chemical components like calcium. Cortical bone, like trabecular bone, has a complex and dynamic microstructure that adjusts over time.

The fundamental morphological and functional unit of cortical bone is the osteon. This primary functional unit of cortical bone has a cylindrical shape at the microscale, with a length of several millimeters and a diameter of around 200 m (*Deuerling et al., 2009*). The osteon is made up of concentric layers called as lamellae that surround the central canal. Because the modulus of elasticity and hardness of the osteon diminish from the centre to the boundary, it has anisotropic qualities like trabecular bones.

2.7.2 Sub-microstructure

2.7.2.1 Lamella

Trabeculae and osteons are formed through the creation of lamellae, which are thin plate-like structures that are very near to one another and have an open space between them. Collagen fibrils are reinforced with apatite crystals to produce a lamella at this structural level (*Fig. 2.9*). The lamellae are aligned in different orientations at the higher structural level to generate either osteons in cortical bone or trabeculae in trabecular bone.

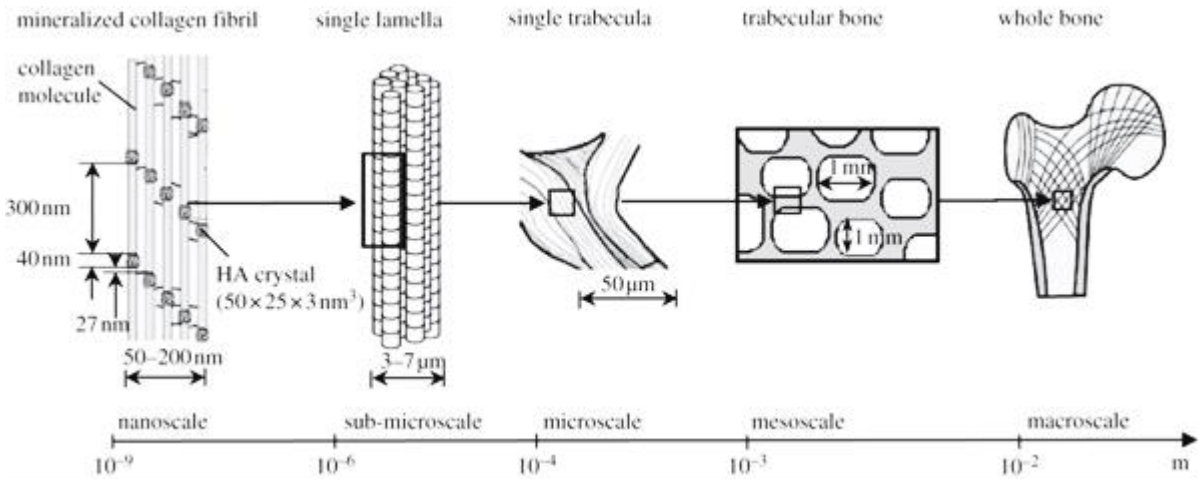

Fig. 2.9: The figure depicts the composite layer's trabeculae-building lamella structure (*Hamed et al., 2012*).

2.7.3 Nanostructure

2.7.3.1 Collagen fibrils and apatite crystals

Although the basic building parts of bone, mineralized collagen fibrils, are generated using the same ingredients, the whole hierarchical structure of bone is exceedingly complicated and changeable. Cross linked collagen molecules, hydroxyapatite, water, and a minor number of non-collagenous proteins make up the collagen fibril (*Giraud et al., 2005; Hamed et al., 2012*). Each fibril is made up of a number of micro-fibrils, which are sub-nanoscale helical assemblages of tropo-collagen molecules.

Bone is a composite material made up mostly of hard hydroxyapatite-like mineral particles buried in a nanoscale elastic matrix made up of collagen fibres. Bones have anisotropic qualities because to the anisotropic shape of mineral particles. The presence of collagen fibres in the bone matrix gives it its viscoelasticity. The fixation of implant materials can be influenced by the anisotropy and viscoelasticity of cortical bone.

Understanding bone shapes and qualities is essential for developing bone replaced materials for bone replacement surgeries, as well as enhancing the design and function of bone implants like the total hip arthroplasty (THA) femoral prosthesis (*Muderis et al., 2011*).

2.7.4 Bone adaptive remodeling

The adaptive process of bone density in response to mechanical forces acting on the bone is known as bone adaptive remodeling (*Rho et al., 1995*). Based on the concept known as Wolff's law, peri-implant bone stress shielding (*Figure 2.10*) causes an implant to loosen due to bone shrinkage in the absence of an appropriate mechanical stimulation (*Schmidt et al., 2003*).

The amount of stress shielding is determined by the implant's size, design, and elastic modulus. Despite the fact that current cementless stems attempt to maximize proximal load transfer via metaphyseal fixation, both cortical and cancellous bone density might diminish in the metaphysis, necessitating revision surgery in the long run (*Pitto et al., 2010*). Cementless femoral stems are most typically made of cobalt–chromium–molybdenum (Co-Cr-Mo) alloys and titanium–aluminum–vanadium (Ti-4Al-6V) alloys. The elastic modulus of titanium alloys is closer to the human bones than that of cobalt–chromium alloys; Co-Cr-Mo has a stronger wear resistance than Ti-4Al-6V (*Takaichi et al., 2013*). As a result, Co-Cr-Mo is often utilized for bearing surfaces, while Ti-4Al-6V is preferred for the stem component, where osseointegration (*Albrektsson and Johansson, 2001*) is desired.

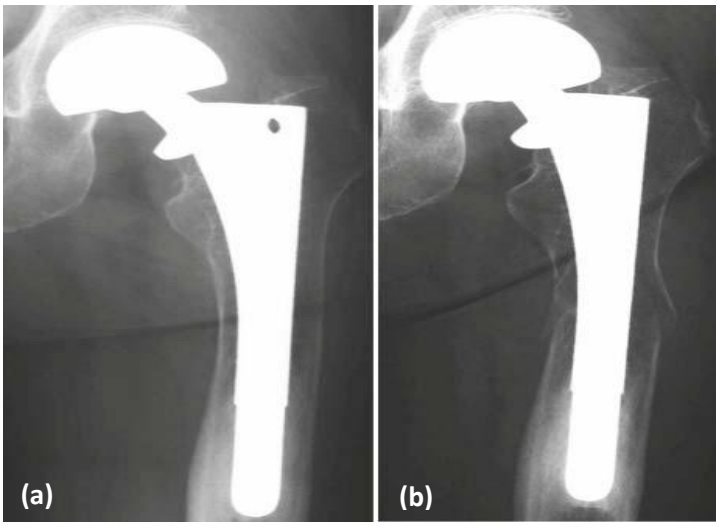

Fig. 2.10: (a) Severe metaphyseal stress shielding after total hip arthroplasty, and (b) Periprosthetic fracture following the implant loosening (*Yamada et al., 2009*).

Ti-4Al-6V should provide less stress shielding than Co-Cr-Mo, according to a finite element study that demonstrates a direct relationship between stem stiffness and the amount of stress shielding. According to *Krishna et al.* (2007), the metaphyseal stress shielding still takes place, however the modulus value of Ti-4Al-6V is still greater than the 17 GPa in cortical bone or around 15 to 25 GPa depending on age, sex, and preparation methods. Since porous structures have a lower rigidity than solid metals, using them or functionally graded materials may lessen the effect of bone adaptive remodeling. Bone is a unique material because of the intricate hierarchical structure that governs many of its mechanical characteristics. The issue for engineers is to connect the multiscale structure of bone to the implant (*Ghanbari et al., 2009*). A porous implant is advantageous because the adaptive remodeling of the peri-implant bone is less affected by it and the pore features also encourage cell proliferation. Since tissues differ, it is challenging to precisely recreate the microstructure of bone. Theoretically, lattice structures with linked pore networks or cellular structures may be replicated using simple structures as opposed to constructing the microstructure of bone.

2.7.5 Cellular structures

Cellular structures are porous materials that are made up of an interconnected network of solid struts or plates that are put together to form a lightweight porous structure (*Gibson, 1989*). Natural materials with a cellular structure abound, including cortical and cancellous bones. It's challenging to perfectly duplicate bone characteristics because bone tissues and synthetic materials have distinct material orientations at the nano and sub-microscales (*Podshivalov et al., 2014*). Although cellular metals and bone appear to have identical morphological parameters, the mechanical characteristics of the porous metals and bones (*Fig. 2.11*) differ significantly due to differences in the composite materials and hierarchical structures of bone and engineered materials (*Guillén et al., 2011*).

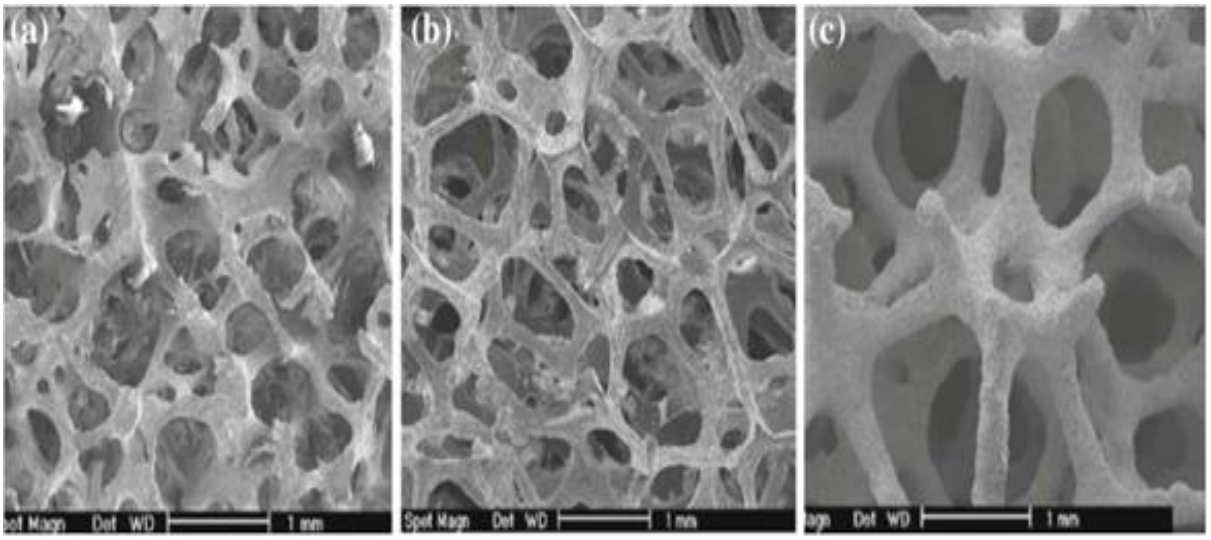

Fig. 2.11: Micro-CT images of bovine cancellous bone (a & b) and three open-cell metallic foams (c) showing similar morphology (*Guillén et al., 2011*).

Because of the high computing costs, predicting the mechanical characteristics of bone morphology-like structures is challenging. Most studies prefer to assess bone trabecular structures as 3D cellular structures to address the limitations associated with large-scale finite element models (*Oxnard, 2004*).

Researchers have concentrated on the basic and regular cellular structures of polyhedra to duplicate the functions of the substituted bones (*Leong et al., 2003; Liulan et al., 2007; Loh et al., 2013 and Van Cleynenbreugel et al., 2002*). To optimize both biological and mechanical performance, these functions require appropriate porosity, pore size, and other characteristics. It is thus vital to characterize the biological, mechanical, and permeability performance of the various constituent components that make up the bone scaffolds (*Bidan et al., 2013; Loh et al., 2013*).

Using computer-aided approaches, elemental units with capabilities similar to bone tissue may be designed and assessed. The following part examines cellular structure methodologies and designs, as well as knowledge gaps in cellular structure design for bone implants.

2.7.6 Computer-aided design-based methods.

Constructive solid geometry (CSG) and boundary representation (B-Rep) are two solid or surface modelling techniques used in commercial computer-aided design (CAD) software. CSG-based models are created using the first technique, which involves marrying the representation of solid primitives using Boolean operations. This method allows for the creation of cellular structures with no dangling edges. CSG algorithms, on the other hand, are frequently limited to simple geometric designs of solid primitives (*Chua et al., 2011*).

The second model, which is based on B-Rep, is characterized by its boundaries, which are made up of a collection of vertices, edges, and loops with no connections between them. Thus, in the B-Rep model, an object consists of an object's faces, edges, and vertices coupled in such a way that the model's topological consistency is maintained. Euler procedures are used to create this topology, while Euclidean computations are used to create the geometry. Euler operations, like Boolean operations in CSG models, are used to generate, alter, and edit the faces, edges, and vertices of a B-Rep model. Using Euler operations, a preliminary assessment of gaps and overlaps between the borders of B-Rep models may be validated (*Giannitelli et al., 2014*).

These two strategies have both advantages and downsides. B-Rep models take up more storage space than CSG models, but they take less time to compute. As a result, when using the B-Rep approach to simulate sophisticated small-scale internal architecture, massive storage data is unavoidable. Topology creation using the B-Rep model is considered nongraphical relational information that is maintained in solid model databases and is not accessible to users; as a result, seeing and manipulating the underlying architecture of the primitives might be difficult or impossible (*Giannitelli et al., 2014*).

2.7.7 Unit block approach

Identification of the fundamental components is necessary for CAD modelling utilizing CSG approaches (primitives or unit blocks). Polyhedral objects are the chosen building blocks in biomedical engineering applications. The connections between planar faces, linear edges, and vertices make up a polyhedron (plane faced polyhedron) (*Cheah et al., 2004*).

Unit blocks can be created in two different ways. The second technique builds a geometric regular polyhedron as a cellular model, while the first way creates a solid geometry as an inclusion of vacant spaces (*Wettergreen et al., 2005*). A solid that fills up space, such a sphere or cube, constitutes the first form of building (*Fig. 2.12*).

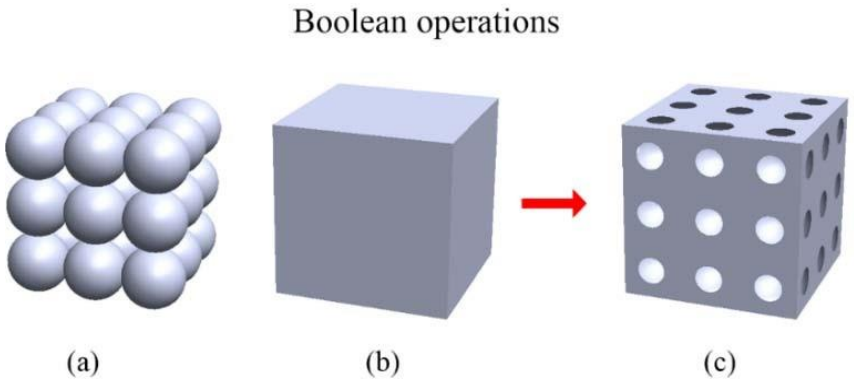

Fig. 2.12: (a) Space-filling units in the form of spheres, (b) overlaid onto a solid structure, and (c) created using standard Boolean operations, resulting in a void structure with the appropriate geometry.

Standard Boolean operations result in a hollow or shelled structure with the desired shape when a void structure is superimposed upon a solid structure (*Sudarmadji et al., 2012*). The proportion of the solid volume to the envelope volume provides information on the porosity of these solid designs. As a result, by altering the volume of the void pieces, space-filling solid designs may have their porosity set to the desired value.

The second technique uses the Archimedean and Platonic solids as a collection of geometric polyhedral in a wire-frame or lattice construction (*Cromwell, 1997*). These polyhedral are advantageous because they may exhibit the appropriate symmetry since they are regular (i.e., both equiangular and equilateral). In contrast to space-filling solids, which represent solid volumes, this model is originally utilized as a volumetric representation to describe the porosity.

Each edge of a polyhedron is transformed to a beam of the equivalent length to generate the open-porous unit components. The thickness of each equilateral beam is the same. The ratio of the total of the beam volumes to the envelope volume of a bounding box

yields information on the porosity of these structures. By changing the unit dimension and/or beam thickness until the desired value is reached, the porosity may be changed.

2.7.8 Computer-aided system for porous scaffolds

The drawback of manually developing and putting together unit cells is that it takes time. *Chua et al.* (2003) and *Cheah et al.* (2004) created an algorithm to automatically build the necessary shape. The user may enter design parameters into this method, also known as the computer-aided system for porous scaffolds (CASPS), and a function will automatically determine the fundamental characteristics, such as void sizes, porosities, and surface area to volume ratio. As only a few structural factors need to be changed, it is simple to create or alter polymeric models. The computer will then modify its internal structures to conform to the required geometry.

But computer-aided systems for porous scaffolds do a terrible job of reproducing intricate porous things, especially bone structures. Computer-aided systems are unable to manage the structures that exhibit graded microstructural morphology as a consequence of automatically processing operations of specialized subroutines.

2.7.9 Influence of unit architecture

Bone scaffold micro-architectures may be created using CAD-based unit cells, which are often derived from simple geometries like polyhedral unit cells. In essence, polyhedral structures are convex, and because of this, CAD modelling can be done with relative ease. The unit cells are duplicated, and their faces are merged with those of the neighboring unit cells to complete the assembly process. *Fig. 2.13* displays some instances of polyhedral unit cells that can be utilized to build scaffolds.

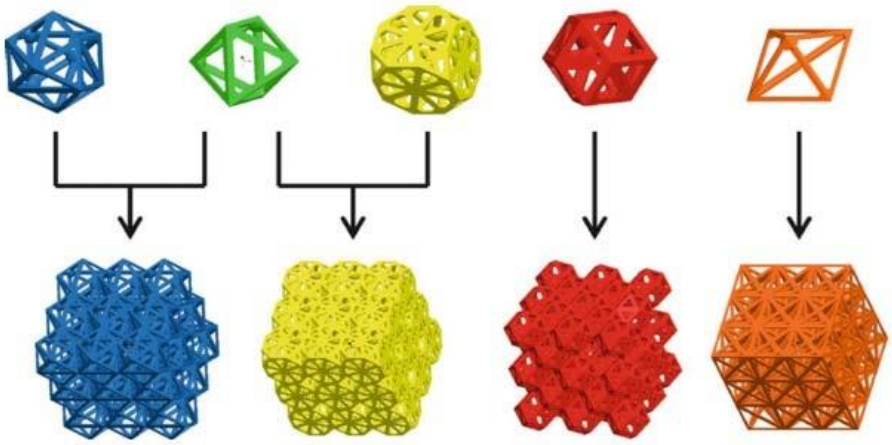

Fig. 2.13: scaffold blocks created by merging polyhedral unit cells (*Sudarmadji et al., 2012*).

Building blocks made of polyhedral material were put through mechanical testing to demonstrate how varied material arrangements or structures may provide variable mechanical properties in architectures that shared the same volume of material (*Tarawneh et al., 2012*). Because of this, the wireframe structure of the unit cells affects how the mechanical performance of such cellular structures with diverse topologies behaves.

2.7.10 Porous biomimetic scaffolds for bone tissue engineering

For bone tissue implants, the material must not only have the right composition but also have a solid structure that closely resembles the structure and mechanical characteristics of bone. There are significant issues with the use of bulk (dense) metallic implants in the human body, despite significant advancements in their manufacture for orthopedic purposes. The biomechanical stiffness mismatch between the implant and bone and the micro-motion of the implants as a result of insufficient initial fixation with host tissue are two important issues (*Robertson et al., 1976 and Ryan et al., 2006*). Because of this, there is no mechanical stress on the bone around the implant, which might cause harmful bone resorption (*Turner et al., 1986; Breme and Helsen, 1998a; Thieme et al., 2001*). For this case, the implant becomes loose because the bone that is keeping it in place weakens. In developing the material and structure of orthopedic implants, any strategy to address the issues posed in providing a suitable load transfer and bone anchoring is crucial.

A new class of materials called as porous materials has recently received a lot of interest. Porous materials can be used to substitute bone since bone is a porous tissue substance, which makes physiological sense. When pores are added to a material's structure, the stiffness values are reduced to levels that are comparable to those of natural bone, which can help with load transmission and encourage the growth of new bones (*Griss and Heimke, 1976*). Moreover, the porosity enables for the growth of new bone tissue into the porous structure, offering a sufficient biological fixation. *Fig. 2.14* shows how bone may grow into an implant's open holes to form a complex interface.

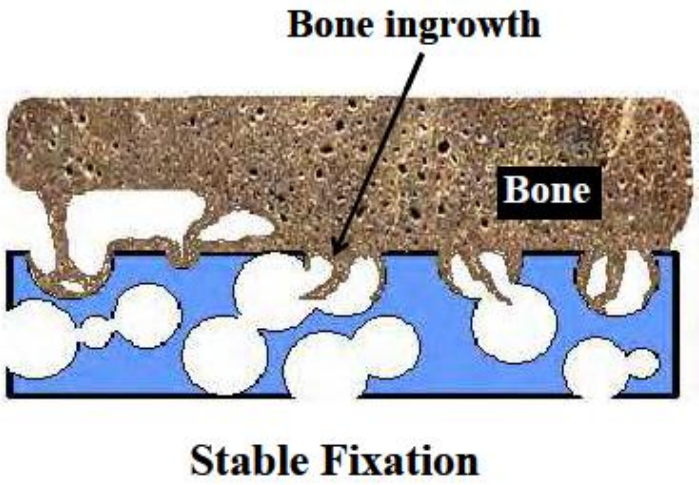

Fig. 2.14: An orthopedic porous scaffold's bone ingrowth into the pores serving as a stable fixing (*Nouri, 2010*).

Porous materials are also thought of as a desirable substitute for bone cement fixing because of their ability to anchor in bone (*Oliveira et al., 2002*). For example, porous ceramic, polymeric, and metallic materials have all been created over the previous three decades. Ceramic materials have great biocompatibility and corrosion resistance, yet they are intrinsically fragile and rapidly break (*Breme and Helsen, 1998b; Rush, 2005*). Similar to how porous polymeric materials can't withstand the mechanical pressures used in joint replacement surgery. In order to find porous metal scaffolds with the right mechanical characteristics for load-bearing applications, researchers are motivated by this (*Breme and Helsen, 1998b*). Strength, stiffness, durability, and biocompatibility are just a few of the qualities that porous Ti scaffolds have, which are also necessary for orthopedic and dental applications.

2.7.10.1 Effects of bone formation on bone tissue scaffolds

It has been suggested that porous cellular architectures can provide adequate microenvironments for mechanical support, physical stimulation, and biochemical inputs for optimal cell development and function while also reducing stiffness (*Hollister, 2005; Inglam et al., 2013 and Tarala et al., 2011*). The mechanical and biological functions of biomedical applications are significantly influenced by the porosity and pore size of cellular materials. Cell nourishment, growth, and movement that lead to tissue blood vessel formation and bone cell production rely on interconnected and porous networks, according to *Hollister* (2005). Additionally, a porous surface aids in the mechanical interlocking of the implant's supporting components with the surrounding bone (*Karageorgiou et al., 2005*). The capacity to effectively transport and exchange bio-factors like proteins, genes, cells, or excellent substrates across this network is another advantage of the linked porosity network, which allows for the guidance and promotion of the development of new tissues.

The essential conditions for bone ingrowth are well known. On biomaterial implants, both in vitro and in vivo, porosity and pore size are crucial for bone development (*Karageorgiou et al., 2005*). Open cellular structures could be the best type of structure for promoting cell activity and reducing the stiffness of metal implants with internal voids. The intricate porous structural model might be produced utilising CAD and AM technology.

2.8 DENSITY AND POROSITY

For the purpose of estimating permeability and mechanical characteristics, a porous metal's density is a crucial factor. The extent to which bone may penetrate and grow into a porous material is known as its permeability (*Despois and Mortensen, 2005*). The mechanical strength is decreased, and the permeability is raised by increasing the porosity (*Eisenmann, 1983*). Yet, a compromise between these two factors needs to be reached to produce an implant that is appropriate for orthopaedic purposes.

The term "relative density" is frequently used in the field of porous metals to define porous materials. It is the proportion of porous metal's density to that of its parent metal. The volume percentage of metal and pores affects the relative density of porous metals. Most porous metal scaffolds have relative densities of less than 0.3 (*Gibson and Ashby, 1982; Kriszt et al., 2002*).

The material must be at least 60% porous to promote the formation of new bone tissue within the pores (*Bram et al., 2006*). Similarly, a minimum porosity of 55% was observed for direct connection of macropores in research by *Esen and Bor* (2007). These levels of porosity would result in a networked porous structure that encourages vascularization, metabolic product movement, and cell ingrowth into the porous area. Porosity is another factor that is thought to be important for biocompatibility. In an experiment conducted by *Tuchinskiy and Loutfy* (2003), mice were implanted with two materials that had identical chemical compositions but varying porosities for up to four weeks. The less porous material was enclosed in a dense, heavily collagenous sack with few blood arteries flowing through it, which elicited a more pronounced foreign body reaction. As a result, the more porous substance had a thinner sac with significantly higher vascularity.

2.9 SHAPE AND SIZE OF PORES

The right pore size must be offered to promote bone growth into porous material. For bone ingrowth to occur, the pore size must be at least on par with bone trabeculae and osteons, which are tens of micrometres thick (*Jasty et al., 1995*).

The ideal pore size for human usage hasn't yet been precisely determined. *Elema et al.* (1990) suggested that the pore size should be at least 200 - 300 µm for bone tissue in growth in the porous materials, but *Pilliar* (1987) claimed that the pore size suited for bone ingrowth is in the range of 75-250 µm. Implants with pore diameters between 100 and 500 µm are appropriate for bone ingrowth (*Engh, 1992; Hungerford and Kenna, 1983 and Laptev et al., 2004*). Pore sizes between 500 µm and a millimetre would more closely resemble a macro-structured surface than a 3D interconnected porous surface, which might hypothetically result in a reduction in interface shear strength (*Jasty et al., 1995*). There have also been theories that new bone production depends more on the degree of interconnectivity than on the actual pore size (*Kuhne et al., 1994; Lu et al., 1999*).

For the implant to be properly fixed and remodelled with the surrounding tissue, the porous structure of the alloys is essential (*Zhang et al., 2007*). This is because it promotes bone tissue formation. *Ayers et al.* (1999) addressed the issue that there does not appear to be a relationship between pore size and bone ingrowth during the cartilaginous phase of bone growth in the NiTi implant. This phenomenon is explained by the utilisation of thin implants that are arranged in thickness order according to pore size.

The degree of cell ingrowth appears to be influenced by the form of the pores in addition to their size. According to *Goodman et al.* (1993), square-shaped pores promote more bone ingrowth than circular ones. Moreover, bigger surface areas for bone ingrowth are provided by pores with more ragged and rough surfaces (*Li et al., 2015*). Yet, the same pore shape may not be optimal for all conceivable purposes due to the diverse functions and locations of the bones in the human body (*Oh et al., 2003*). According to reports, additional variables may also affect how quickly bones grow into the pores. The bone ingrowth rate is greater in portions put in cancellous bone than in cortical bone, according to research by *Bobyn et al.* (1980). *Clemow et al.* (2004) found that the square root of pore size was inversely linked to the percentage of bone developing into the surface.

2.10 PROPERTIES OF HUMAN BONES

As shown in *Fig. 2.15*, human bone has an intricate hierarchical structure composed of multiple strata: macro level (overall shape of bone includes cortical and cancellous bone), micro level (e.g., haversian systems, osteons, single trabecular), fine micro level (e.g., lamellae), sub-micro level (e.g., fibrillar collagen and embedded mineral), sub-micro level (e.g., fibrillar collagen and embedded mineral), micro level (*Wang et al., 2016*).

As a result, human bone is prone to shattering under high loading conditions, which may arise because of an unintentional injury or because of density loss over time. The cortical bone's UTS and E are much greater than the cancellous bone's (*Singh et al., 2017*). Bending or torsion causes tensile and compressive stresses on the cortical bone (*Nishiyama et al., 2018*). Because the tensile strength of the bone is lower than its compressive strength, failure occurs in the area under severe tensile stress (*Johannesdottir et al., 2018*). The mechanical characteristics of various human bones of various age groups are summarised in *Table 2.1*. Porous structured implants are designed to mimic a variety of qualities. The mechanical characteristics of trabecular bone are influenced by the architectural arrangement of individual trabeculae as well as its porosity (*Ralston, 2013 and 2017*).

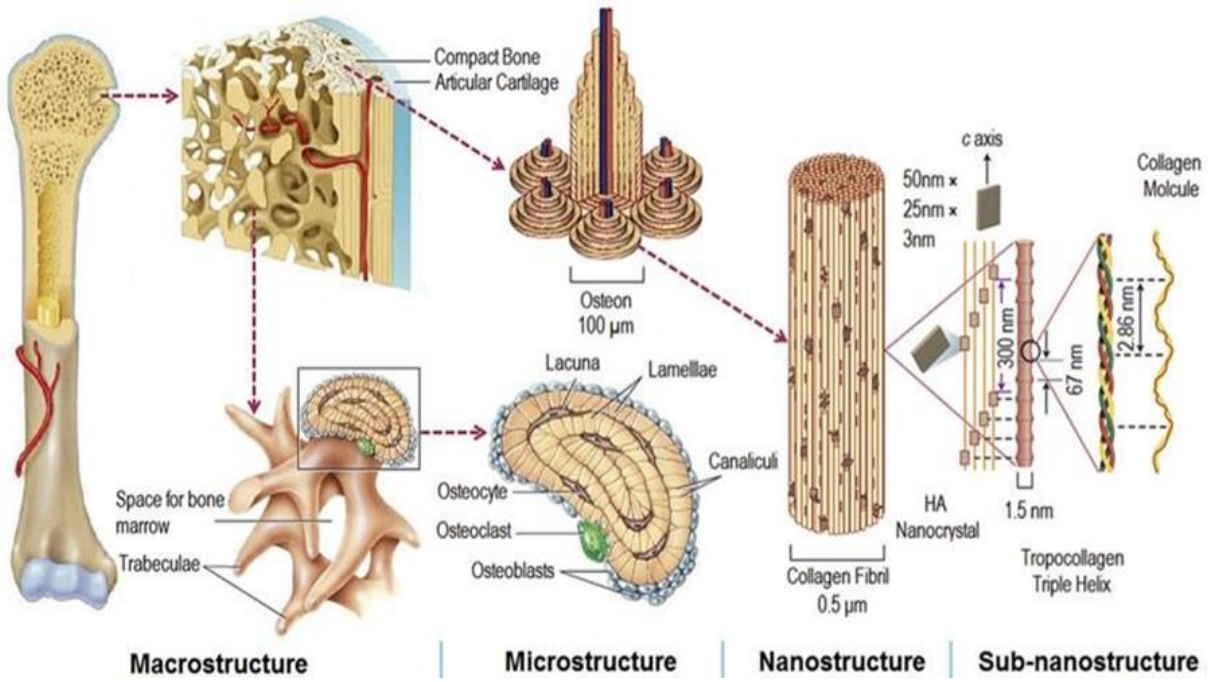

Fig. 2.15: Hierarchical structure of human bone (*Li et al., 2013*).

The mechanical characteristics of bone change with age, as seen in *Table 2.3*. The most essential properties for biomedical implants are UCS and E.

Table 2.3 - Mechanical properties of different human bones.

Sl. No.	**Bone Type**	**Age** (Range)	**TYS** (MPa)	**UTS** (MPa)	**UCS** (MPa)	**E** (GPa)	**G** (MPa)	**e** (%)	**Reference**
1	Femur	20-29	120	140	209	18.1± 2	3.58	3.40	*(Bank, 1960)*
2	Femur	30-39	120	136	209	18.6	3.58	3.40	*(Bank, 1960)*
3	Femur	40-49	121	-	200	18.7	3.70	-	*(Bank, 1960)*
4	Femur	41.5	-	102	-	14.9	-	1.32	*(Evans, 1976)*
5	Femur	50-59	111	131	192	18.2	3.23	2.80	*(Bank, 1960)*
6	Femur	60-69	112	129	179	15.9	3.10	2.25	*(Bank, 1960)*
7	Femur	70-79	111	129	190	18.0	3.17	2.25	*(Bank, 1960)*
8	Femur	80-89	104	120	180	15.4	3.17	2.24	*(Bank, 1960)*
9	Fibula	33	-	100	-	19.2	-	2.10	*(Evans, 1976)*
10	Fibula	59	-	80	-	15.2	-	1.19	*(Evans, 1976)*
11	Tibia	20-29	-	-	-	-	3.58	-	*(Bank, 1960)*

12	Tibia	30-39	-	-	213	35.3	3.58	-	*(Bank, 1960)*
13	Tibia	40-49	-	-	204	30.6	3.70	-	*(Bank, 1960)*
14	Tibia	41.5	-	106	-	18.9	-	1.76	*(Evans, 1976)*
15	Tibia	50-59	-	-	192	24.5	3.23	-	*(Bank, 1960)*
16	Tibia	60-69	-	-	183	25.1	3.10	-	*(Bank, 1960)*
17	Tibia	72	-	84	-	16.2	-	1.56	*(Evans, 1976)*
18	Tibia	70-79	-	-	183	26.7	3.17	-	*(Bank, 1960)*
19	Tibia	80-89	-	-	197	25.9	3.17	-	*(Bank, 1960)*

The tensile properties of cortical fibular and femoral bone deteriorate with age, whereas the tibia's tensile properties remain same, except for changes in ultimate strain.

UCS and E of human bone are averaged to be 190 MPa and 18.5 GPa respectively, according to *Table 2.3*. To minimize the stress shielding effect and extend the life of an implant without requiring revision surgery, the mechanical and biological characteristics of the implant should be comparable to those of the bone.

2.11 BIO-RELATED PROPERTIES

Materials for medical purposes must fulfil several requirements, and implants should be morphologically similar to bone structure and facilitate the creation of new bone tissue (osteogenesis). The essential components that must be considered are biocompatibility and biodegradability.

2.11.1 Non-toxicity and biocompatibility

A clinical-grade orthopedic implant must be extremely biocompatible and toxic-free in order to guarantee that cell activities are secure and beneficial. Metals substances used for implantation should not be harmful. A hazardous chemical compound or chemical combination can have negative effects on living cells and organisms. The presence of a toxin in a material is referred to as its toxicity (*Li YU*). Metals may be cytotoxic or hazardous, as can their derivatives. Most heavy metals pose a serious hazard to human life by harming organs and cells, including mercury (Hg), lead (Pb), and cadmium (Cd) (*Jaishankar et al*,

2014). The human body requires certain metals, including barium (Ba), chromium (Cr), iron (Fe), selenium (Se), beryllium (Be), cobalt (Co), lithium (Li), strontium (Sr), boron (B), copper (Cu), molybdenum (Mo), tungsten (W), cerium (Ce), iodine (I), nickel (Ni), and zinc (Zn) (*Chen et al, 2015*). Some necessary minerals can be hazardous in large doses, but (*Plum et al, 2010*).

Additionally, because metal complexes are susceptible to chemical breakdown in aquatic conditions, they may also pose health hazards (hydrolysis). Such chemicals may produce hazardous byproducts or leave behind intractable residues after a chemical reaction (*Egorova et al, 2017*). Instead of describing a straightforward attribute of a material, biocompatibility defines a complicated characteristic of a system between the substance and the biological host. A biocompatible substance should interact positively with live cells or tissues, promoting tissue integration, wound healing, and rebuilding.

Because of this, the meaning of the term "biocompatibility" has evolved from just meaning "non-toxic" to include "having a favourable impact on interacting with live cells and actively expressing new tissue" (*Williams, 2014*). Metal implants must be biocompatible to support the activities of cells and tissues. For instance, scaffolds in tissue engineering serve as a template for osteogenesis and their materials should be compatible with the main bone cells (osteoblasts, osteocytes, and osteoclasts) to promote the production, remodelling, and repair of new bone (*O'Brien, 2011; Little et al, 2011 and Terrier et al, 2017*).

2.11.2 Biodegradability for temporary implant materials

Most recently, the parameters for low elastic modulus, new bone tissue ingrowth, and vascularization capacity for implantation have been substantially satisfied by the manufacture of metal implants with an open-cellular structure utilizing modern additive manufacturing technology. Yet, there are still issues with implants' long-term instability. Particularly, metallic biomaterials like titanium and its alloys do not deteriorate over time, making them a permanent foreign object in the human body. As a result, bacterial infections, chronic endothelial dysfunction, ongoing physical irritability, and localized chronic inflammatory responses might impact a patient's quality of life (*Moravej et al, 2011*).

Medical implants composed of non-biodegradable substances, such as titanium alloys and stainless steels, can occasionally halt the normal development of bones, necessitating further surgery to assist future bone ingrowth. Hence, creating biodegradable (*Alishiri et al, 2016*) metals for use in implants may be a preferable answer to these issues. Eventually, the biodegradable implants will vanish and be replaced by freshly created tissues. For temporary medical implant applications such as bone fixation and vascular stents, biodegradability, also known as bio-absorbability, is taken into consideration. These implants often use alloys based on magnesium (Mg), iron (Fe), and zinc (Zn). With biodegradable implants, the rate of breakdown is crucial (*Wen P et al, 2018*). According to reports, among biodegradable metal compounds, the degradation of Zn-based alloys occurs at a rate of 20 to 300 µm/year in vitro (*Wen et al, 2001 and Katarivas et al, 2017*). In vitro, the deterioration rates of Mg-based alloys and Fe-based alloys, respectively, are typically higher than 300 µm/year and lower than 50 µm/year.

Over six months, *Bowen et al.* (2013) observed the corrosion behaviour of pure Zn wire used as cardiac stents in rats. According to their research, the stents' cross-sectional area decreased by an average of 20 µm/year during the first three months before more than doubling by the sixth. The biodegradable metallic materials created using additive manufacturing techniques also exhibit mechanical qualities suitable for implant applications during immersion testing. *Li et al.* (2018) created a Fe-based diamond lattice scaffold using selective laser melting (SLM). They discovered that the scaffold's mechanical characteristics were remained adequate for implant applications after a four-week immersion test, even though the samples' elastic modulus and yield strength had reduced by 7% and 5%, respectively.

2.12 CHARACTERISTICS OF A SUCCESSFUL Ti-6Al-4V IMPLANT

A successful porous metallic implant aids the healing of bone tissue at the wounded site (*Chen et al., 2017*). The characteristics of an excellent scaffold include biocompatibility (*Lin et al., 2018*), a good surface for cell attachment (*Pyka et al., 2012*), proliferation (*Douglas et al., 2018*), differentiation, and a highly porous pore network for cell ingrowth and to minimize mechanical failure, less or no stress shielding is also required (*Fig. 2.16*) (*Kadkhodapour et al., 2015*), which may be achieved by mechanical characteristics of

implants and surrounding tissues being comparable (*Krijger et al., 2017*). Furthermore, to avoid mechanical failure, anatomic loading criteria must be satisfied. *Frame et al., 2018* studied mechanical driven homeostasis, and mechanostat modeling demonstrated that bone adaptation stable structure is affected by loading magnitudes and directions. Pore size increases bone development, with a pore size of 600 micron showing to be the best rated value for SLM formulation of joint prosthesis surface structure (*Taniguchi et al., 2016*).

However, when porosity raises, static mechanical properties decrease, resulting in shorter fatigue lifetimes (*Yavari et al., 2014a and 2014b*). The relationship between compressive strength and porosities follows a linear pattern, apart from the impact of pore size distributions. *Douglas et al.* (2018) modified the surface of human bone marrow stem cells (HBMSCs) with A-ALP (apple derived alkaline phosphatase) and found that adhesion and proliferation of HBMSCs increased after 7 days, indicating that surface modification aided adhesion and proliferation (*Liu et al., 2004*). *Bobbert et al.* (2017) tested primitive, Gyroid, and diamond Ti-6Al-4V porous structures with pore sizes of 500, 600, 700, and 800 microns and found that SLM manufactured porous biomaterials have a balance between static and fatigue testing and resemble trabecular bone. To obtain great clinical outcomes, careful selection of porosity, pore size, and pore interconnectivity are thus key considerations for developing porous metallic implants (*Cools et al., 2018*).

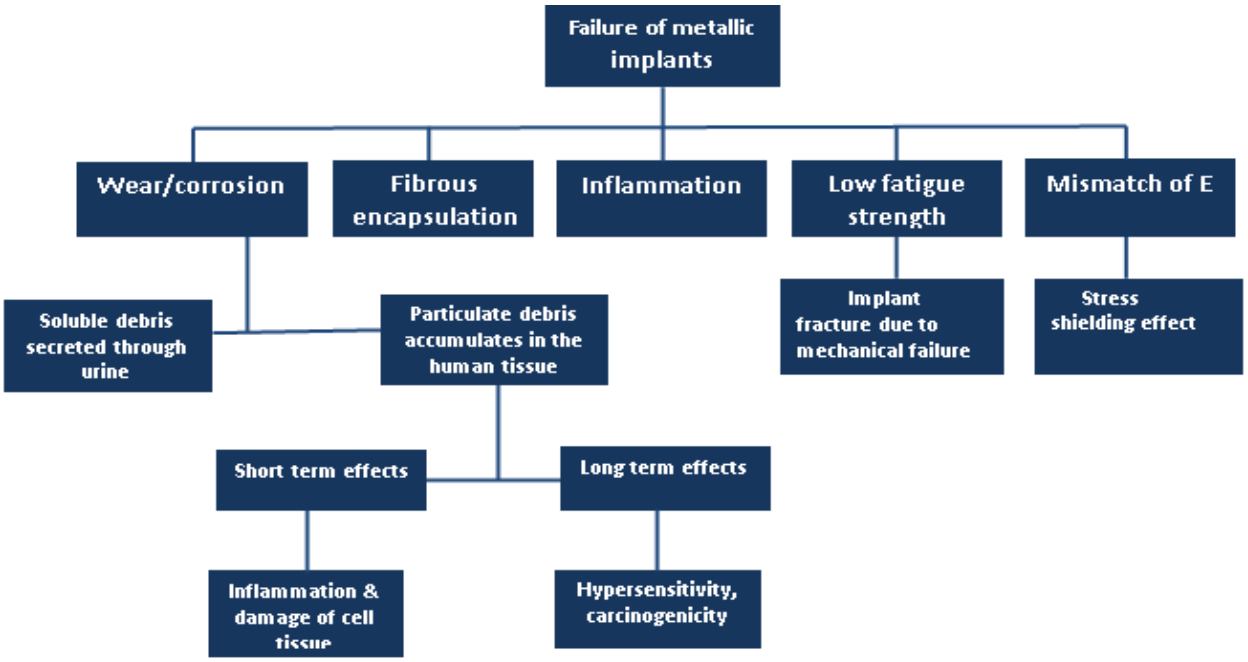

Fig. 2.16: Failure possibilities of bio-implant.

2.13 ADDITIVE MANUFACTURING (AM) TECHNIQUES

The production of intricate structures with accurate geometry by merging data supplied from CAD has substantially improved since the advent of additive manufacturing (AM) technology in the late 1980s. In the past, AM methods were applied to the manufacture of prototypes for creating new products. For the preparation of a final product, AM techniques have been developed to replace the time-consuming processing procedures of conventional prototype techniques, which require mould-making and casting phases. AM techniques may drastically reduce the amount of time needed to fabricate items, down to hours. The advancement of AM technology lowers the cost of production and enhances the characteristics of the parts produced. These additive manufacturing (AM) techniques may be used to produce finished products in small batches as well as prototypes quickly.

AM techniques refer to a range of solid freeform manufacturing methods that may create prototypes or finished goods with almost perfect shapes based on CAD models by employing a layer-by-layer build process. Because AM technologies can produce lightweight complex structures that are suited for bone tissue-engineered materials, they are currently utilized in the biomedical industry (*Melchels et al., 2010*).

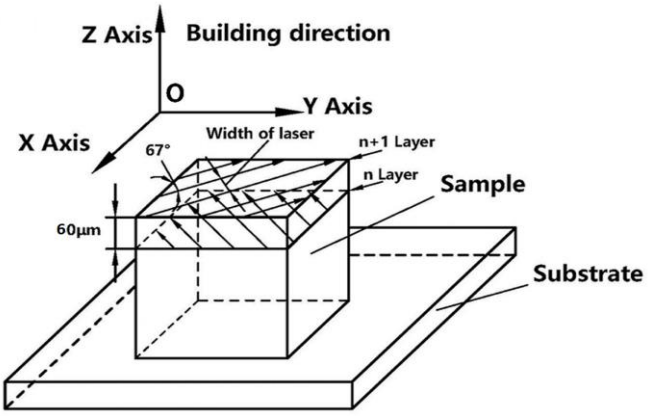

Fig. 2.17: SLM Manufacturing Process.

In general, CAD data are transformed into a sequence of two-dimensional cross-sectional layers and sent to process in all AM processes using a standard tessellation language type (STL) file format. The solid model is then treated, working its way up from the base

layer. According to the CAD model, each layer is adhered or bonded to the layer before it to create a solid object (*Fig. 2.17*).

In the recent decades, more than 20 AM systems have been created and put on the market. According to the processing ingredients, these stacking techniques may be divided into three groups: liquid-based, solid-based, and powder-based AM systems (*Peltola et al., 2008*).

Table 2.4 - Overview of AM processes employed in orthopedic applications.

	AM Processes			
	SLA	**FDM**	**3DP**	**SLS/SLM**
Principle	Photopolymerisation	Melt extrusion	Powder + binder deposition	Powder sintering/melting
Polymers	✔	✔	✔	✔
Ceramics	✔	✔	✔	✔
Metals	✘	✘	✘	✔
Hydrogels	✔	✔	✔	✘
Cells	✔	✔	✔	✘

Stereolithography (SLA) is a solid-based technique, whereas fused deposition modeling (FDM) is a liquid-based technology. As powder-based technologies, selective laser sintering (SLS), selective laser melting (SLM), and 3D printing (3DP) provide a range of material options, including metals, ceramics, and polymers. An Overview of additive manufacturing (AM) technologies used for biomedical applications is shown in *Table 2.4*.

2.13.1 Stereolithography (SLA)

The regulated photopolymerization of a liquid resin serves as the foundation to produce SLA techniques (*Fig. 2.18*). A computer-driven construction stage manages a laser beam or a

digital light projector. It creates a layer pattern on the resin's surface by shining an ultraviolet (UV) light there. This pattern's resin is hardened to a specific depth, which makes it stick to a layer or platform below it. The platform is lowered from the liquid surface after the first layer has been photopolymerized to allow the liquid resin to fill the subsequent created layer. The second layer is then used to cure the design.

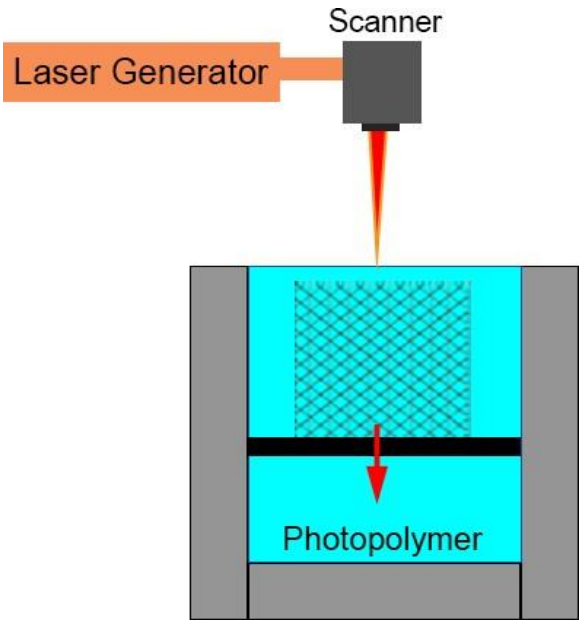

Fig. 2.18: Scheme of the SLA process.

In general, photopolymerization of printing techniques typically yields insufficient results, necessitating further post-curing with UV radiation to enhance the mechanical qualities of the structures (*Hutmacher et al., 2004*). The layer movement resolution of 1.3 mm and the laser spot size of 80 - 250 mm affect the quality of the SLA products (*Harris et al., 2004*).

It is necessary to manage the accuracy of each layer's thickness through complete curing of the material since the solidification of the liquid resin in proportion to the layer resolution is vital for bonding these patterns between connecting layers. The energy of the light that the resin is exposed to determines the cure depth for a certain resin. By choosing the right light source's power, scanning speed, and exposure duration, this energy may be managed. The actual polymerization process contains multifunctional monomers and is difficult to confirm, even though the kinetics of the curing processes (initiation, propagation, and termination) can be predicted analytically.

The difficulty in producing anatomical models for surgical planning due to shrinking of the treated products is a restriction of SLA fabrication in biomedical applications. Due to the laser beam's absorption and dispersion, this might result in noticeable distortion when producing tiny and complex shapes.

2.13.2 Selective laser sintering (SLS)

SLS processes employ a CO_2 laser beam to layer-by-layer sinter ceramic and polymeric powders to create solid three-dimensional objects (*Fig. 2.19*). A material powder is heated by the laser beam to a temperature that is slightly over the glass transition point, which causes the powder's particles to sinter and solidify into a mass. Then, a fresh layer of powder is applied by a roller, right on top of the top surface of the previously sintered layers, to create the following layers (*Paul et al., 1996*).

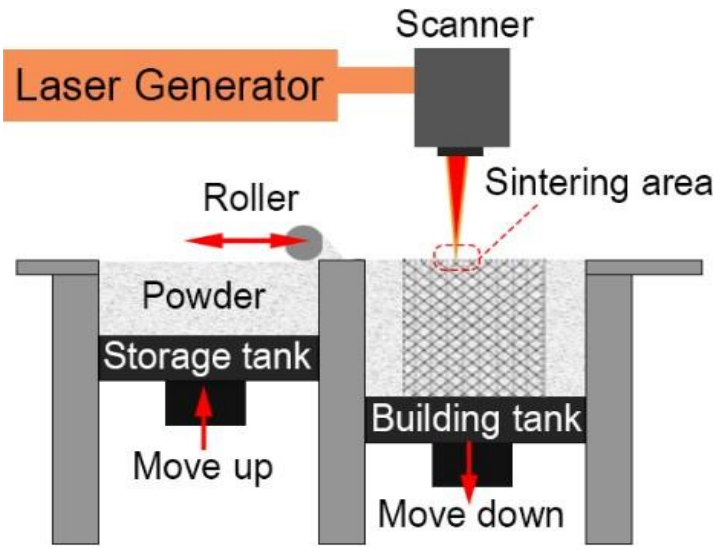

Fig. 2.19: Scheme of the SLS process.

SLS procedures are ideal for designing bone tissue structures manufactured with polymers, bio-ceramics, or composites since they are better able to create a precise geometry than SLA. Practically, SLS manufacturing requires powdered biomaterials that can fuse but do not disintegrate when exposed to a laser beam. Furthermore, unlike 3DP procedures, SLS does not call for the use of any organic solvent. This economical and successful technology is

therefore used for building scaffolds that include the intricate anatomical geometry of bone structures.

2.13.3 Fused deposition modeling (FDM)

A team of engineers and medical professionals from the National University of Singapore and National University Hospital used FDM to construct polycaprolactone (PCL) scaffolds. A hole in the skull has been patched using PCL scaffolds that have undergone FDM processing. In a way similar to that employed in other AM processes, the FDM operation is controlled by an extrusion head movement in a horizontal axis while the platform descends in a vertical plane at every new layer to construct scaffolds. The thermoplastic polymer, such as PCL, in a semi-liquid condition, is precisely extruded into position by the head. The substance that was extruded later solidifies and clings to the layer below. Because FDM requires connection during filament extrusion to build the item in each layer, it is limited to constructing solid pieces rather than extremely complicated bone structures (*Fig. 2.20*).

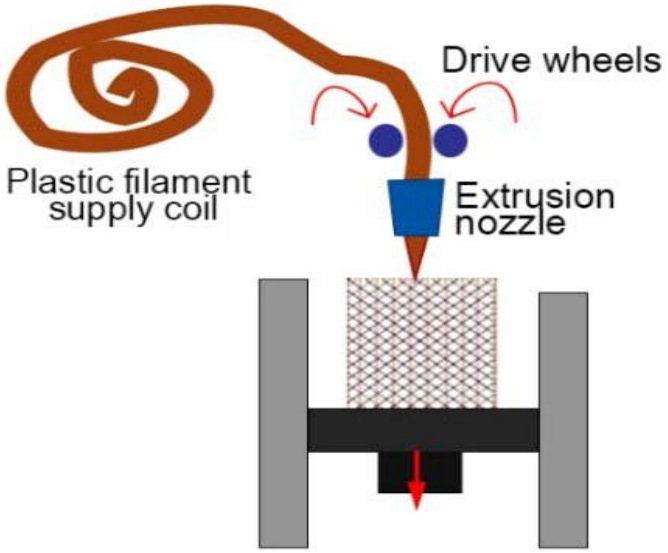

Fig. 2.20: Scheme of the FDM process.

2.13.4 Three-dimensional printing (3DP)

The method uses standard inkjet printing technology. The initial layer of new powder is applied to a constructing tank to create a 3D model. An inkjet print head deposits an adhesive binder solution onto the powder layer. A new layer of powder is applied once the 2D layer pattern has printed entirely. Up to the finished product, the printing is repeated in cycles to use a binder to combine nearby layers (*Fig. 2.21*).

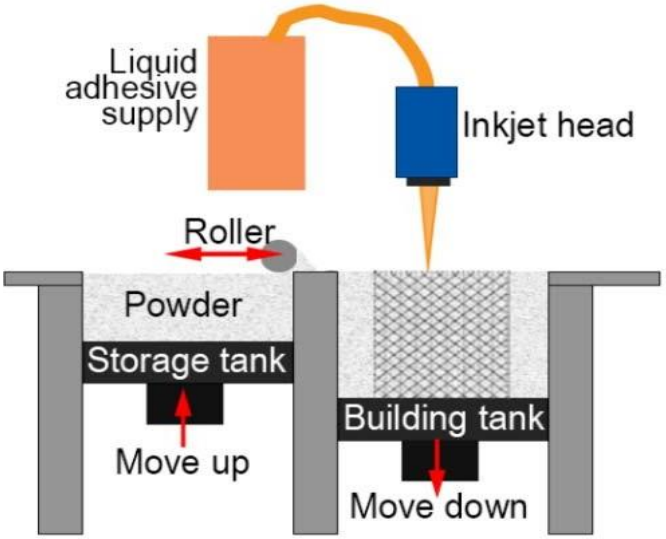

Fig. 2.21: Scheme of the 3DP process.

To get the completed component, the binder and unbound powder are taken out. The size of the nozzle limits the printing resolution, while the layer thickness (80 - 250 µm) is determined by the particle size (*Hutmacher et al., 2004*). The difficulty in removing the interior unbound powder and binders, which can be poisonous to cells, is a disadvantage of employing the binder for the porous sections. Therefore, using biocompatible powder-binder systems is a crucial necessity for 3DP of tissue-engineering materials. Calcium phosphates, which resemble bone, are an example of a very biocompatible material that has been adapted to 3DP procedures since it is possible to process it without the use of hazardous chemical solvents.

2.13.5 Selective laser melting (SLM)

Based on better lasers, SLM was created from SLS (*Gorny et al., 2011*). SLM technique uses a laser beam to locally melt metal powder layer by layer as instructed by CAD data, *Fig. 2.22*, to produce 3D metal components.

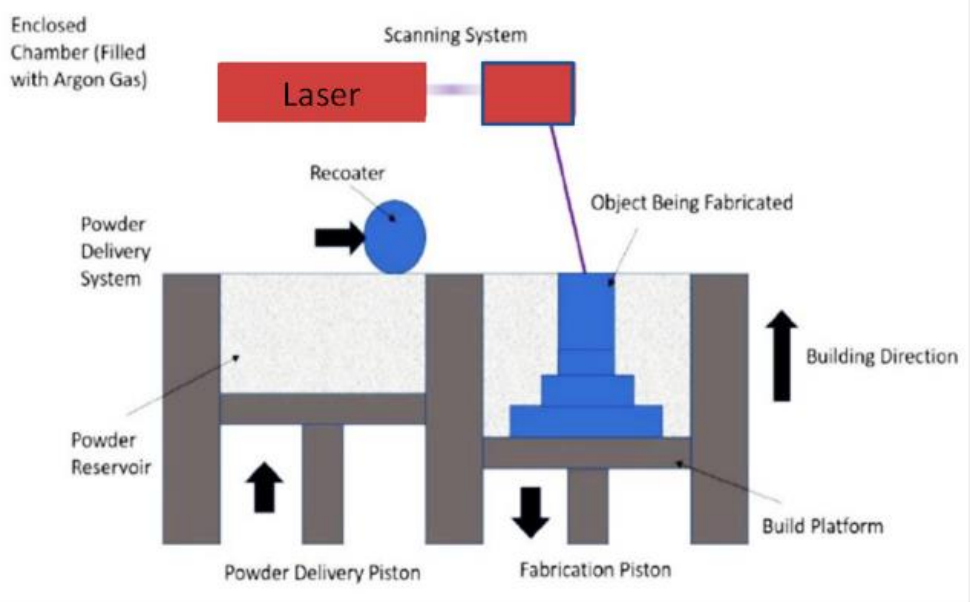

Fig. 2.22: Scheme of the SLM process.

SLM has recently been employed in the production of medical implants, including as knee and hip replacements, as well as dental implants. The enhanced mechanical, chemical, and biological compatibility of the finished products have been the subject of several researches (*Brenne et al., 2013; Girardin et al., 2016 and Mengucci et al., 2016*). Powder-based manufacturing technologies, which may manufacture with a variety of metal alloys such as titanium, stainless steel, and cobalt-chrome alloys, are the materials utilized in SLM processes.

Due to the numerous variables involved in the processing, there is no agreement on the mechanical behaviours and structural integrity of metallic components made using SLM methods compared to conventional manufacturing procedures. However, the most significant limiting issues that may impact SLM products are often the level of surface polish, unsupported facing surfaces, and thermal residual stresses (*Mengucci et al., 2016*).

2.14 SUMMARY

To repair broken bones and joints, hip implants are employed. Metal implants cannot produce an original organ as bone scaffolds can, which is how original orthopedic bone implants differ from bone-substituting scaffolds. Metallic implants can, however, operate in a way that is more in line with the functional requirements of the targeted bone when the multiscale structure of bone tissue and functionally graded notions are considered.

The ability to fabricate cellular structures in free form has improved because to AM methods. Different materials, including polymers, ceramics, and metals, are produced using different AM techniques. The precision of AM fabrications is processing dependent, but layer printing ideas remain the same. These cellular structures demonstrate the advantages of lightweight construction and support a setting for maintaining bone functions. Metallic bone implants can more nearly resemble bone tissues by grading the porosity inside the cellular structures in accordance with mechanical and biological needs. The effects of graded materials used in orthopedic biomedical devices have not been extensively studied (*Chua et al., 2011; Khanoki et al., 2012; Kuiper et al., 1997; Leong et al., 2008 and Oshkour et al., 2013a*).

Hip implants are a good example of a bone implant that has a more natural load transfer to the bone and lessens the stress shielding effect and peri-implant bone resorption. The mechanical features of grading direction along implants, however, are not fully understood. Most of the research has used computer simulation to study this (*Gong et al., 2012; Hazlehurst et al., 2014; Kuiper et al., 1997; Oshkour et al., 2013b*).

The manufacturing of cellular materials and the application of mechanical forces that are resistible on a large scale are both dependent on the microstructural architecture. This study concentrated on how an implant's architecture may support the environment and enable cells, collagen fibres, apatite crystals, and other materials to adapt to its framework and help the implant mechanically and physiologically resemble bone at a larger scale. Uncertainty exists over the ideal configuration of the internal architecture of the graded cellular structures that will be combined with bone implants. To find the best structures in terms of physiological, mechanical, and biological performance, it is crucial to investigate the impact of graded cellular structures on load-transferring capabilities.

CHAPTER 3 PROBLEM FORMULATION, OBJECTIVES AND METHODOLOGY

3.1 INTRODUCTION

The reduction of bone stress shielding may be facilitated by a cellular structure or porous substance. In addition to being lighter and more energy-absorbing, these structures have pores that help lessen the relative stiffness and density mismatch between the materials. Although the bone cells can connect to, move through, multiply, and perform other tasks in the porous networks (*Gibson, 2005; Wu et al., 2014*), the mechanical characteristics of porous structures are solely dependent on internal pore architecture (*Gümrük et al., 2013*).

The biological processes of bone tissue and the mechanical characteristics of cellular structures are both governed by the internal architecture. Because of the reduced pore diameters, which restrict cell penetration within the structures, an insufficient internal design might result in occlusion. The internal architecture of pore size, pore geometry, and pore interconnectivity of porous materials created using conventional techniques, such as solvent casting, salt leaching, and gas foaming techniques, cannot be precisely controlled, leading to poor biomechanical properties (*Naing et al., 2005; Peltola et al., 2008*). Contrarily, layer fabrication-based additive manufacturing (AM) methods may accurately create intricate 3D internal architecture (*Tarawneh et al., 2012; Williams et al., 2005*).

The porosity and pore size of the cellular structures are also determined by the polyhedron-shaped unit cell. The space-filling unit cells of polyhedral forms used by *Sudarmadji et al.* (2012), *Tarawneh et al.* (2012) *and Wettergreen et al.* (2005) were used to produce the cellular structures, and the unit dimensions made it simple to manage the mechanical performance. According to studies by *Hazlehurst et al*. (2013), *Mullen et al.* (2009 and 2010), *Wieding et al.* (2013) *and Williams et al.* (2005), cellular structures with cubic form units have equivalent stiffness and strength (E = 1.06 - 17.98 GPa and = 0.5 - 350 MPa) to cortical and cancellous bones. On the other hand, octahedral form units might also be used to create cellular structures with bone-equivalent rigidity (*Ahmadi et al., 2014 and 2017; Gorny et al., 2011; Smith et al., 2013*). It is unclear what internal structures for bone implants should be used.

Although the mechanical behaviour of polyhedral form units under uniaxial compression has been studied, the effect of the loading mode remains unclear. There haven't been many researches done to far looking at how 3D interior designs affect both mechanical and biological behaviour.

The poor mechanical strength of PCL restricts their usage for bone implants even though it has been widely employed for bone scaffolds. One of the robust, biocompatible polymers is Visi Jet material (3D System, USA), which may be processed using 3D printing (3DP) methods. It can be produced using AM methods and has three times the strength and elastic modulus of PCL.

Pore size, strut thickness, surface roughness, actual porosity, compression testing, and FE simulation of porous structures with various 3D internal architectures were investigated in this chapter. The results showed that these porous structures had a promising future in the biomedical field as bone implants.

3.2 PROBLEM FORMULATION

The following conclusions may be drawn from the literature review:

- Due to the excellent mechanical properties (low Young's modulus, high fatigue performance, high corrosion resistance, and low density) and compatibility compared to human biological system, titanium and its alloys, particularly Ti-6Al-4V alloy, have recently attracted more attention as metallic biomaterials.
- Metal additive manufacturing is a relatively recent manufacturing method that may be used commercially in the biomedical industry to produce implants that are patient-focused. The qualities of the printed item are influenced by the interaction of several process factors and printing techniques in additive manufacturing.
- To make implants more functional and bone-integrated, several lattice architectures have been employed to create porosity in the implants. According to the literature study, the mechanical properties of cubic lattice structures with varied pore sizes have not yet been studied and demand attention under diverse loading circumstances.

3.3 OBJECTIVES

The proposed research project has several goals, including the following:

- To examine the relationship between pore morphology and the mechanical behaviour of cubic lattice systems.
- To examine the failure criterion under loading circumstances.
- To use experimental data to confirm the results of the finite element analysis.
- To achieve the optimum strut dimension and pore size that imitates human bone to improve osseointegration.

3.4 EXPERIMENTAL TECHNIQUES AND PROCEDURES

3.4.1 Selection of the material

As shown in *Figs. 3.1 (a) & (b)*, porous scaffolds were manufactured using Ti-6Al-4V powders (supplied by EOS GmbH, Germany) that were nearly spherical in shape, smooth on the surface, and had particle diameters under 90 µm. *Fig. 3.1(a)* also depicts the distribution of particle size determined by the method of laser diffraction in accordance with the Coulter principle. A powder monolayer and mounted, polished samples are examined visually using an optical microscope, such as the Olympus BX41 or GX51 (EOS, Finland). *Tables 3.1 and 3.2* illustrate, respectively, the examination of the particle size distribution and powder characteristics in this work.

Table 3.1 - Particle size distribution analysis.

Size Characteristics	Test Method	Result(µm)
d10	Laser Diffraction	29.48
d50		47.05
d90		71.92

Table 3.2 - Powder property analysis.

Property	Test Method	Result
Apparent density	ASTMB212	2.42 gm/cm^3
Tap density	ASTMB527	2.9 gm/cm^3
Density	ISO3369	4.41 gm/cm^3
Water content	Karl Fischer titration	25.6 ppm

The scaffolds were manufactured based on the chemical composition (shown in *Table 3.3*), and it was discovered that Ti64 powder had very low percentages of iron, carbon, hydrogen, oxygen, and nitrogen. The physical properties of Ti64 alloy in this work are shown in *Table 3.4*.

Table 3.3 - Chemical composition of Ti-6Al-4V powder used in this work.

Element	Ti (wt %)	Al (wt %)	V (wt %)	Fe (ppm)	C (ppm)	H (ppm)	O (ppm)	N (ppm)
Mass	Balance	5.5 - 6.75	3.5 - 4.5	<3000	<800	<150	<2000	<500

Table 3.4 - Physical properties of Ti-6Al-4V alloy in this work.

Parameter	Value
Melting Temperature	1604 - 1670^{0}C
Transus Temperature	995^{0}C
Density	4.41 g/cm^3
Water Content	25.6 ppm
Electrical Resistivity	1.67 μΩ-m
Specific Heat Capacity	530 J/kg/K
Thermal Conductivity	7 W/m/K
Linear Thermal Expansion Coefficient	9x10^{-6} /K

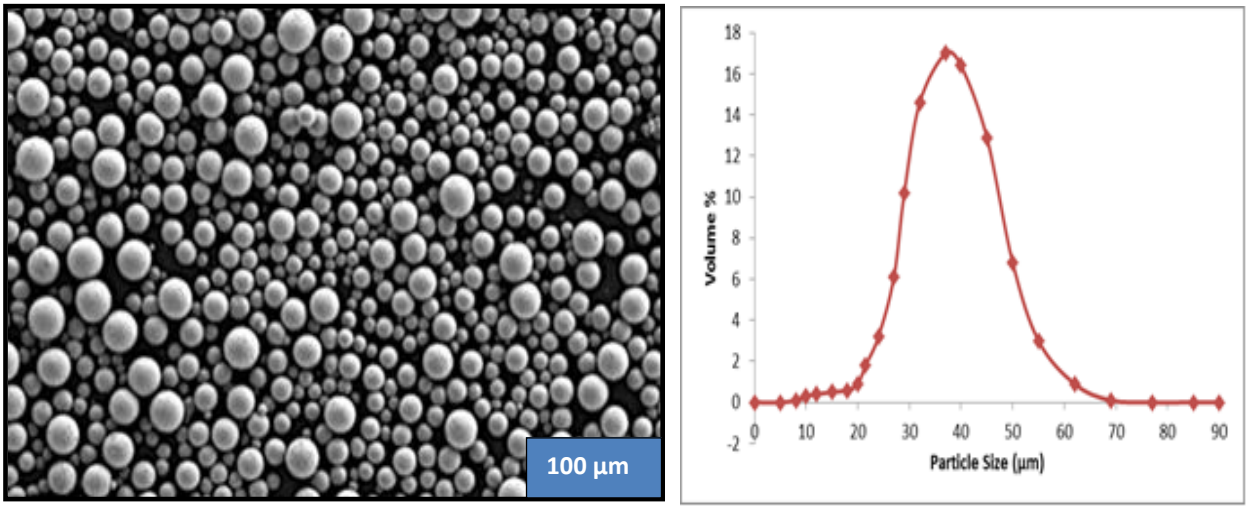

Fig. 3.1: (a) Morphological micrograph of Ti-6Al-4V raw powder for SLM Manufacturing; (b) Particle size distribution of Ti-6Al-4V powder.

The SLM process is dependent on variables including the kind of material, scanning, laser source, and environmental factors. Because the porosity has a significant impact on the mechanical properties of the components, a parametric analysis was carried out for the chosen materials to optimise the entire process, including the density of parts. Specifically, four parameters- laser power, layer thickness, scanning speed, and hatch distancing have been chosen during the procedure for testing. The energy that the laser beam provides is governed by (*Vandenbroucke, 2007*):

$$E_d = \frac{P_l}{(v_s ht)} \tag{3.1}$$

Where E_d = energy density, P_l = laser power, v_s = scan speed, h = hatch distancing and t = layer thickness.

The quantity of energy used per unit volume of the powder substance is described by its energy density. The density and quality of the fabricated components are also impacted by variations in the input process parameters along with changes to the volume energy density. According to the equation above, melting increases with higher energy and decreases as layer thickness, scanning speed, and hatch distance rise. To thoroughly melt the particles and produce significant densification, a high energy density is necessary. The process parameters have an impact on the energy input for the SLM process as well, as is illustrated by (*Liu, 2015)*:

$$E_i = \frac{4P_l}{(\pi d_l^2 v_s)} \tag{3.2}$$

Where E_i = energy input, P_l = laser power, d_l = diameter of laser beam and v_s = scan speed.

Another is linear energy density (LED), which is similarly useful for calculating the energy input of powdered materials as follows [*Attar, 2019*]:

$$LED = \frac{P_l}{v_s} \tag{3.3}$$

Where P_l = laser power and v_s = scan speed.

The relationship between the process variables, energy density (E_d), scanning speed (v_s), laser power (P_l), and hatch distancing (h), and the porosity percentage (P), may be written as follows:

$$P = f\left(\frac{E_d v_s h^2}{p_l}\right) \tag{3.4}$$

The scanning speed (vs), hatch distancing (h), and layer thickness (t) are all directly proportional to the building rate. The layer thickness and scanning speed are constrained by the available laser power. The product of scanning speed, hatch distancing, and layer thickness, which represents the construction rate of the SLM process, is represented as follows:

$$V_b = v_s h t \tag{3.5}$$

Where V_b is the building rate in mm^3/s.

3.4.2 Designing of porous Ti-6Al-4V lattices

Seven distinct types (Diamond, Cross, Grid, Vinties, Tesseract, Star, and Octet) of porous scaffolds were modeled using Rhino 6 software as shown in *Fig. 3.2*, each having dimensions of 15mm x 15mm x 15mm and a porosity of 65%. The EOS Direct Metal Laser

Sintering Machine (Model-EOSINT M-280) was used to print all the seven separate 3D models (2 of each, n = 14 Nos.) then they are converted to 2D standard STL files. For Ti64, a specific density of 4.41 g/cm^3 and a relative density of around 100 g/cm^3 were used.

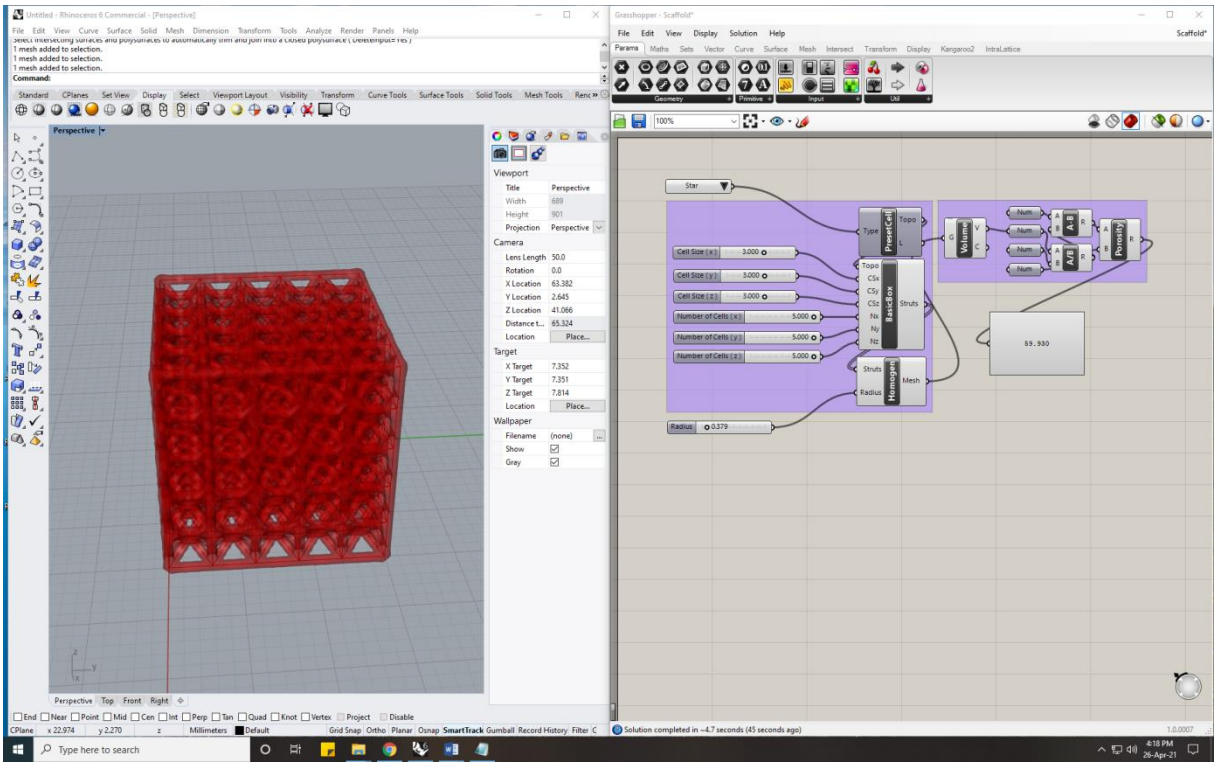

Fig. 3.2: Designing of the scaffolds in Rhino 6 software.

3.4.3 Fabrication of porous Ti-6Al-4V alloy structures by SLM

By importing data from 3D software such as CAD, Rhino 6, and others, additive manufacturing (AM) technologies, in particular selective laser melting (SLM), are utilised to considerably enhance the production process of complicated structures with small geometries. When compared to the conventional manufacturing of samples, it uses less time and less labour-intensive procedures since the casting and mould-making processes are not necessary. As a result, AM techniques may dramatically reduce the time needed to fabricate parts within an hour while also lowering production costs, material waste, improving characteristics, and consuming less energy. A layer upon layer of items are built using the AM process to create samples that are close to net form and based on 3D models. The computer modelled 3D standard tessellation language (STL) file contains number of 2D slices. The process of creating a solid model is then started using a typical SLM machine by adding materials, as shown in *Figs. 3.3 & 3.4*. The SLM technique uses metal powders as the

raw material, a laser, beam focusing apparatus, feeder mechanism, and build plate (shown in *Fig. 3.5*). The initial layer of Ti64 powder was applied to the metallic build plate at 35°C using a roller-based recoater mechanism in order to print the 3D scaffolds. The powder layer was maintained at a thickness of 60 µm. A concentrated laser beam scans across the surface of the prescribed model while melting the specific powder layer parts. A 1kW Ytterbium fibre laser of wavelength ranging from 1.06 - 1.08 µm with an 80 µm diameter circular spot was employed. The F-theta (Model No.: FTH100-1064) lens controls the beam travel while the galvanometer regulates the beam focus. To prevent oxidation during the melting, the entire procedure was carried out in an atmosphere of inert gas (argon). The EOS Direct Metal Laser Sintering Machine (EOSINT M280), as seen in *Fig. 3.4*, was used to create all Ti-6Al-4V lattices of various types. SLM laser is rotated 67^0 between two neighbouring layers during manufacturing. Due to its capacity to create intricate porous structures, the SLM technology was employed in this work to construct various Ti lattices. The STL files of scaffolds with names and fabricated scaffolds on the printing board for SLM are depicted in *Fig. 3.6(a-b)* and *Fig. 3.7(a-d)*. The fabricated 3D porous Ti64 scaffolds (Diamond, Cross, Grid, Vinties, Tesseract, Star, and Octet) by SLM are shown in *Fig. 3.8(a-g)*.

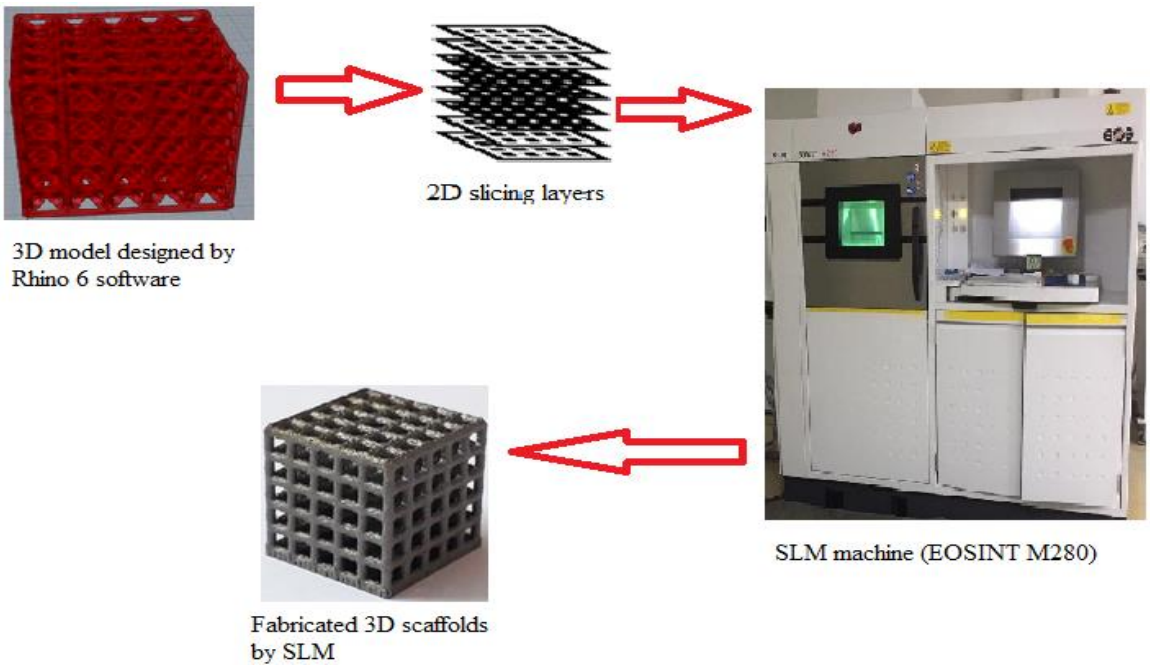

Fig. 3.3: An overview of additive manufacturing processes used in present work.

Fig. 3.4: EOS Direct Metal Laser Sintering Machine (Model: EOSINT-M280) at Central Tool Room & Training Centre (CTTC), MSME Tool Room (Govt. of India), Bhabaneshwar.

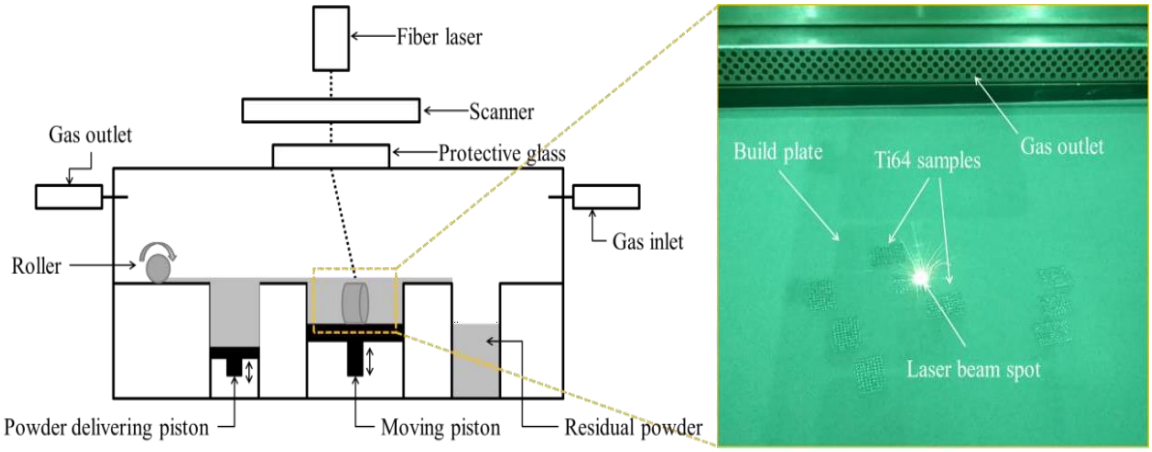

Fig. 3.5: Schematic of fabrication process of Ti64 PLS using SLM system EOSINT M280.

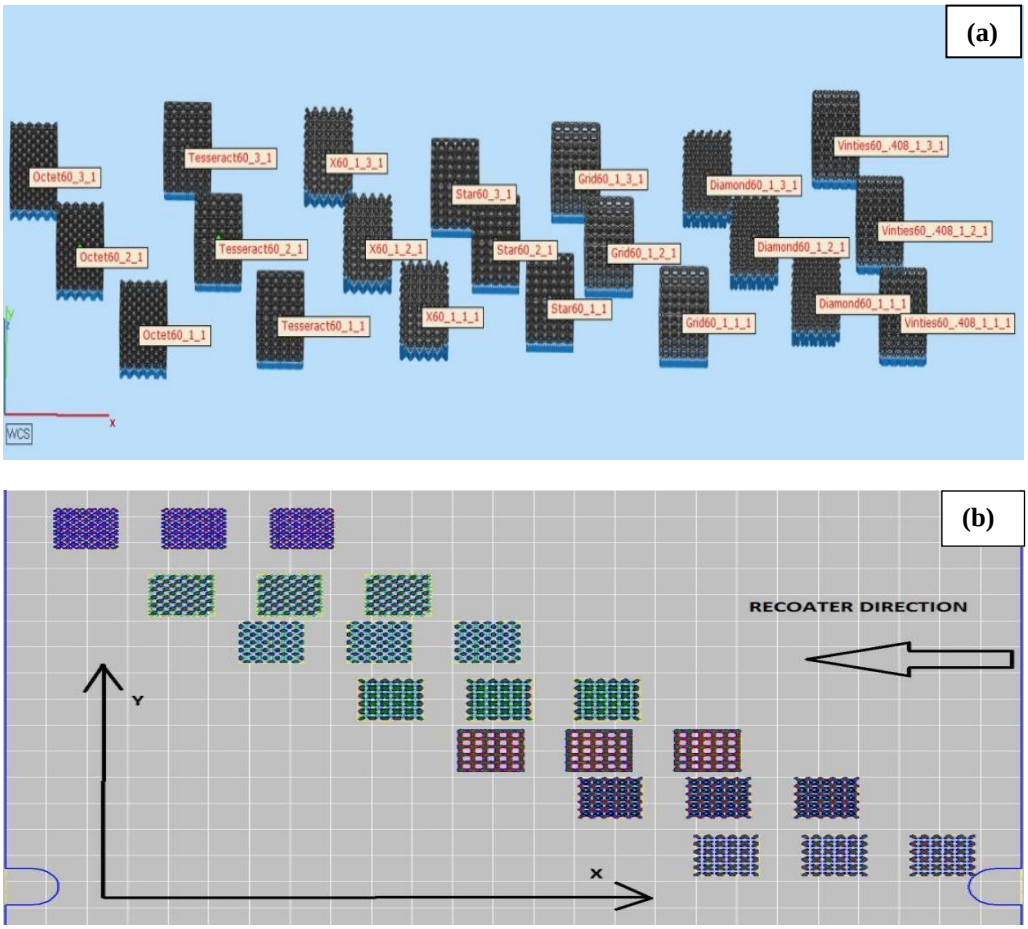

Fig. 3.6: (a) Parts arrangement with names, (b) STL files on printing board of the laser sintering machine.

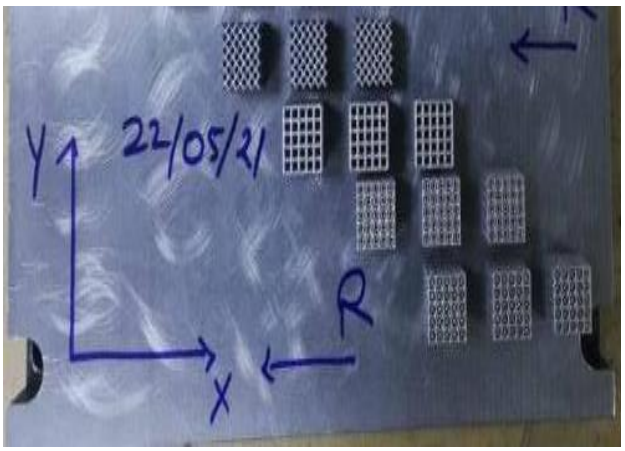

(a)

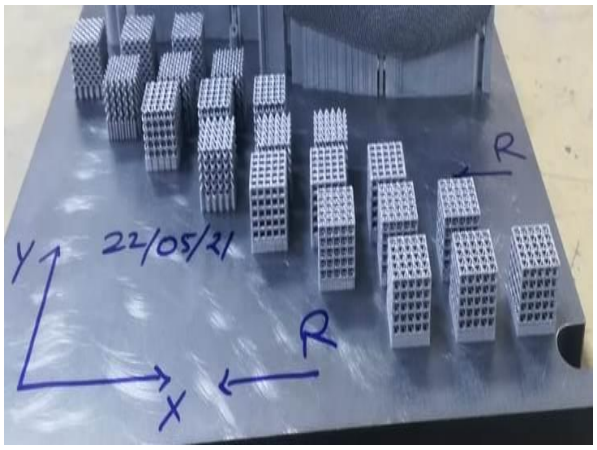

(b)

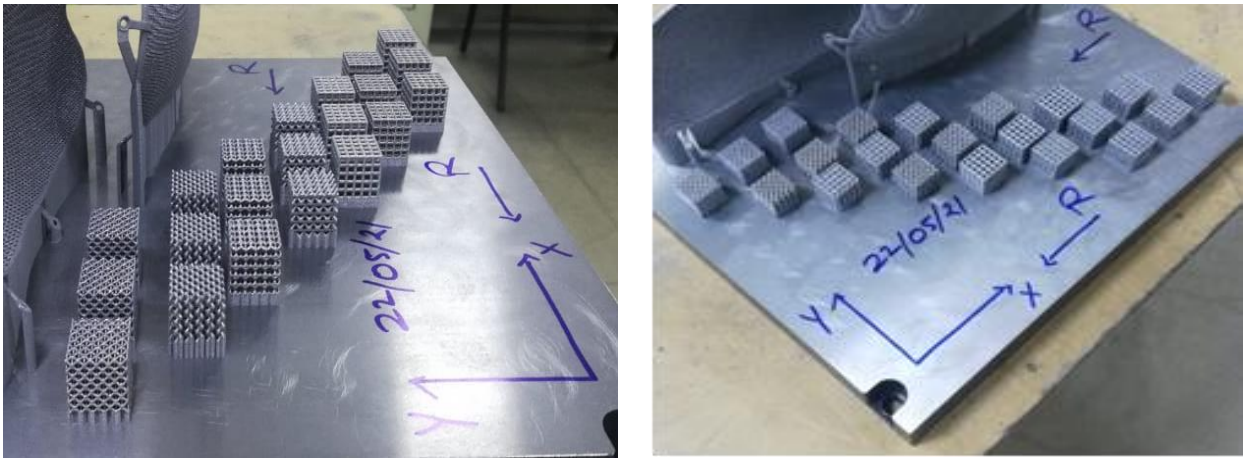

(c) (d)

Fig. 3.7 (a-d): Porous lattice scaffold samples obtained after fabrication.

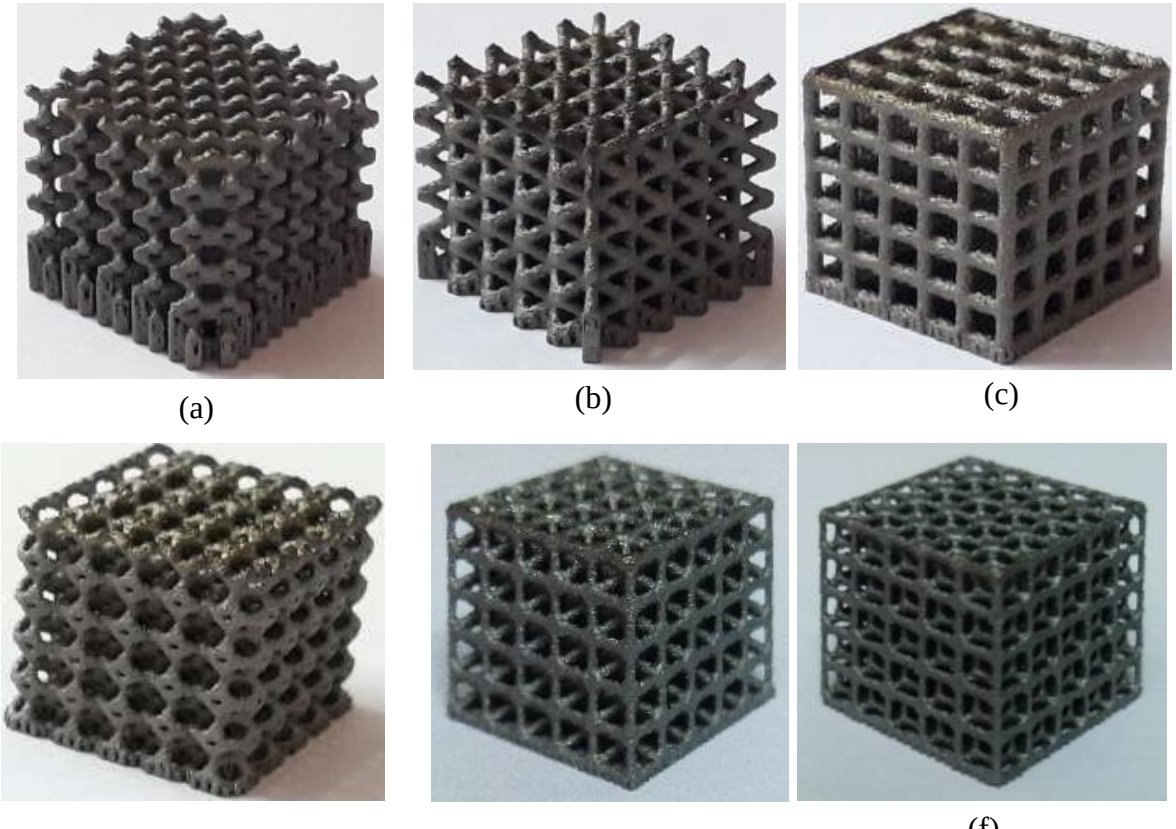

(a) (b) (c)

(d) (e) (f)

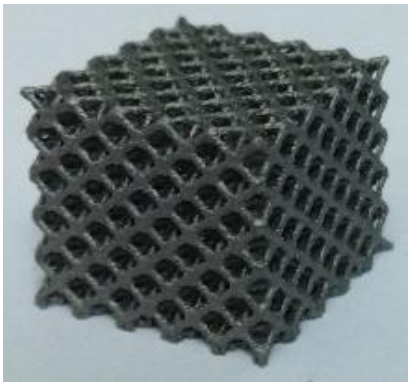

(g)

Fig. 3.8: Computer Model of Ti-6Al-4V Porous Scaffolds: (a) Diamond (b) Cross (c) Grid (d) Vinties (e) Tesseract (f) Star and (g) Octet.

3.4.4 Morphology characteristics

The cubic PLS samples that were successfully constructed using the SLM approach is depicted in *Fig. 3.8* with various unit cell dimensions. The produced PLS parts showed that they perfectly imitated the intended structures. All of the porous scaffolds' strut thickness and pore size were assessed using an optical/stereo microscope, as illustrated in *Fig. 3.9*. The general specifications of the stereo microscope are listed in *Table 3.5*. Additionally, by comparing the dimensions with those specified in the Rhino 6 model, optical microscopic pictures (shown in *Fig. 3.10*) proved the successful approximation of the constructed structures. The strut thickness and pore size of the manufactured PLS samples varied dimensionally by 2 to 6%. The main cause of this variance is the shrinkage that happened in the solidified section. The minimum laser beam spot size (*Metel, 2018*) and powder properties (*Farzadi, 2015*) are two examples of system capabilities that might cause variance. In contrast to the intended structures, it was discovered that the actual pore size was raised and the strut size was lowered. It was discovered during the examination of PLS samples that the struts primarily contained micro-pores at the bottom portions of the PLS components. This may be because there are unsintered particles, which would cause inappropriate melting (*Sola, 2019*).

The increased porosity at the lower parts may also be caused by the base plate's temperature. The PLS samples' relative density (RD) was calculated and found to be between

27 and 56%. It is crucial to note that the actual value of RD deviates from the intended PLS by an average of 7 - 8%. The larger pores and smaller struts are the causes of this variance. This is mostly caused by system capabilities and shrinking.

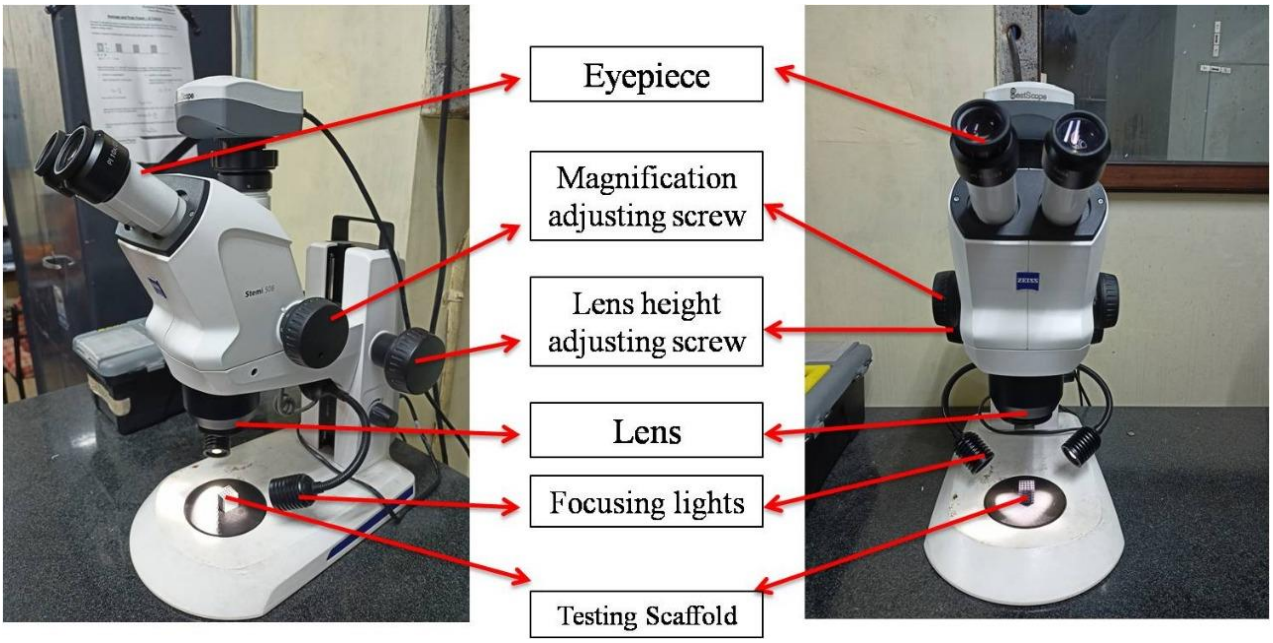

Fig. 3.9: Stereo microscope (Model-Stemi 508) for measuring pore size and strut thickness.

Table 3.5 - General specifications of the microscope.

Type of Microscope	**Stereo microscope, Greenough design**
Design Principle	Two zoom systems, tilted by the stereo angle
Stereoscopic View	Three dimensional observation through eyepieces
Apochromatic Corrected Zoomand Front Optics	Image free of color fringes in complete magnification range
Manual Zoom, Zoom Range	8:1 (0.63×...5.0×)
Quality of Zoom Optics	Distortion free, excellent contrast, apochromatic corrected
Ergonomic Viewing Angle	35^0
Adjustment of Interocular Distance	55 – 75 mm
Eyepieces	d = 30 mm
Stemi Mounts	d = 76 mm
Illuminators	d = 53 mm; Illuminators d = 66 mm via clamp ring d53/66

Working Surface	W255 × D215 mm
Height / Lifting range	360 mm / 190 mm
Load capacity of Stemi mount	5 kg

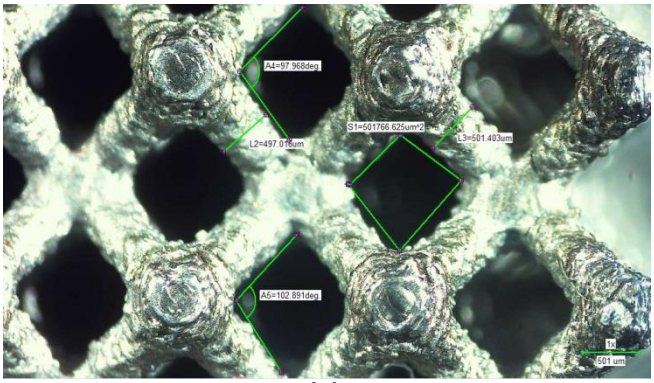

(a)

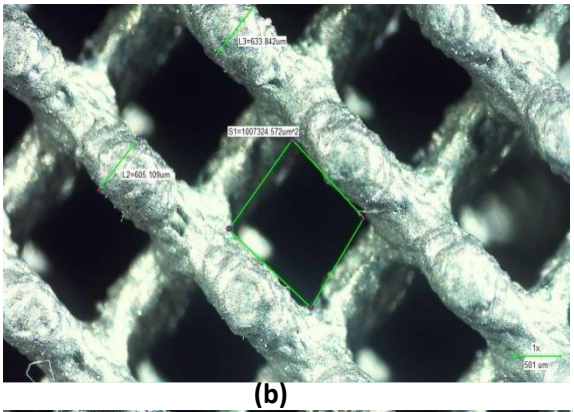

(b)

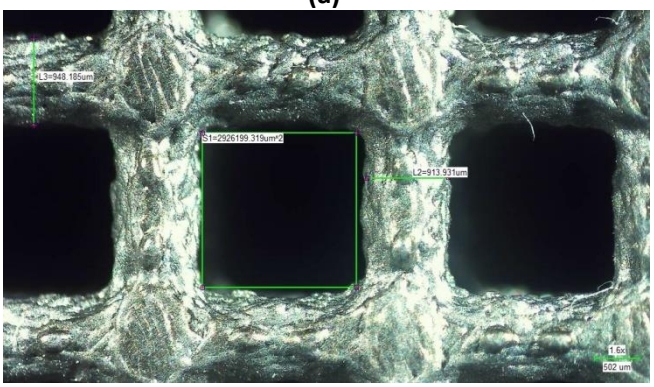

(c)

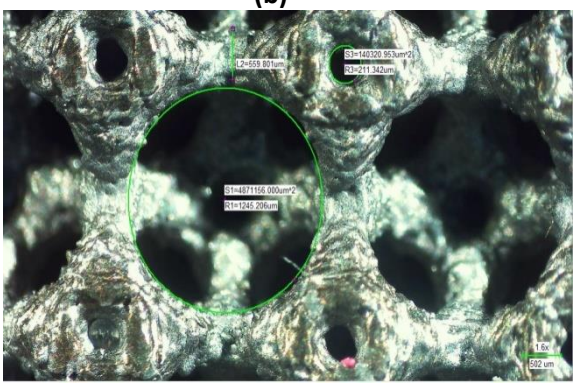

(d)

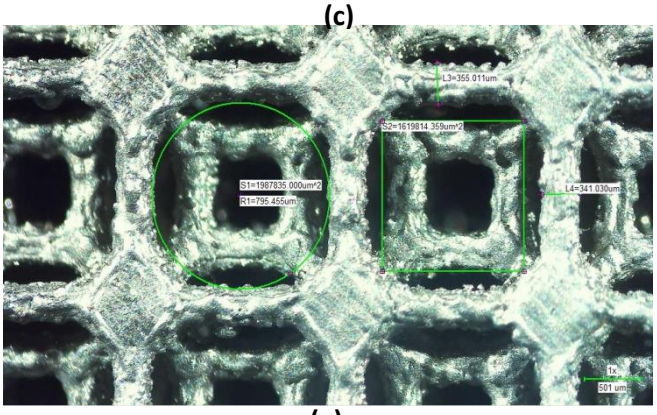

(e)

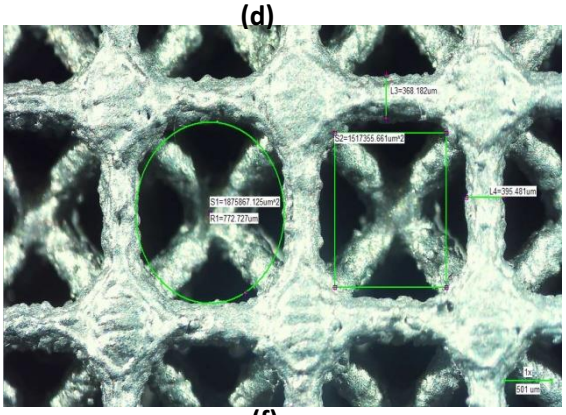

(f)

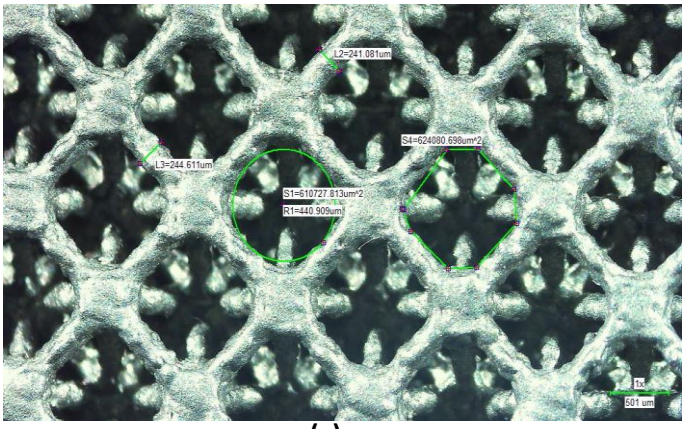

(g)

Fig. 3.10: Measurement of pore area and strut thickness using stereo microscope (Stemi 508) of fabricated porous scaffolds: (a) Diamond, (b) Cross, (c) Grid, (d) Vinties, (e) Tesseract, (f) Star & (g) Octet.

The pore area and strut thickness of scaffolds (shown in *Fig. 3.10*) are measured by stereo microscope (Model - Stemi 508) as shown in *Fig. 3.9* and it is observed that the pore area and strut thickness of the diamond, grid, cross, vinties, tesseract, star, and octet scaffolds are 586787.302 μm^2, 4253703.533 μm^2, 2417618.517 μm^2, 1290453.750 μm^2, 4783524.14 μm^2, 2484045.93 μm^2 & 1175303.449 μm^2 and 496.929 µm, 601.184 µm, 740.249 µm, 485.438 µm, 451.570 µm, 407.651 µm & 467.599 µm respectively.

3.4.5 Heat treatment process

The specimens with the construction plate underwent heat treatment after manufacturing. As-built SLM with no heat treatment and annealed SLM with heat treatment at 900^0C for 120 minutes are the two heat treatment modalities. In an argon atmosphere, the entire heat-treating procedure was carried out at a rate of 5^0C/minute, followed by cooling in the furnace. *Table 3.6* provides a list of the heat treatment steps that SLM applied to porous scaffolds as-built.

Table 3.6 - Heat treatment process of as-built scaffolds by SLM.

Sample	Temperature (^{0}C)	Time (minutes)	Cooling
Diamond	900	120	Furnace cooling (annealing)
Cross	900	120	Furnace cooling (annealing)

Grid	900	120	Furnace cooling (annealing)
Vinties	900	120	Furnace cooling (annealing)
Tesseract	900	120	Furnace cooling (annealing)
Star	900	120	Furnace cooling (annealing)
Octet	900	120	Furnace cooling (annealing)

3.4.6 Surface roughness test

The implant and bone tissue may be affected by surface roughness and energy, which can also inhibit osteoblastic cell adhesion, growth, proliferation, and differentiation (*Guehennec, 2008*). The implant surface can be enhanced by acid etching, sandblasting, and plasma spraying to achieve the desired roughness (*Guehennec, 2007*). The procedures based on metal powder can provide implants with the necessary level of surface roughness for osteointegration. Numerous Ti particles with spherical shapes are partly bound to the porous walls during the SLM process. The specimens are then heated to 900^0C in an argon environment, where microcavities are created on the walls and further encouraged to interlock with neighbouring tissues when transplanted into people. *Biemond et al.* (2013) published a comparison of the surface quality of trabecular implants produced by SLM and EBM. The specimens, which were created using SLM and EBM procedures, show various morphological traits and surface roughness: Individual granules were easily visible in the specimens made using the EBM process, but the surface roughness was flattened in the specimens made using the SLM technique. The discrepancy in porosity and post-treatment surfaces is caused by the disparity in accuracy between these two methods.

The Ti-6Al-4V powder is observed to have a smooth surface and a nearly spherical form in the SEM picture displayed in *Fig. 3.1*. According to the literature (*Ponader, 2008*), surface roughness has a positive effect if R_a is less than 25 µm and a negative effect if R_a is larger than 57 µm. Porous implants do not require surface treatment up to a roughness value of 25 µm; however, if the roughness value is greater than 25 µm, surface treatment is required. The roughness value (R_a) of the produced samples is determined using a Talysurf surface roughness tester (MITUTOYO SJ-210) and shown in *Fig. 3.11.*

Fig. 3.11: Talysurf surface roughness tester (Mitutoyo SJ-210).

Various researches have shown that the information on how to create the following surface treatments (*Bordjih et al., 1996*) is largely conflicting. The findings on osteoblasts made by *Ponder et al.* (2008) in relation to the surface roughness of implants by EBM indicated that the arithmetic average value of the absolute roughness values (R_a) plays a crucial role in the differentiation and as well as proliferation of human osteoblasts.

3.4.7 Porosity measurement of manufactured scaffolds

Titanium alloys are extensively employed in orthopedic applications due to its superior Young's modulus and corrosion resistance, high specific strength and stiffness, and great biocompatibility (*Challis et al., 2014*). However, dense Ti alloys have a higher elastic modulus of around 110 GPa, compared to 3 to 30 GPa in native bones. In the SLM method, Ti64 materials have stronger strength and stiffness, but poorer ductility (E = 110 GPa, yield strength = 945 MPa, UTS = 1050 MPa, and = 14%) (*Yu et al., 2020 and Trevisan, et al., 2018*). To minimize stress shielding, the implants should have mechanical, biological, and chemical properties similar to human bones (E = 3 - 30 GPa). As a result, a porous network has been introduced into dense materials to get desired mechanical properties by varying porosity.

The density principle is used to determine how porous the prepared samples are. Each sample was submerged in water in a measuring cylinder with minute graduations, and the amount of the water displaced provided the theoretical volume of the scaffold with porosity as seen in *Fig. 3.12*.

The porosity of Ti-6Al-4V scaffolds can be determined as:

$$P = (1 - \frac{W_p}{W_d}) x 100\% \qquad (3.6)$$

Where P = Porosity, W_p = Weight of the porous sample and W_d = Weight of the dense samples.

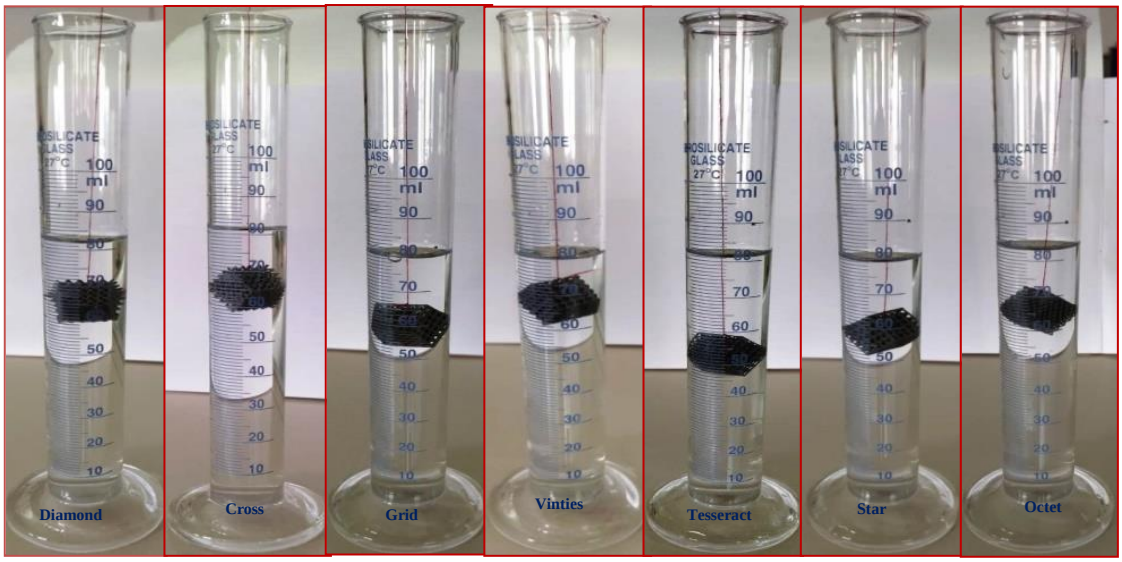

Fig. 3.12: Porosity measurement of fabricated porous scaffolds by measuring cylinders.

3.4.8 Mechanical properties

The materials' microstructure enhances their mechanical qualities, which are profoundly influenced by the additive manufacturing process. In this method, materials are produced layer by layer while being repeatedly heated and cooled to produce scaffolds. In particular, the first particles pass through by rapidly heating to the point of melting while absorbing energy from a laser or electron beam source. After being scanned by the energy source, the material's melting part soon hardens to form coarse-grained microstructures. The remaining portion of the material is repeatedly heated in order to process the subsequent layers. The metastable microstructures and structural phases produced by this compound heat cycle can

modify the component volume. Different AM techniques might vary the depth of the melt region depending on the heat transfer. Typically, the heat transmission in laser metal deposition (LMD) comprises convection to the shield gas, conduction to the substrate, and built material. However, in SLM procedures, a powder bed covers the whole component, which limits heat conduction, lowers gas flow rates, and diminishes convectional contribution. In general, at low cooling rates, EBM produces Ti-6Al-4V components with a coarser microstructure than those made by SLM or LMD. On the other hand, in SLM and LMD processes, a very high degree of undercooling is only caused by a higher cooling rate greater than 104 K/s and a very high thermal gradient.

In an ISO17025 recognised laboratory, the mechanical characteristics of Ti-6Al-4V alloys made using the SLM technique will be evaluated in accordance with ISO 6892-1 or ASTM E8. Due to the rapid solidification and heating cycles used in the AM method, metastable microstructures and phases may quickly be changed to have improved mechanical characteristics. In general, the choice of treatment choices can also have a great influence on stress reduction, precipitation, densification, phase evolutions, and grain size and orientation.

By using the simplified formula, it is possible to approximately calculate the connection between the modulus of elasticity and porosity %. (*Su, 2012*):

$$E_p = E_s(1-P)^2 \qquad (3.7)$$

Where E_p = effective Young's modulus of porous material, E_s = Young's modulus of dense or solid material and P = porosity.

The computer-modelled scaffold has a theoretical porosity of 65%. However, maintaining the actual porosity during fabrication is challenging, and the scaffold porosity may differ from the planned porosity. A correlation analysis was also carried out to exploit the tiny deviated porosity. The elastic modulus and strength of porous materials are affected by porosity or relative density, and it is necessary to understand how elastic properties vary with prepared samples. As a result, the Gibson-Ashby Correlation model is used to investigate the relationship between porosity and elastic characteristics in this study (*Silva and Gibson, 1997*). The relationship between elastic modulus, strength and porosity can be written as:

$$E_p/E_s = C_1(W_p/W_s)a \quad (3.8)$$

$$\sigma_p/\sigma_s = C_2(W_p/W_s)b \quad (3.9)$$

Where E_p, W_p, and σ_p represent the elastic modulus, weight and strength of porous scaffolds and E_s, W_s and σ_s represent the elastic modulus, weight, and strength of Ti alloy and a, b, C_1 and C_2 are the constants. Consider E_s is equal to 112 GPa and σ_s is equal to 1050 MPa. Using equation (3.1), equations (3.2) and (3.3) can be re-written as:

$$E_p/E_s = C_1(1 - P)a \quad (3.10)$$

$$\sigma_p/\sigma_s = C_2(1 - P)b \quad (3.11)$$

Where, a = 2, b = 1.5, C_1 = 1 and C_2 = 0.3 is used as per in Gibson-Ashby model.

3.4.9 Experimental setup and compression test

To determine the mechanical properties of each sample, a compression test was conducted in an INSTRON machine with maximum load cell capacity of ± 25 kN. An additional attachment made of two HSS compression plates with a thickness of 5 mm is created in order to correctly fit the samples in the INSTRON testing machine during the compression test and also to prevent the slipping of small samples in size (15 mm cube) shown in *Fig. 3.13*. The top plate is depicted in *Fig. 3.13(a)*, and the bottom plate is displayed in *Fig. 3.13(b)*. The plate's main job is to hold the sample in place and lessen the impact of sample compression. The scaffold is then positioned between the plates as seen in *Fig. 3.14* & *Fig. 3.15* and the attachment is then set up to the INSTRON machine. The machine's initial settings and control functions are configured on a TAB that is linked to it. Throughout the testing, a computer connected to the INSTRON machine records the variations in applied loads and deformation behaviours for each sample. Atmospheric conditions are normal, and all of the scaffolds are squeezed at a crosshead movement rate of 0.02 mm/s (27^0C and 65% RH).

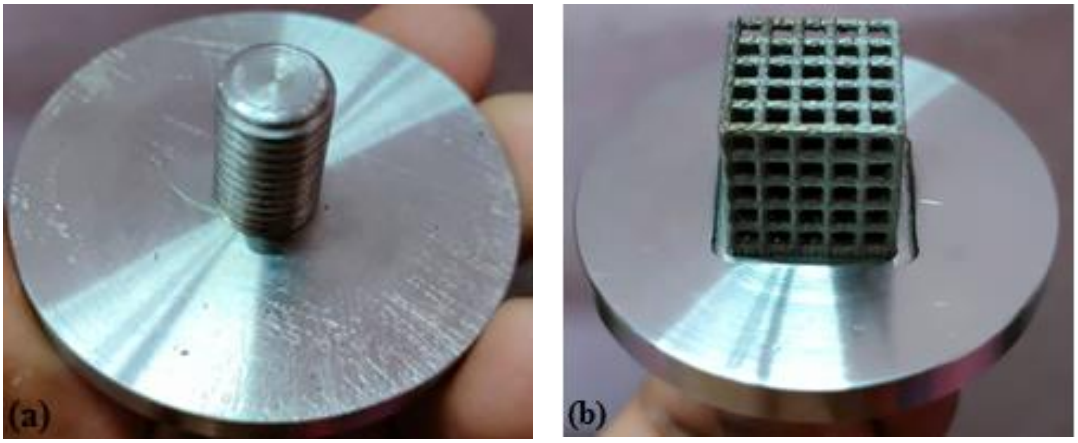

Fig. 3.13: HSS plates to be fitted with INSTRON machine: (a) Upper plate and (b) Lower plate.

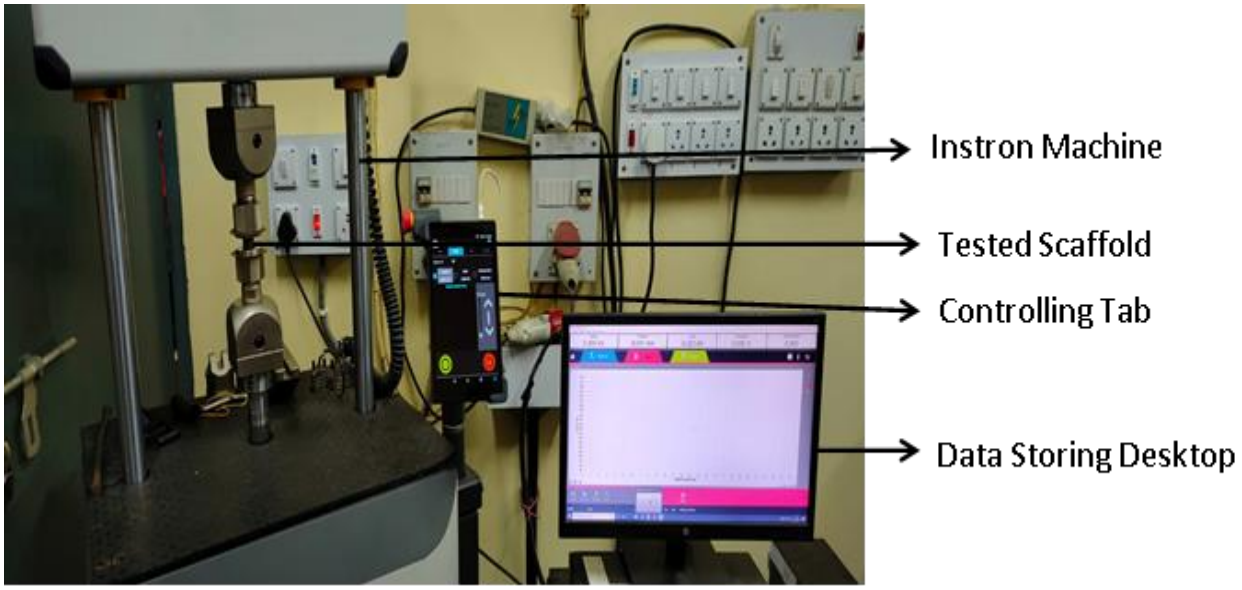

Fig. 3.14: Compression test set up for INSTRON.

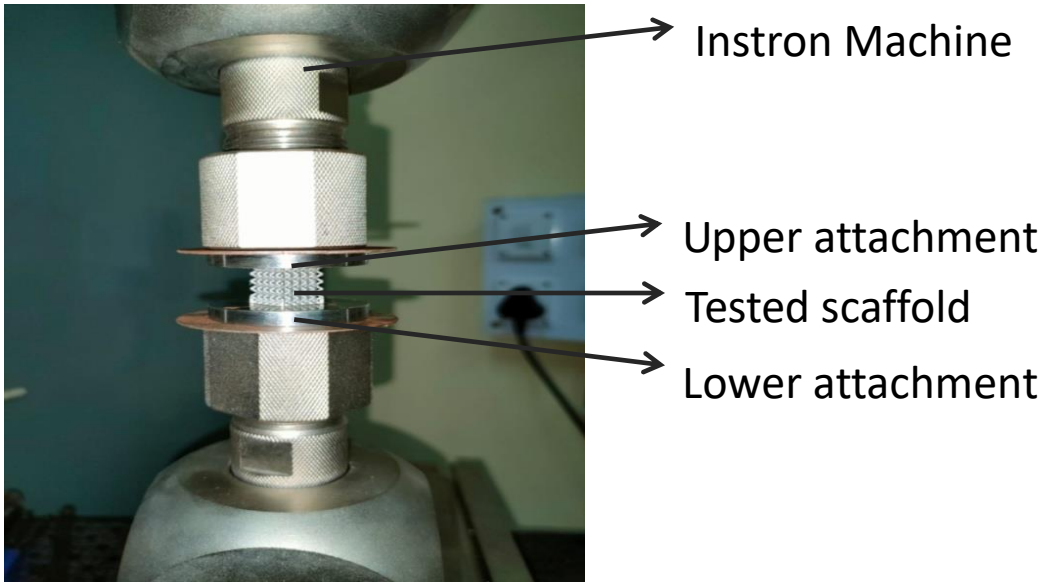

Fig. 3.15: Sample held in INSTRON testing machine with two additional attachments.

3.5 FINITE ELEMENT ANALYSIS

Finite Element Analysis (FEA) is a simulation method for predicting how a part will react under a particular set of circumstances. A mathematical technique known as the Finite Element Method (FEM) is used to make this prediction. FEM breaks down a big system into smaller pieces called finite elements through spatial discretization to solve an issue. This is accomplished by building a mesh out of the item under examination that has a limited number of points. This method of expressing a boundary issue yields a set of algebraic equations that may be used to calculate the unknown function over the specified domain. These straightforward equations are then combined to form a more complex system of equations that models the overall issue.

3.6 SUMMARY

This research examined the design and production of a porous structure using SLM techniques for Ti64 material. These methods may be used to create the Ti64 porous structures of several architectural types, including the Diamond, Cross, Grid, Vinties, Tesseract, Star, and Octet. By optical/stereo microscopy (Stemi-508), the Ti64 porous structures manufactured by the SLM technique in this work showed actual pore size in the range of

407.651 µm to 740.249 µm and porosity varying from 62.55% to 64.4%. These structure's pore size and porosity values fall within the permissible range of morphological specifications for bone osseointegration.

The Ti-6Al-4V porous structures manufactured in this thesis were biocompatible and low in cell toxicity. The reduced bioactivity of this material allows it to be manufactured as orthopaedic implants when osseointegration is not necessary. However, the bioactive layer of hydroxyapatite (HA) coated on the surface of the laser-melted Ti-6Al-4V material greatly improved cell osseointegration, proliferation, and differentiation as well as biocompatibility. To increase osseointegration between Ti-6Al-4V porous implants and bone, HA coating is applied to the surface of laser-melted Ti-6Al-4V porous structures. To use these designs to create orthopaedic bone implants that behave more like human bone, the mechanical properties, and stress-transferring features of laser-melted Ti-6Al-4V porous structures were further studied.

CHAPTER 4

RESULTS AND DISCUSSION

4.1 INTRODUCTION

Ti-6Al-4V powders with particle diameters below 90 µm are used as raw material to fabricate the porous scaffolds. Then based on the internal procedures, the visual observation of powder is done using optical microscope Olympus BX41 or GX51 (EOS, Finland) to investigate powder monolayer. Ti-6Al-4V powder is almost spherical in shape with smooth surface and contains very less amount of iron, carbon, hydrogen, oxygen and nitrogen. Seven numbers of porous 3D scaffolds (Diamond, Grid, Cross, Vinties, Tesseract, Star and Octet) of 15 mm cube were designed by Rhino 6 software using Ti-6Al-4V powders with 65% porosity and a specific density of 4.41 gm/cm^3. All the samples have been manufactured by selective laser melting (SLM) machine EOSINT M280-400W, optimized by 60 µm thickness of layer, a laser power of 340 W and the diameter of laser beam of the laser source is 100 µm. During SLM manufacturing, the laser is rotated through 67^0 between the two adjacent layers. Porous scaffolds were heat treated at 900^{0}C for 2 hours in an inert atmosphere, and at last cooled at room temperature in a furnace to improve the mechanical properties.

4.2 SURFACE ROUGHNESS

The roughness value (R_a) of the produced samples was determined using a Talysurf surface roughness tester (MITUTOYO SJ-210) shown in *Fig. 3.11* and is reported in *Table 4.1*. The grid kind of sample has a lower level of surface roughness. The grid type sample has the least amount of surface roughness, whereas the diamond type sample has a higher level of surface roughness.

Table 4.1 - Roughness value (R_a) of prepared samples.

Sample Type	Roughness value (R_a) (µm)	
	Sample1	Sample2
Diamond	46.2	49.6
Cross	43.7	41.8
Grid	23.2	21.6
Vinties	27.7	29.8
Tesseract	31.3	30.6
Star	33.8	35.1
Octet	29.3	31.6

4.3 POROSITY VARIATION OF FABRICATED SCAFFOLDS

The porosity % of the fabricated scaffolds is slightly lesser than the scaffolds designed in Rhino 6 software because of the powder materials attached to the scaffold walls during fabrication by SLM. It is important to mention that the actual porosity % of fabricated scaffolds showed a decrease of averagely 1 - 4% as compared to the designed scaffolds in Rhino 6 software as shown in *Table 4.2*.

Table 4.2 - Measured porosity of the prepared samples.

Sample Type	Theoretical porosity	Measured porosity	
		Sample 1	Sample 2
Diamond	65%	62.7%	62.4%
Cross	65%	63.4%	63.8%
Grid	65%	64.3%	64.5%
Vinties	65%	64.1%	64.2%
Tesseract	65%	63.2%	63.9%
Star	65%	64.5%	64.0%
Octet	65%	62.7%	62.7%

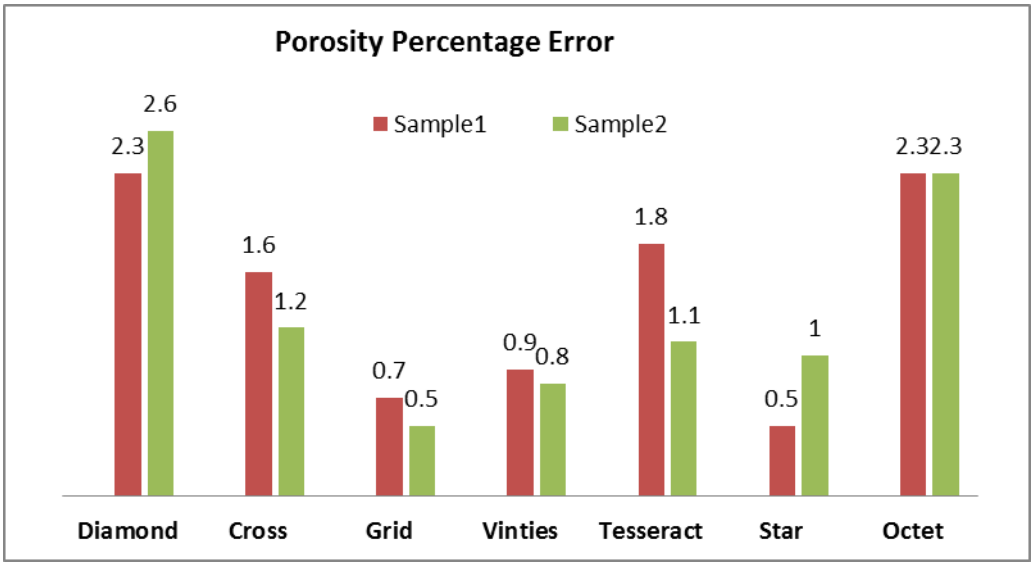

Fig. 4.1: Percentage of error in porosity of different prepared samples.

Fig. 4.1 shows that the porosity error % for the grid type of sample is the lowest, while the porosity error percentage for the diamond type is the highest, according to the porosity measurements of the produced samples. The porosity variation in the grid type sample is the smallest.

4.4 OPTIMISATION OF PROCESS PARAMETERS

The Minitab software is used in the Design of Experiments (DOE). The porosity of the various samples is determined using Archimedes principle, and the findings are then evaluated for optimization using the Minitab software. An optimization analysis of the percentage of porosity vs scan speed (mm/s), hatch distance (mm), and laser power (W) is carried out. Mean and Signal to Noise ratio responses and graphs were produced. Every sample is studied at two levels, and the results are documented.

Minitab generates a table of estimated regression coefficients for each response feature. The signal-to-noise ratio (S/N) and the means are chosen as response characteristics in this investigation. The absolute value of the coefficient represents the relative importance of each element. The component with the highest coefficient has the most significant impact on that responsecharacteristic. The amount of the factor coefficient in Minitab generally corresponds to the factor rankings in the response tables.

The response tables display the mean of each response characteristic for each factor level. The ranks in the tables are based on Delta statistics, which measure the relative size

of impacts. The delta statistic is calculated by subtracting the highest from the lowest mean for each component. The Delta statistic is calculated by taking the highest minus the lowest average for each element. Based on Delta values, Minitab gives ranks, with rank 1 being the highest, followed by rank 2 and so on. We always strive to optimize the S/N ratio in Taguchi trials.

The main effects graphs demonstrate how each component influences the response characteristic (S/N ratio, means). A major impact arises when various amounts of a component have varied effects on the characteristic. For a factor with two levels, we can see that one level raises the mean more than the other. This distinction is a significant consequence.

The main effects plot is produced by Minitab by plotting the typical average for each factor level. These averages correspond to those shown in the answer table.

a) When the line is horizontal, there is no primary impact. Each level of the factor has an equal effect on the characteristic, and the average characteristic remains constant across all factor levels.

b) The line's non-horizontal position has a primary effect. The feature is impacted differently by the component at various levels. As the vertical positions of the displayed points diverge, the magnitude of the major influence grows (the more the line is not parallel to the X-axis).

4.4.1 Diamond

The main effects plots display the effect of different parameters and its extent in relation with porosity. In the scaffold of diamond, scan speed (mm/s) shows huge variation in comparison tohatch distance (µm) and laser power (W). The porosity is greatly affected by the scan speed and thereby it is ranked 1 in the response tables for signal to ratio and means. The slope of scan speed is more inclined towards the vertical axis i.e. showing major deviation from horizontal axis therefore establishing higher impact upon porosity. *Table 4.3 & 4.4* shows the response table for signal to noise ratio and *Fig. 4.2* represents the main effect plots for signal to noise ratio and means. In the diamond scaffold, laser power is ranked second, and lastly the hatch distance. These parameters are ranked on the

basis of their effect on the porosity of the scaffold.

Table 4.3 - Response Table for Signal to Noise Ratio.

Level	Scan Speed (mm/s)	Hatch Distance (µm)	Laser Power (W)
1	35.92	36.1	36.14
2	36.29	36.11	36.08
Delta	0.37	0.01	0.05
Rank	1	3	2

Table 4.4 - Response Table for Means.

Level	Scan Speed (mm/s)	Hatch Distance (µm)	Laser Power (W)
1	62.55	63.85	64.1
2	65.25	63.95	63.7
Delta	2.7	0.1	0.4
Rank	1	3	2

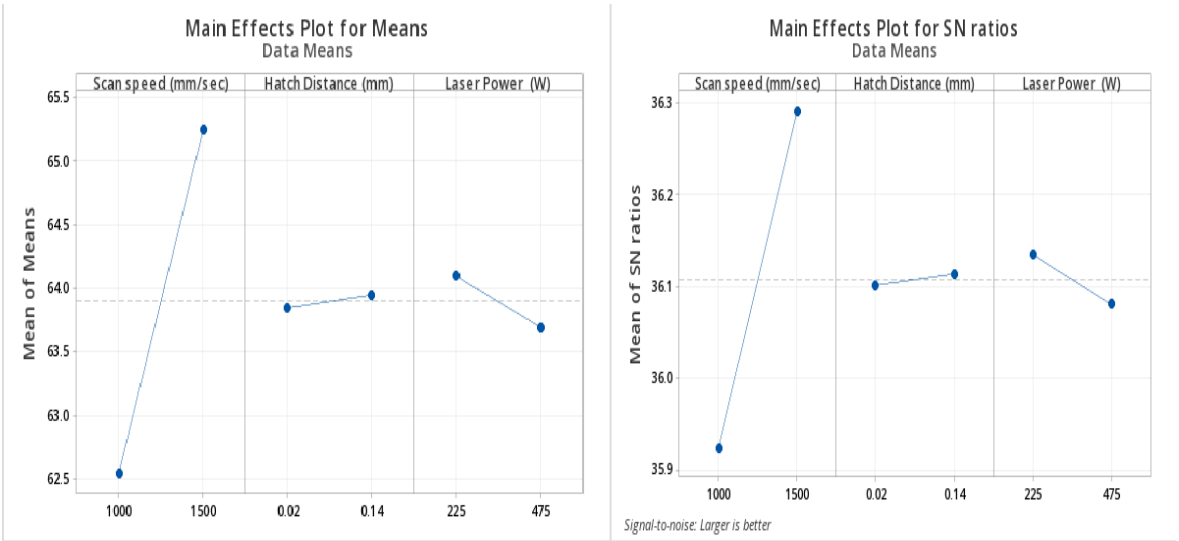

Fig. 4.2: Main Effects Plots for Means and SN Ratios for Diamond.

4.4.2 Cross

The main effects plots display the effect of different parameters and its extent in relation with porosity. In the cross scaffold, scan speed (mm/s) shows huge variation in comparison to hatchdistance (µm) and laser power (W). The porosity is greatly affected by the scan speed and thereby it is ranked 1 in the response tables for signal to ratio and means. The slope of scan speed is more inclined towards the vertical axis i.e. showing major deviation from horizontal axis, therefore, establishing a higher impact upon porosity. *Table 4.5 & 4.6* shows the response table for signal-to-noise ratio and *Fig. 4.3* represents the main effect plots for means and signal-to-noise ratio. In this scaffold, hatch distance is ranked second, and lastly the laser power.

Table 4.5 - Response Table for Signal to Noise Ratios.

Level	Scan Speed (mm/s)	Hatch Distance (µm)	Laser Power (W)
1	36.07	36.15	36.18
2	36.29	36.21	36.18
Delta	0.22	0.06	0.01
Rank	1	2	3

Table 4.6 - Response Table for Means.

Level	Scan Speed (mm/s)	Hatch Distance (µm)	Laser Power (W)
1	63.6	64.2	64.45
2	65.25	64.65	64.4
Delta	1.65	0.45	0.05
Rank	1	2	3

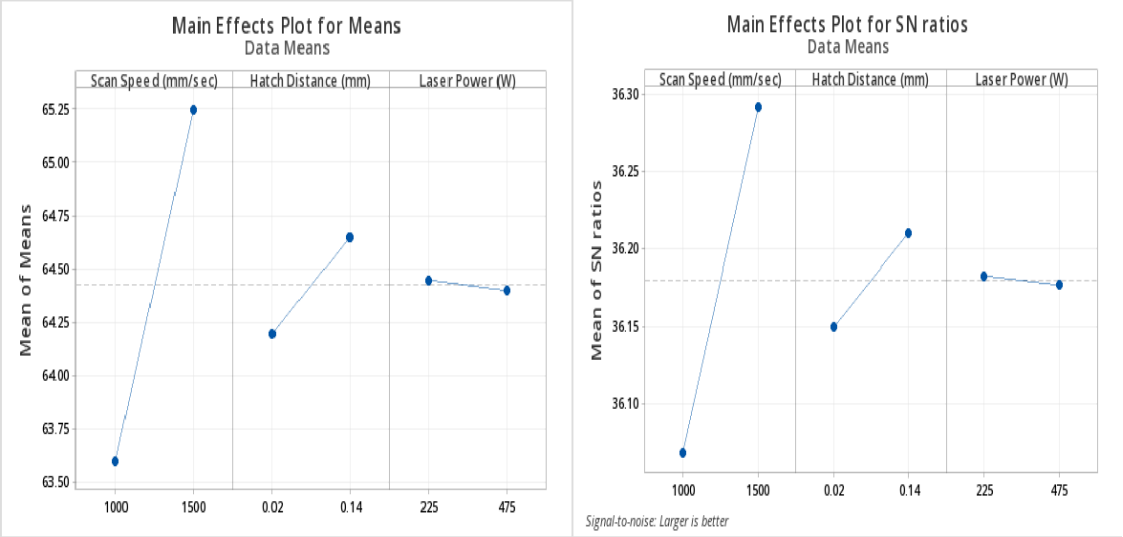

Fig. 4.3: Main Effects Plots for Means and SN Ratios for Cross.

4.4.3 Grid

The main effects plots display the effect of different parameters and its extent in relation with porosity. In the grid scaffold, scan speed (mm/s) shows huge variation in comparison to hatch distance (µm) and laser power (W). The porosity is greatly affected by the scan speed and thereby it is ranked 1 in the response tables for signal to ratio and means. The slope of scan speed is more inclined towards the vertical axis i.e. showing major deviation from horizontal axis therefore establishing higher impact upon porosity. *Table 4.7 & 4.8* shows the response table for signal to noise ratio and *Fig. 4.4* represents the main effect plots for signal-to-noise ratio and means. In this grid scaffold, hatch distance is ranked second and lastly the laser power. Hatch distance also shows greater impact on porosity as compared to the Diamond and Cross structures. The laser power used is same as before for other scaffolds.

Table 4.7 - Response Table for Signal to Noise Ratios.

Level	Scan Speed (mm/s)	Hatch Distance (µm)	Laser Power (W)
1	36.17	36.2	36.24
2	36.29	36.26	36.22
Delta	0.12	0.05	0.01
Rank	1	2	3

Table 4.8 - Response Table for Means.

Level	Scan Speed (mm/s)	Hatch Distance (µm)	Laser Power (W)
1	64.35	64.6	64.85
2	65.25	65	64.75
Delta	0.9	0.4	0.1
Rank	1	2	3

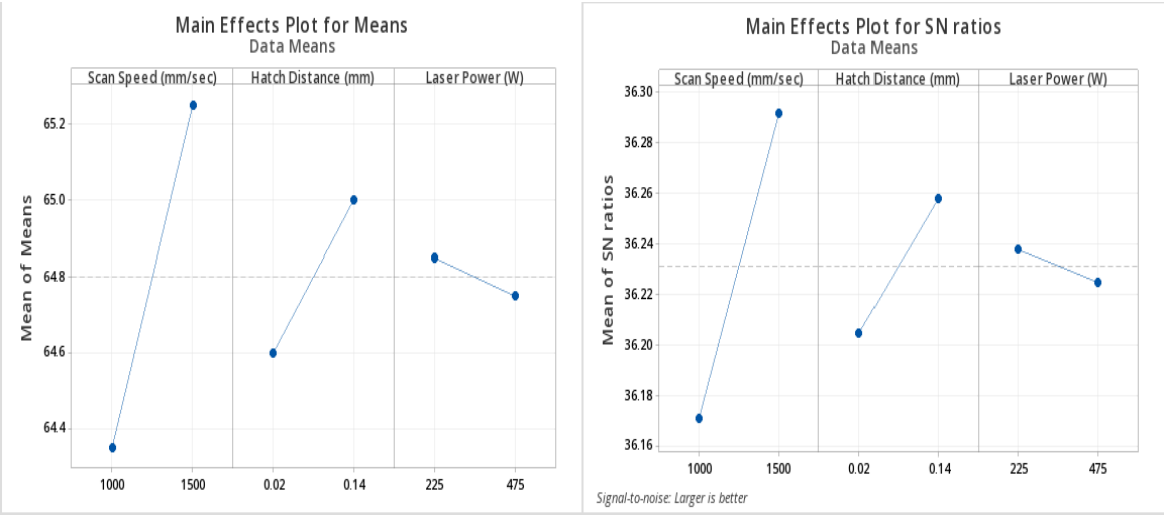

Fig. 4.4: Main Effects Plots for Means and SN Ratios for Grid.

4.4.4 Vinties

The main effects plots display the effect of different parameters and its extent in relation with porosity. In the vinties scaffold, scan speed (mm/s) shows huge variation in comparison to hatch distance (µm) and laser power (W). The porosity is greatly affected by the scan speed and thereby it is ranked 1 in the response tables for signal to ratio and means. The slope of scan speed is more inclined towards the vertical axis i.e. showing major deviation from horizontal axis therefore establishing higher impact upon porosity. *Table 4.9 & 4.10* shows the response table for signal to noise ratio and *Fig. 4.5* represents the main effect plots for signal to noise ratio and means. In this vinties scaffold, hatch distance is ranked second and lastly the laser power. Hatch distance also shows greater impact on porosity as compared to the Diamond and Cross structures. In this case laser power is also having significantly much impact in comparison to Diamond, Cross and

Vinties scaffold.

Table 4.9 - Response Table for Signal to Noise Ratio.

Level	Scan Speed (mm/s)	Hatch Distance (µm)	Laser Power (W)
1	36.19	36.22	36.25
2	36.29	36.26	36.23
Delta	0.1	0.05	0.02
Rank	1	2	3

Table 4.10 - Response Table for Means.

Level	Scan Speed (mm/s)	Hatch Distance (µm)	Laser Power (W)
1	64.5	64.7	64.95
2	65.25	65.05	64.8
Delta	0.75	0.35	0.15
Rank	1	2	3

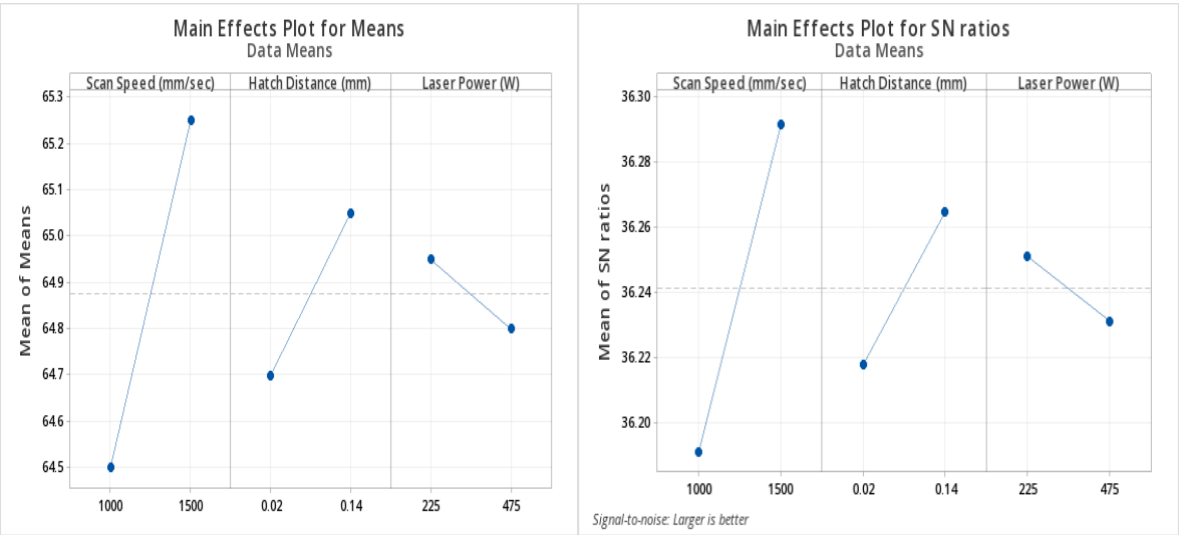

Fig. 4.5: Main Effects Plots for Means and SN Ratios for Vinties.

4.4.5 Tesseract

The main effects plots display the effect of different parameters and its extent in relation with porosity. In the scaffold of tesseract, scan speed which is in mm/s shows huge variation in comparison to hatch distance (µm) and laser power (W). The porosity is greatly affected by the scan speed and thereby it is ranked 1 in the response tables for signal to ratio and means. The slope of scan speed is more inclined towards the vertical axis i.e. showing major deviation from horizontal axis therefore establishing higher impact upon porosity. *Table 4.11 & 4.12* shows the response table for signal to noise ratio and means and *Fig. 4.6* represents the main effect plots for signal to noise ratio and means. In the tesseract scaffold, hatch distance is ranked second and lastly the laser power as can be seen in the tables of signal to noise ratio and means. These parameters are ranked on the basis of their effect on the porosity of scaffold.

Table 4.11- Response Table for Signal to Noise Ratios.

Level	Scan Speed (mm/s)	Hatch Distance (µm)	Laser Power (W)
1	36.06	36.14	36.17
2	36.29	36.22	36.18
Delta	0.23	0.08	0.01
Rank	1	2	3

Table 4.12 - Response Table for Means.

Level	Scan Speed (mm/s)	Hatch Distance (µm)	Laser Power (W)
1	63.55	64.10	64.35
2	65.25	64.70	64.45
Delta	1.70	0.60	0.10
Rank	1	2	3

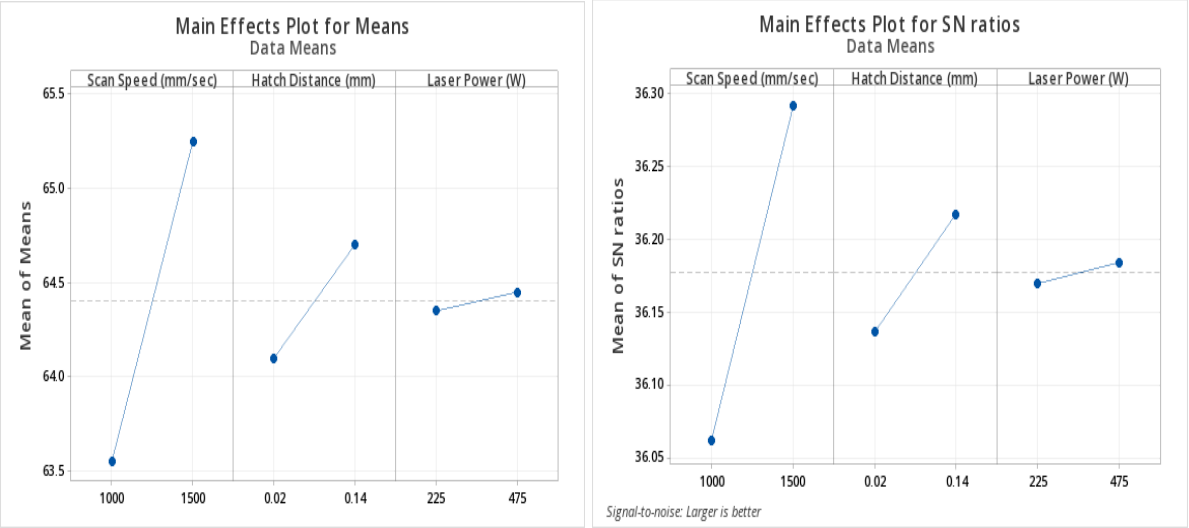

Fig. 4.6: Main Effects Plots for Means and SN Ratios for Tesseract.

4.4.6 Star

In star specimen, scan speed (mm/s) demonstrates enormous disparity in contrast to hatch distance (µm) and laser power (W). In the optimization of parameters larger is better is opted for obtaining the response tables and graphs. The porosity is significantly affected by the scan speed and thus it is ranked 1 in the response tables for signal to ratio and means. The inclination of scan speed is more in the direction of the vertical axis i.e. displaying nonconformity from horizontal axis therefore establishing greater impact upon porosity. *Table 4.13 & 4.14* displays the response table for signal to noise ratio and means whereas *Fig. 4.7* denotes the main effect plots for signal to noise ratio and means. In this star scaffold, hatch distance is ranked third as it has almost lesser impact when compared with scan speed and laser power.

Table 4.13 - Response Table for Signal to Noise Ratios.

Level	Scan Speed (mm/s)	Hatch Distance (mm)	Laser Power (W)
1	36.16	36.22	36.26
2	36.29	36.22	36.19
Delta	0.13	0.00	0.07
Rank	1	3	2

Table 4.14 - Response Table for Means.

Level	Scan Speed (mm/s)	Hatch Distance (mm)	Laser Power (W)
1	64.25	64.75	65.00
2	65.25	64.75	64.50
Delta	1.00	0.00	0.50
Rank	1	3	2

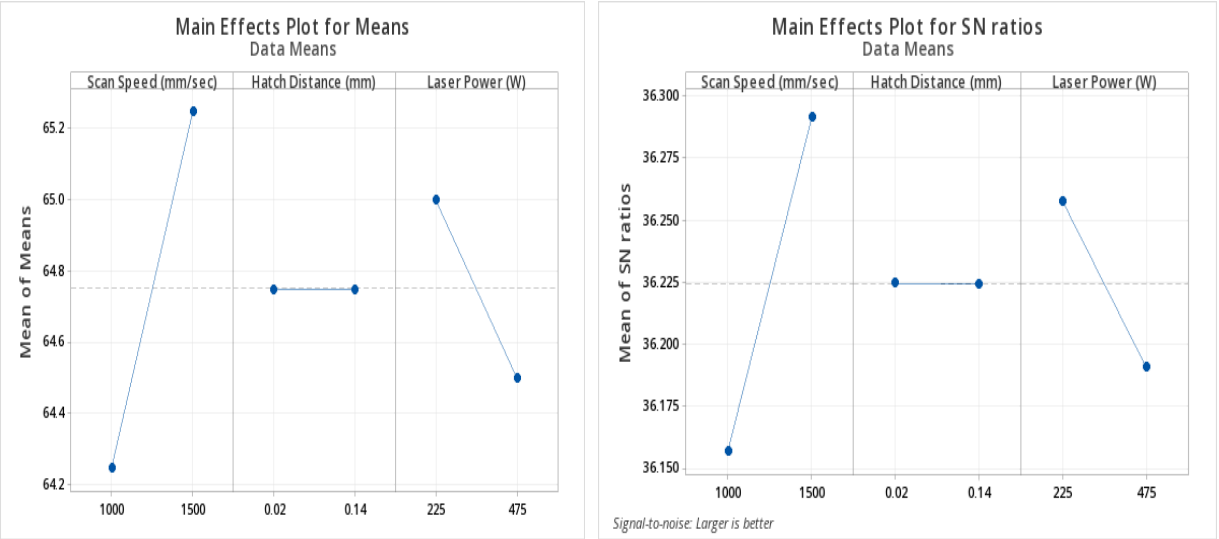

Fig. 4.7: Main Effects Plots for Means and SN Ratios for Star.

4.4.7 Octet

In the octet scaffold, scan speed (mm/s) demonstrates enormous disparity in contrast to hatch distance (µm) and laser power (W). The porosity is significantly affected by the scan speed and thus it is ranked 1 in the response tables for signal to ratio and means. The inclination of scan speed is more in the direction of the vertical axis i.e. displaying nonconformity from horizontal axis therefore establishing greater impact upon porosity. *Table 4.15 & 4.16* display the response table for signal to noise ratio and means whereas *Fig. 4.8* denotes the main effect plots for signal to noise ratio and means. In this octet scaffold, hatch distance and laser power are ranked similar.

Table 4.15 - Response Table for Signal to Noise Ratios.

Level	Scan Speed (mm/s)	Hatch Distance (µm)	Laser Power (W)
1	35.95	36.10	36.14
2	36.29	36.14	36.10
Delta	0.35	0.03	0.03
Rank	1	2.5	2.5

Table 4.16 - Response Table for Means.

Level	Scan Speed (mm/s)	Hatch Distance (µm)	Laser Power (W)
1	62.70	63.85	64.10
2	65.25	64.10	63.85
Delta	2.55	0.25	0.25
Rank	1	2.5	2.5

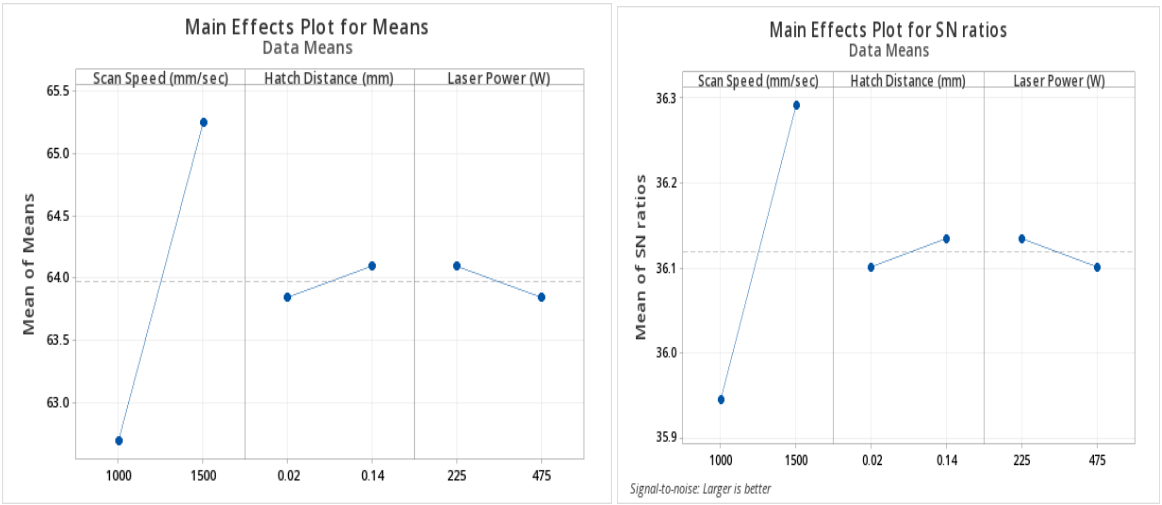

Fig. 4.8: Main Effects Plots for Means and SN Ratios for Octet.

4.5 EFFECT AND OPTIMISATION OF PROCESS PARAMETERS DURING SLM

The characteristics of AM porous scaffolds are influenced by various input process parameters during the SLM process. The improvement of density is the main concern for the porous scaffolds manufactured by SLM. Fully dense struts are also desirable in

porous scaffolds. Furthermore, because of the severe non-equilibrium conditions during SLM, a unique microstructure has been observed. This is due to the rapid cooling of the melt pool during the process, which causes the variation of mechanical properties.

All the seven samples are fabricated by a SLM machine (Model: EOSINT M280-400W) with the following input process parameters for Ti-6Al-4V materials as shown in *Table 4.17*.

Table 4.17 - Input process parameters generally used for porous Ti-6Al-4V scaffolds during SLM process.

Parameters	**Value**
Type of Laser	Ytterbium Fibre Laser
Shape of Spot	Spherical
Scan Speed (SS)	800-1500 mm/s
Diameter of Particle (PD)	80 μm
Hatch Distance (HD)	0.1- 0.14 mm
Power of Laser (LP)	217- 400 W
Diameter of Laser (LD)	80 micron
Density (ρ)	4.41 g/cm^3
Thickness of Layer (LT)	60 μm
Initial Temp. of Bed (T_i)	35^{0}C
Scan Angle of Rotation	67^0
Building Space	200 mm x 200 mm x 200 mm
Environment Maintained	Inert
Scan Path	"X" & Rotational

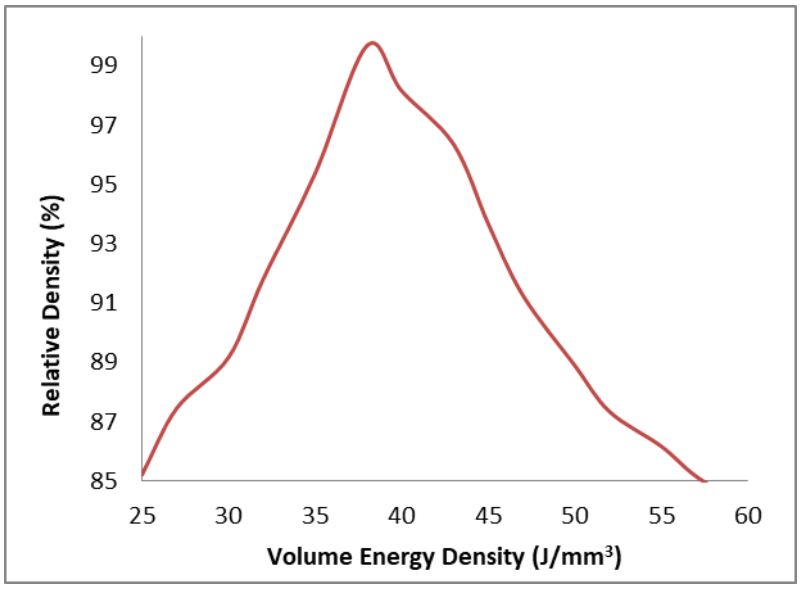

Fig. 4.9: Variation of relative density (%) with volume energy density (J/mm^3).

It has been observed from *Fig. 4.9* that the effects of process parameters (such as laser power, scan speed, and hatch distance) on relative density of Ti-6Al-4V samples made using SLM and the scanning speed has also a significant effect on relative density. Now an optimization study is required to determine the ideal processing parameters for achieving the desired density during fabrication by SLM (*Junfeng and Zhengying, 2017*). The goal is to achieve maximum density with no restrictions on process parameters. To determine the suitable process parameters, an optimization study is required for achieving the desired density during fabrication by SLM, are optimized using Minitab software as shown in *Table 4.18*.

Table 4.18 - Optimized process parameters and build system of Ti-6Al-4V during SLM.

Parameters	Result
Scan Speed (SS)	1250 mm/s
Laser Power (LP)	340 W
Hatch Distance (HD)	0.12 mm
Layer Thickness (LT)	60 µm
Particle Diameter (PD)	80 µm

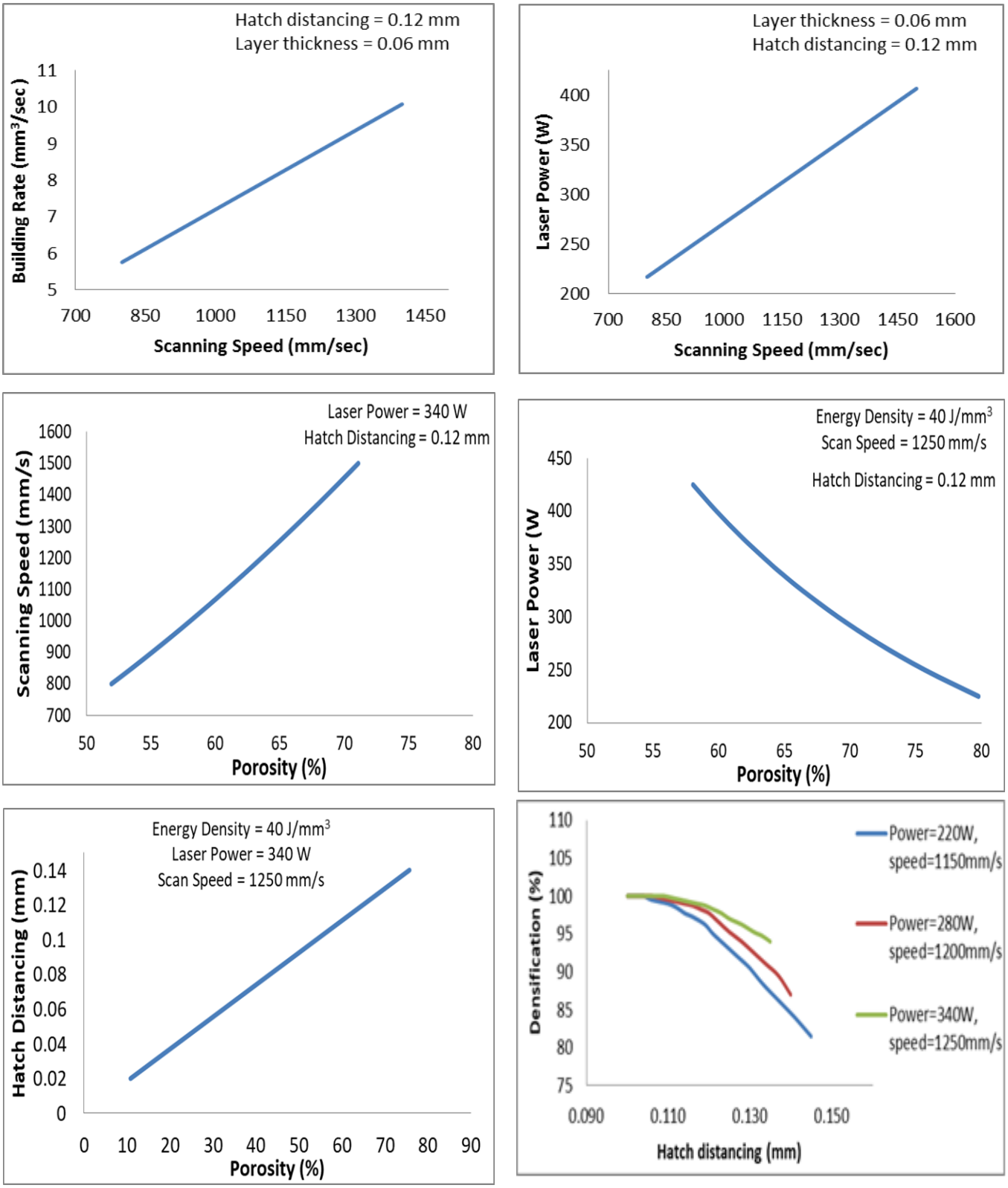

Fig. 4.10: Effect of input process parameters during fabrication by SLM.

The density of the scaffolds play a key role to optimize the process parameters since it has a direct impact on the mechanical, physical and also biological properties of the part. The relationship between relative density and the product of three factors is characterized as volume energy density (VED) and expressed as Equation No. (3.1). *Fig. 4.9* shows the relationship between relative density and VED. The relative density first increased, and then decreased as VED increased. The relative density reaches its highest value, which is close to 100%, when the VED is around 40 J/mm^3. From *Fig. 4.10*, it is observed that with increase in scanning speed, hatch distancing and layer thickness, the porosity percentage increases except laser power obtained from Equation No. (3.4). When the ratio of laser power and scan speed is too low, the melting channel depth is reduced and spheroidization occurs, resulting in poor bonding between the layers and un-melted powder particles, resulting in a low relative density. And when the ratio of laser power and scan speed is too high, the melting track depth is increased, the height is small, making it difficult to form, and the phenomena of element evaporation and ablation is easy to occur during the forming process, resulting in density reduction. Increase in hatch distance resulting partial melting of the powder and inclusion. As a result, only the appropriate ratio of laser power to scan speed and hatch distance may achieve higher relative density and are optimized at 0.272 J-mm and 0.12 mm respectively.

Using simulations (combination of selective process parameters like energy density, relative density, laser power, scan speed, layer thickness and hatch distancing), similar studies might be done to investigate how hatch spacing affects densification. In *Fig. 4.10*, densifications observed by changing hatch spacing from 10 μm to 140 μm for various laser power and scanning speed combinations. And it is found that the increasing hatch distancing results in inadequate melt pool overlap, which leads to poor compaction between neighbouring scan tracks, leading in lower densifications. From result, it can also be seen that higher hatch spacing up to 120 μm can be used to achieve high densification upto 99.5% but at a significantly lower combination of laser power (220 W) and scanning speed (1150 mm/s), the lower speed allowing enough time for heat build up results in proper melting and compacting of material. To get a higher densification, a higher building rate is desired then a higher value power (340 W) and speed (1250 mm/s) with a hatch spacing of 120 μm can be employed. As a result, the simulation model allows us to make an accurate choice regarding the optimum range of process parameters to utilize ahead of time and reduce the need for

prolonged testing.

Aside from the machining input process parameters, there are a number of scaffold design factors that have a significant effect on mechanical and biological properties. Pore morphology, unit cell shape, and strut thickness are factors to consider. From *Fig. 10*, it is observed that the process parameters are the most important factors which affect the porosity of SLM-fabricated samples.

4.6 COMPRESSION TEST

The stress-strain curve is plotted from the received data shown in *Fig. 4.11*. The effective elastic moduli of scaffolds are measured by the slope of the graph obtained from compression test on an INSTRON machine and listed in *Table 4.19*.

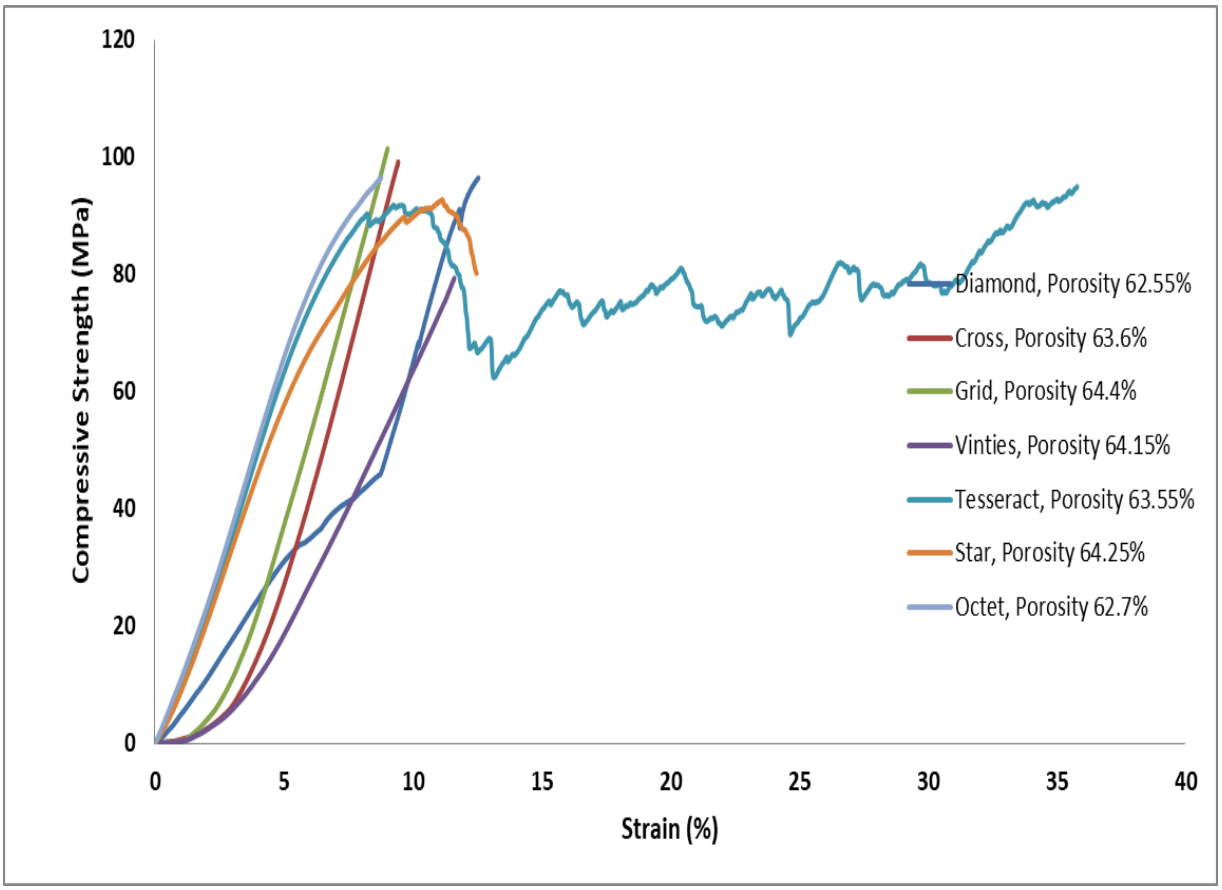

Fig. 4.11: Compressive stress-strain curve of porous Ti-6Al-4V scaffolds obtained from INSTRON.

Table 4.19 - Mechanical properties of manufactured porous Ti-6Al-4V scaffolds and natural cortical bones.

Scaffolds Type	Actual Porosity %	Pore Size (μm^2)	Strut Thickness (µm)	UCS (MPa)	E (GPa)
Diamond	62.55	586787.302	496.929	96.41	6.5
Cross	63.6	4253703.533	601.184	98.42	11.15
Grid	64.4	2417618.517	740.249	101.39	10.33
Vinties	64.14	1290453.750	485.438	95.63	7.16
Tesseract	63.55	4783524.141	451.570	94.92	5.87
Star	62.45	2484045.93	407.651	92.71	7.9
Octet	62.7	1175303.449	467.599	96.49	11.16
Natural bones	-	-	-	0.45 - 25.8	3 - 30

Elastic modulus and compressive strength values for the diamond, grid, cross, vinties, tesseract, star, and octet scaffolds are 6.5 GPa, 11.15 GPa, 10.33 GPa, 7.16 GPa, 5.87 GPa, 7.9 GPa & 11.16 GPa and 96.41 MPa, 98.42 MPa, 101.39 MPa, 95.63 MPa, 94.92 MPa, 92.71 MPa & 96.49 MPa. Pore area and strut thickness of the tested scaffolds using the same stereo microscope are shown in *Fig. 4.12*.

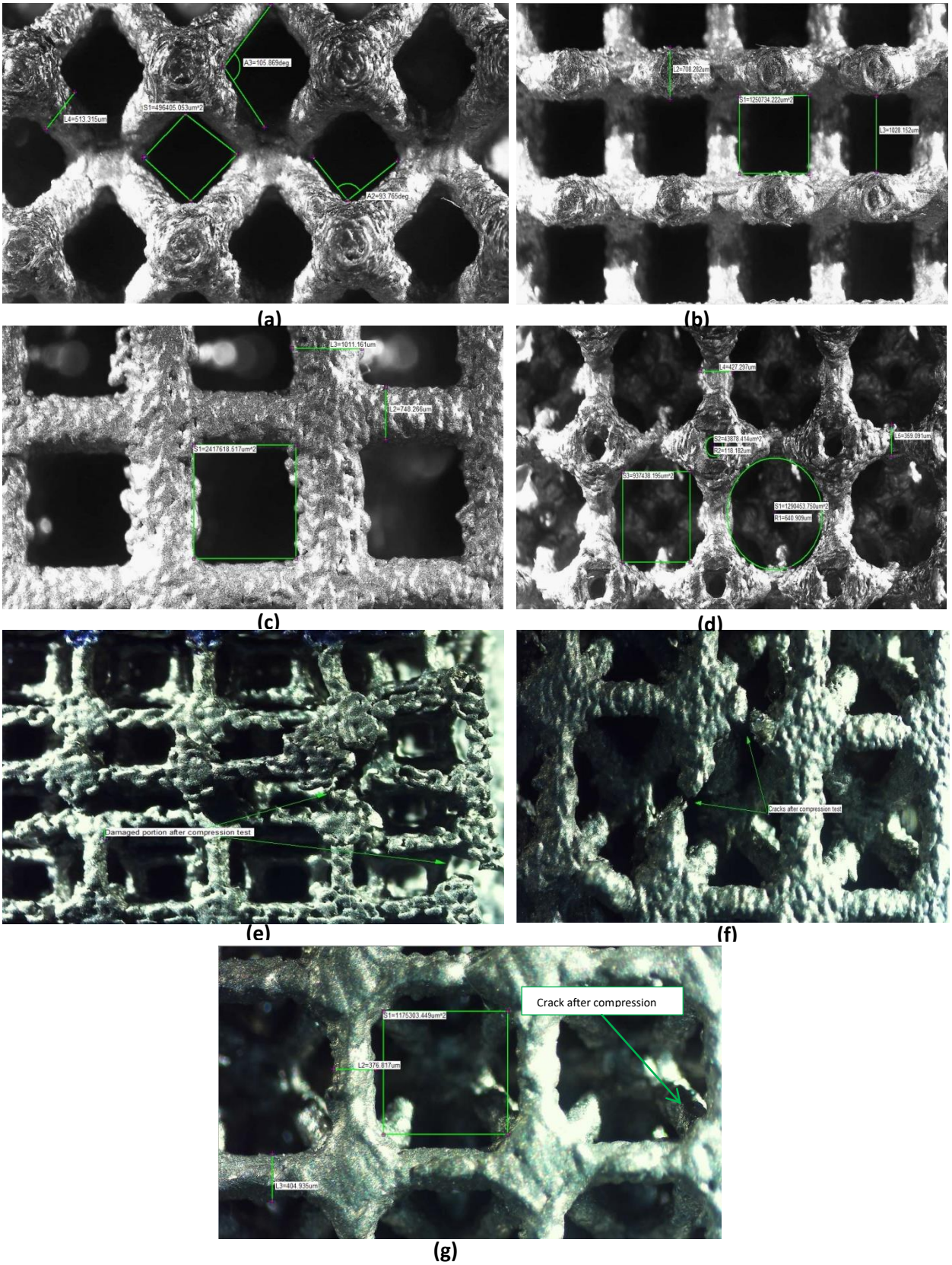

Fig. 4.12: Measurement of pore area and strut thickness using stereo microscope (Stemi 508) of the tested scaffolds: (a) Diamond, (b) Cross, (c) Grid, (d) Vinties, (e) Tesseract, (f) Star & (g) Octet.

For grid type sample, the greatest value of compressive strength (101.39 MPa) and average elastic modulus (10.33 GPa) was observed. The results show that the grid samples are slightly hard at first due to their form, but when additional load is applied, they become soft and strain increases. The octet type sample has the greatest elastic modulus value (11.16 GPa). But tesseract, star and octet scaffolds don't meet the biomedical needs as metallic implants in case of compressive load of 25 kN and above as they are fractured. On the other hand, diamond, cross, grid and vinties scaffolds were remain unchanged even after compressive loading of 25 kN due to their higher strut thickness as compared with tesseract, star and octet types and to reach the fracture point for these scaffolds additional load is required. The microstructure of all seven scaffolds at same compressive load is shown in *Fig. 4.11*. The manufactured scaffolds have a promising elastic modulus that is similar to natural cortical bones (E = 3 - 30 GPa [*Frosch et al., 2002*]) which will reduce the effect of stress-shielding. *Table 6* reveals that porous Ti64 scaffolds have higher compressive strength than bone (UCS = 0.45 - 25.8 MPa [*Ponader et al., 2008*]). The greater compressive strength lengthens the implant's life.

4.7 MECHANICAL PROPERTIES

Fig. 4.13 shows that when the porosity is around 60-70%, the Ti porous scaffolds have a value that is comparable to human bones. Mechanical property is inversely proportional to the porosity. With increase in porosity %, effective elastic modulus decreases. The theoretical effective elastic modulus may be determined using equation (7) and is equal to 13.475 GPa (assuming a Young's modulus of 110 GPa and a porosity of 65%), which is comparable to human bones (E = 3 – 30 GPa).

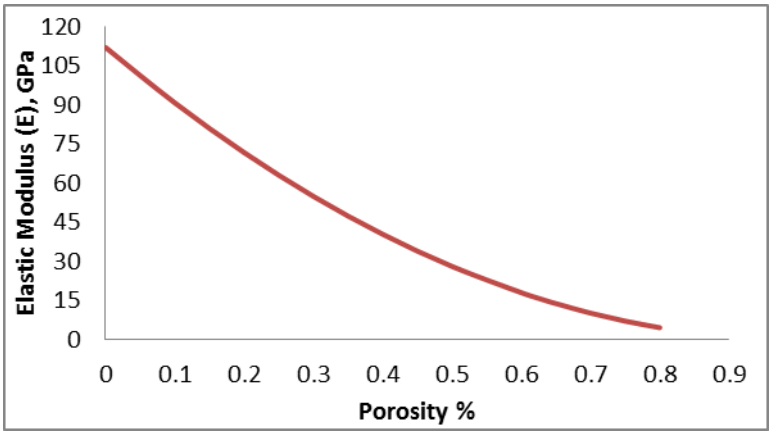

Fig. 4.13: The effect of porosity on elastic modulus.

The relative elastic modulus (modulus ratio of porous portion to solid part) and relative compressive strength (stress ratio of porous part to solid part) of the scaffolds with changing porosity are depicted in *Figs. 4.14 & 4.15*. As the percentage of porosity increases, the relative compressive strength and relative elastic modulus decreases. This relative compressive strength and relative elastic modulus can be used as a fast reference for the user-specific demand based on the needed strength of bone implant for the individual application.

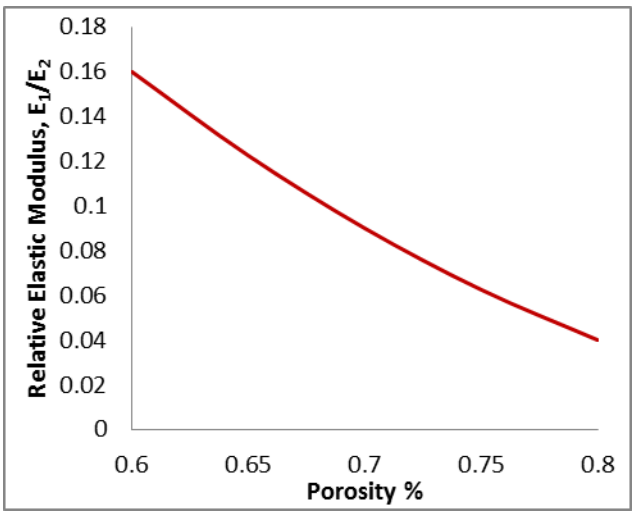

Fig. 4.14: Relative elastic modulus, E_1/E_2 vs Porosity %.

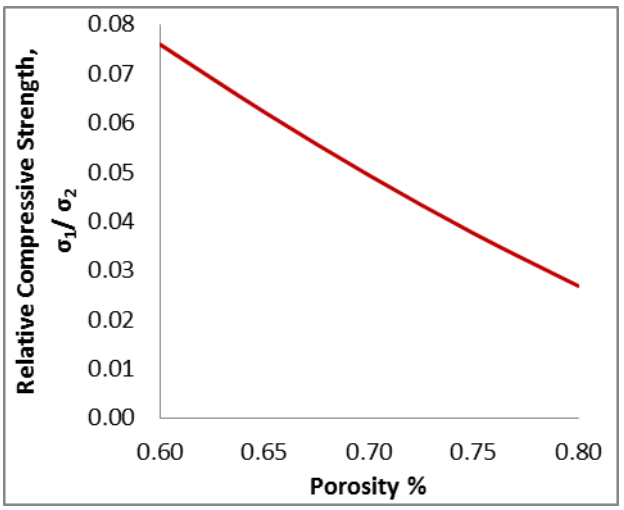

Fig. 4.15: Relative compressive strength, σ_1/σ_2 vs Porosity %.

4.8 FINITE ELEMENT SIMULATION

The STL files from Rhino 6 modeled scaffolds are imported into ANSYS (2019 R3 & 2020 R2) finite element software, and mesh refinements were created to produce accurate results. The meshed model was used to apply input parameters, with the lower surface of the porous scaffolds fixed and a 25 kN compressive force evenly distributed on the top surface. A SOLID187 3-D element of higher order is considered due to its efficiency in handling complex geometries. It exhibits quadratic displacement characteristics and is particularly effective for simulating irregular meshes, often generated by different CAD/CAM systems. Each of its nodes is defined by three degrees of freedom: translation along the x, y, and z axes.

4.8.1 Mesh convergence study

Mesh convergence studies are performed for each seven types of scaffolds separately. The converged mesh sizes are considered for the further analysis. The porous Ti-6Al-4V scaffolds meshed and analysed with different mesh sizes to get the optimal mesh size. Starting with a coarse mesh, the analysis calculates key mechanical parameters such as von Mises stresses, strain distribution, and displacements. A too-coarse mesh may yield inaccurate results, while an overly fine mesh escalates computational demands without significantly improving accuracy. The results from the convergerd mesh sizes are then compared to experimental data or established analytical solutions to validate the model. Mesh convergence studies for the numerical simulation are shown in Table 4.20.

Table 4.20 - Mesh convergence study for the numerical simulation.

Sl No	Scaffold Type	Element Type	Total Element Count (Nos)	Maximum Von Mises Stress (MPa)	Comments
1		SOLID187	187025	97.350	
2		SOLID187	235487	96.050	
3	Diamond	SOLID187	299365	95.835	
4		SOLID187	**326599**	**95.077**	Considered for further analysis
5		SOLID187	353256	95.076	
1		SOLID187	186025	99.219	
2		SOLID187	236487	97.894	
3	Cross	SOLID187	289365	97.675	
4		SOLID187	**322725**	**96.902**	Considered for further analysis
5		SOLID187	353256	96.901	
1		SOLID187	187021	102.606	
2		SOLID187	236485	101.236	
3	Grid	SOLID187	297457	101.009	
4		SOLID187	**328157**	**100.210**	Considered for further analysis
5		SOLID187	350256	100.209	
1		SOLID187	187025	95.215	
2		SOLID187	235487	93.944	
3	Vinties	SOLID187	298543	93.733	
4		SOLID187	**326935**	**92.992**	Considered for further analysis
5		SOLID187	353256	93.191	
1		SOLID187	187025	90.993	
2		SOLID187	235487	89.777	
3	Tesseract	SOLID187	299365	89.576	
4		SOLID187	**328157**	**88.868**	Considered for further analysis
5		SOLID187	359215	88.967	
1	Star	SOLID187	187025	85.821	

2		SOLID187	235487	84.675	
3		SOLID187	297315	84.485	
4		SOLID187	**336595**	**83.817**	Considered for further analysis
5		SOLID187	353256	83.816	
1		SOLID187	187025	86.365	
2		SOLID187	235487	85.014	
3	Octet	SOLID187	295313	84.824	
4		SOLID187	**322513**	**84.153**	Considered for further analysis
5		SOLID187	363252	84.152	

The convereged mesh size as shown in the *Table 4.20* provides guidance for future FEA simulations on similar porous scaffolds under compressive loads. the mesh size that are considered for the further analysis are also shown in the table. It ensures reliable results are obtained without excessive computational resources, optimizing the analysis process for engineering applications.

4.8.2 Result analysis

The experimental results validated the FE analysis, as shown in *Fig. 4.16*. For the diamond, cross, grid, vinties, tesseract, star, and octet, the Ansys simulation of maximum Von-Mises stresses and strain percent of modelled scaffolds yielded 95.07 MPa, 96.90 MPa, 100.21 MPa, 92.99 MPa, 88.86 MPa, 83.38 MPa & 84.15 MPa, and 12.07%, 13.00%, 8.28%, 9.15%, 8.8%, 9.19% and 10.35% respectively. The findings from both the compressive test and the finite element analysis software are identical for each kind of scaffold.

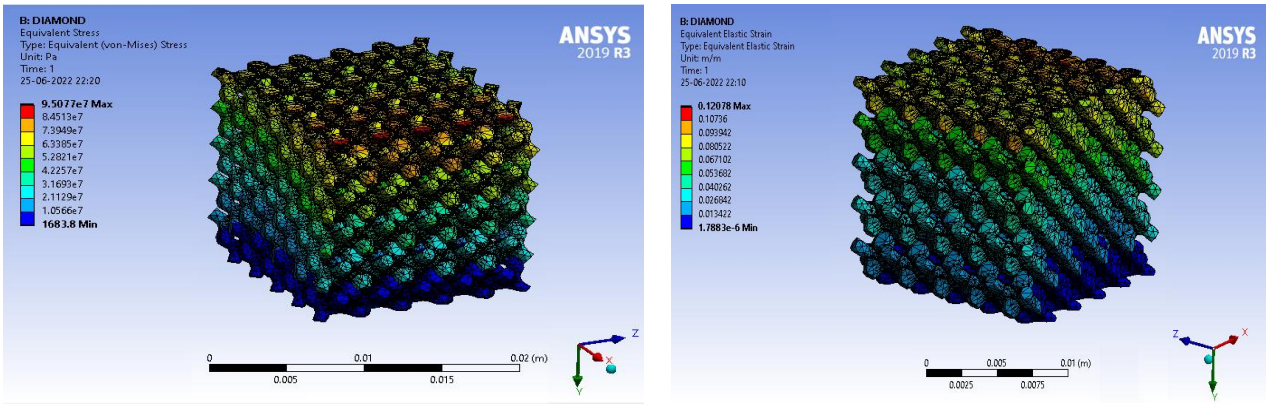

(a)

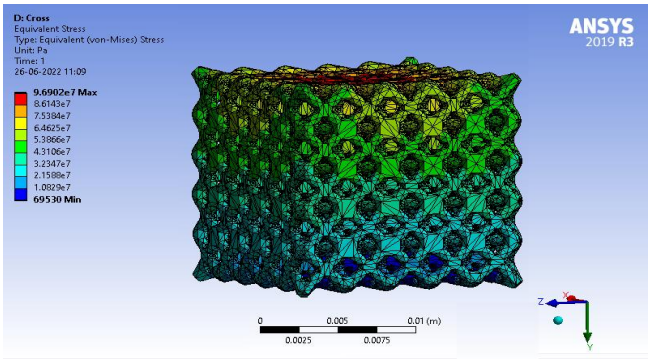
D: Cross
Equivalent Stress
Type: Equivalent (von-Mises) Stress
Unit: Pa
Time: 1
26-06-2022 11:09
9.6902e7 Max
8.6143e7
7.5384e7
6.4625e7
5.3866e7
4.3106e7
3.2347e7
2.1588e7
1.0829e7
69530 Min
ANSYS
2019 R3

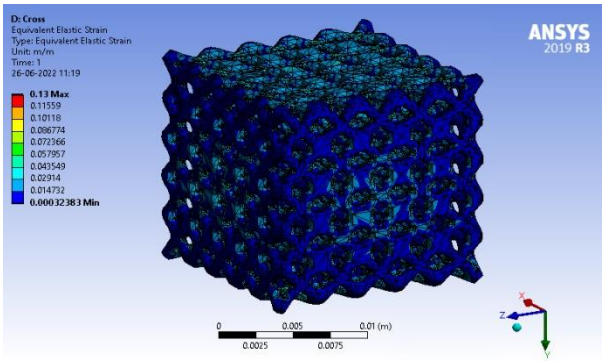
D: Cross
Equivalent Elastic Strain
Type: Equivalent Elastic Strain
Unit: m/m
Time: 1
26-06-2022 11:19
0.13 Max
0.11559
0.10118
0.086774
0.072366
0.057957
0.043549
0.02914
0.014732
0.00032383 Min
ANSYS
2019 R3

(b)

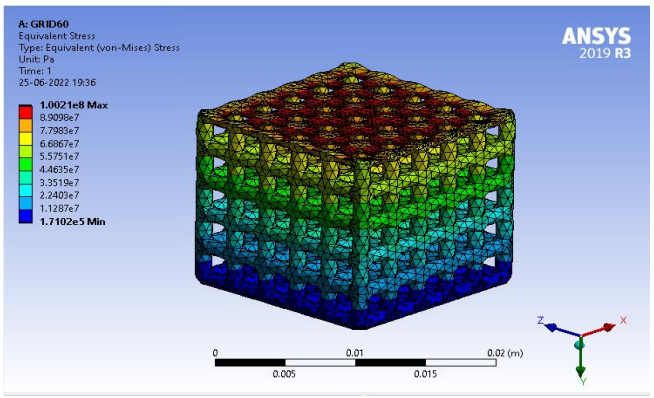
A: GRID60
Equivalent Stress
Type: Equivalent (von-Mises) Stress
Unit: Pa
Time: 1
25-06-2022 19:36
1.0021e8 Max
8.9098e7
7.7983e7
6.6867e7
5.5751e7
4.4635e7
3.3519e7
2.2403e7
1.1287e7
1.7102e5 Min
ANSYS
2019 R3

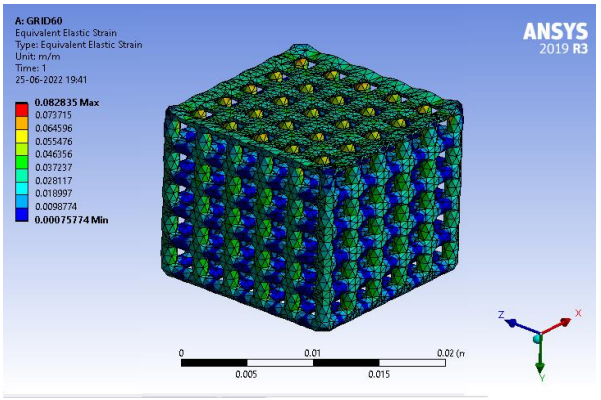
A: GRID60
Equivalent Elastic Strain
Type: Equivalent Elastic Strain
Unit: m/m
Time: 1
25-06-2022 19:41
0.082835 Max
0.073715
0.064596
0.055476
0.046356
0.037237
0.028117
0.018997
0.0098774
0.00075774 Min
ANSYS
2019 R3

(c)

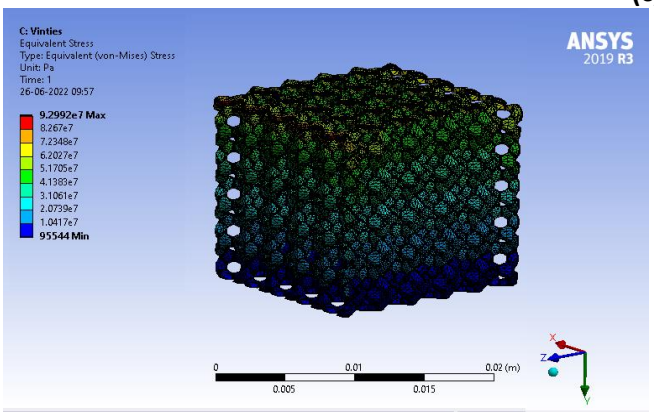
C: Vinties
Equivalent Stress
Type: Equivalent (von-Mises) Stress
Unit: Pa
Time: 1
26-06-2022 09:57
9.2992e7 Max
8.267e7
7.2348e7
6.2027e7
5.1705e7
4.1383e7
3.1061e7
2.0739e7
1.0417e7
95544 Min
ANSYS
2019 R3

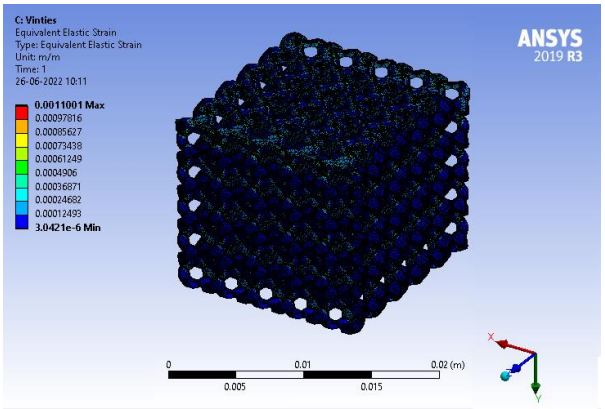
C: Vinties
Equivalent Elastic Strain
Type: Equivalent Elastic Strain
Unit: m/m
Time: 1
26-06-2022 10:11
0.0011001 Max
0.00097816
0.00085627
0.00073438
0.00061249
0.0004906
0.00036871
0.00024682
0.00012493
3.0421e-6 Min
ANSYS
2019 R3

(d)

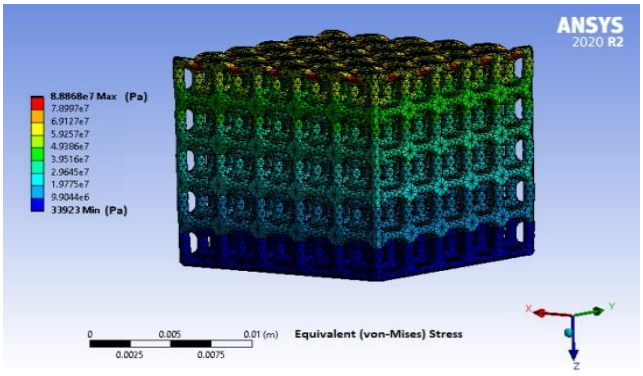
8.8868e7 Max (Pa)
7.8997e7
6.9127e7
5.9257e7
4.9386e7
3.9516e7
2.9645e7
1.9775e7
9.9044e6
33923 Min (Pa)
Equivalent (von-Mises) Stress
ANSYS
2020 R2

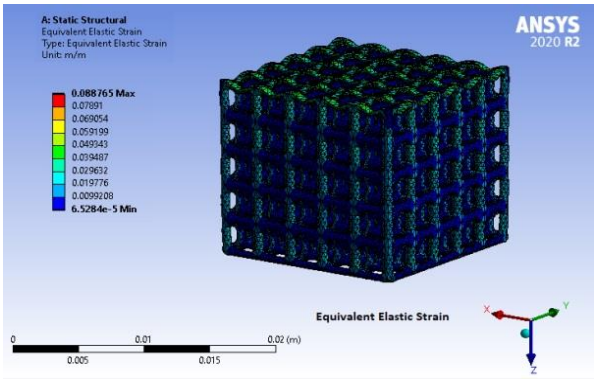
A: Static Structural
Equivalent Elastic Strain
Type: Equivalent Elastic Strain
Unit: m/m
0.088765 Max
0.07891
0.069054
0.059199
0.049343
0.039487
0.029632
0.019776
0.0099208
6.5284e-5 Min
Equivalent Elastic Strain
ANSYS
2020 R2

(e)

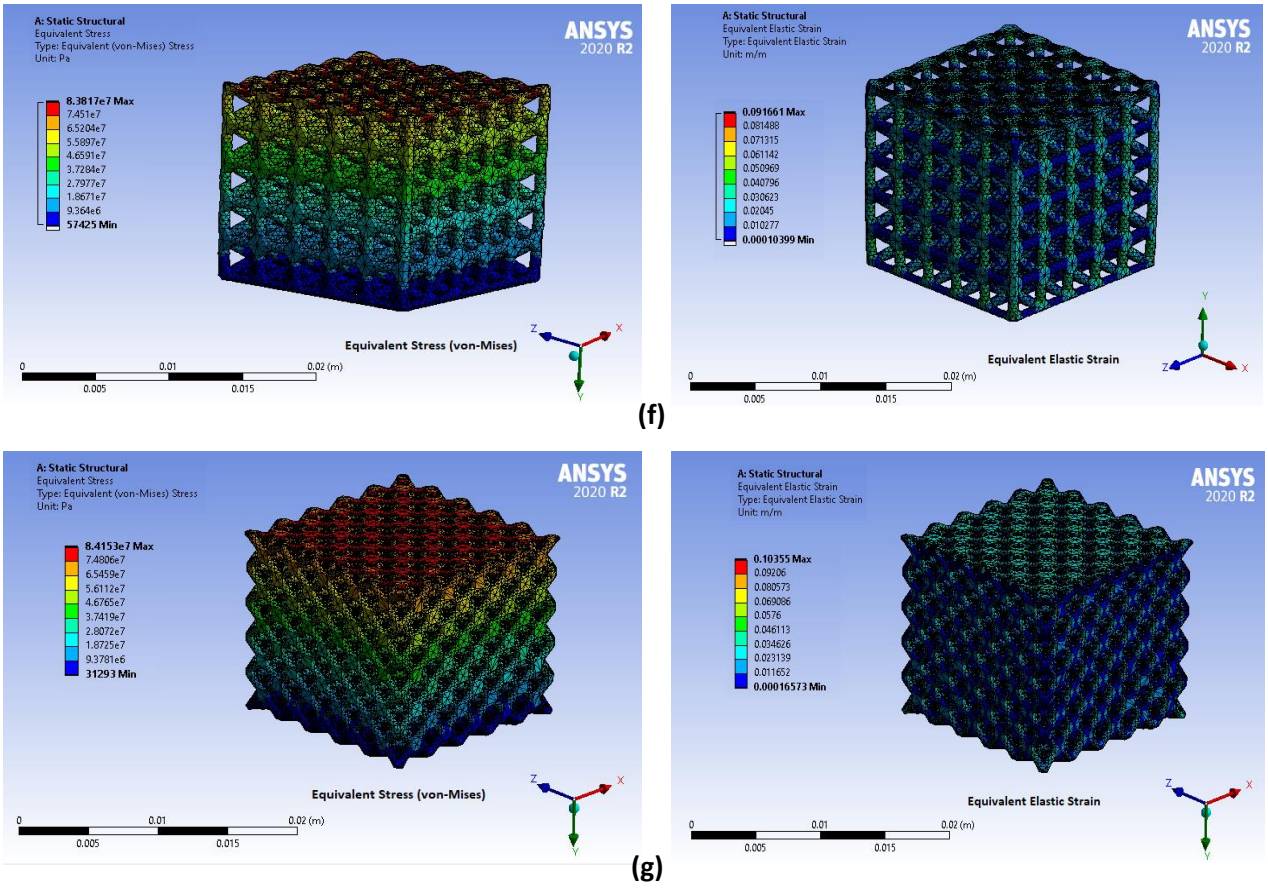

Fig. 4.16: Finite element simulations of designed porous scaffolds by Ansys 2020 R2: (a) Diamond, (b) Cross, (c) Grid, (d) Vinties, (e) Tesseract, (f) Star & (g) Octet.

The significant differences of the results obtained from compressive test and finite element analysis software are due to slightly changes in dimensions and porosity of the fabricated sacffolds than the designed models because of the metal powders are attached to the wire surface.

4.9 SUMMARY

As we illustrated, titanium cellular structures with the stiffness values suggested in this work could be successfully produced by additive manufacturing methods. The optimal strut thicknesses and pore sizes of the interior architecture that produce the desired stiffness will be found by examining the titanium porous structures with different unit cells.

The application of FEA for forecasting the mechanical characteristics of Ti-6Al-4V porous structures was constrained by unexpected surface imperfections brought on by SLM manufacturing procedures. Since there is no established standard procedure, substantial

variances are anticipated from the various melting settings and machine effectiveness. As a result, physical testing seems to be the primary way for validating the mechanical properties of the laser-melted porous structures during an early stage of SLM production procedures. FEA findings typically overestimate the stiffness of porous structures.

The probability of structural failure will rise since the compressive characteristics of Ti-6Al-4V porous structures showed similar stiffness (6.5 - 11.16 GPa) but higher compressive strength (92.71 - 101.39 MPa) than those of bone. As a result, Ti-6Al-4V porous scaffolds would be perfect for replacing bone components that require strength, such as inter-spinal cages and long-bone defects.

CHAPTER 5

CONCLUSIONS

5.1 CONCLUSION AND REMARKS

It is usually preferable to create bone implants that can replicate both the macro and microstructures of real bones. It is possible to create porous structures with suitable unit cells, pore size, surface area, and porosity that have balanced mechanical and biological properties from multi-scale structures. In addition, porous bone implants are anticipated to retain the necessary mechanical strength while reducing stress shielding on the bone tissue around the implant.

The selective laser melting (SLM) technology is used to create porous Ti-6Al-4V scaffolds for biological purposes. For the acceptability of a biomedical implant, porosity, surface roughness, and mechanical compression tests are done. To employ the porosity deviated scaffold, the relative elastic modulus is also investigated. Optimization and microscopic studies of the fabricated scaffolds were also performed. The following findings may be drawn from the current work:

i. Rhino 6 software is used to design seven distinct porous Ti64 scaffolds (each of two, n = 14 scaffolds) with 65% porosity, which are then manufactured using AM, specifically SLM.

ii. The porous scaffolds were heat treated at 900^0C for 2 hours in an inert environment, then cooled at ambient temperature in a furnace to enhance mechanical properties.

iii. The grid type sample has the least amount of surface roughness, but the diamond type sample has a greater value of surface roughness.

iv. The grid type sample has the lowest error % of porosity difference, whereas the diamond type has the highest, and the grid type sample may produce better likeness with the lowest deviation.

v. The elastic modulus of Ti alloy scaffolds with 60–70% porosity is comparable to that of human bones resulting reduces the effect of stress-shielding.

vi. When volume energy density (VED) is 40 J/mm^3, the relative density reaches its highest value, which is close to 100%.

vii. The porosity % increases with an increase in scanning speed, hatch distancing, layer thickness and decreases with laser power.

viii. The mechanical properties are influenced by the porosity % of scaffolds. The effective elastic modulus and relative compressive strength decrease as the porosity percentage increases.

ix. The process parameters have a significant impact on the relative density of Ti64 scaffolds manufactured by SLM. By optimising the process parameters, the microstructure of porous Ti64 alloy scaffolds may be controlled by SLM, which are: 340 W laser power, 1250 mm/s scanning speed, 0.12 mm powder layer thickness, and 0.06 mm hatch spacing.

x. For grid type scaffolds with a height strut thickness of 740.249 µm, the greatest ultimate compressive strength was determined to be 101.39 MPa, which is much more than human bones resulting in improved implant.

xi. Titanium alloys have been successfully linked in biomedical sectors due to additive manufacturing technologies, which have the capacity to construct any complicated porous scaffold for biomedical applications, and so serve to give further support for material engineers and prospective designers.

3D printed implants have significant benefits as patient specific customized implants can be printed based on need and urgency in situation. Unique mechanical and biological properties of Ti-6Al-4V porous scaffolds structures can successfully replace the solid implants including hip replacement or bone replacement. The rapid development of AM technology will enhance the lead time of implant.

5.2 SCOPE OF FUTURE WORK

Future study in the following areas is advised to advance the development of bone-biomimetic implants with porous interior architecture:

i. Recent statistical modeling of lattice structure manufacturing utilizing SLM has revealed the essential processing factors influencing lattice structure attributes. To validate the effects, the work might be expanded to include thermal modeling of thin struts or the entire three- dimensional (3D) lattice systems. The experimental data acquired in this study may then be used to validate the thermal models.

ii. Apatite forming ability, live/dead viability cytotoxicity, and alkaline phosphatase activity can be used to gain further biological responses. The dynamic habitat could also be employed since the behaviour of planted cells on scaffolds differs in static and dynamic environments.

iii. Histological tests may be performed to determine the path travelled by cells in vitro to penetrate the scaffolds.

iv. More testing about the physical and biocompatible qualities is necessary to have a better understanding of the possibilities for this innovative method in producing porous Ti scaffolds forhard tissue engineering.

v. Enhance the accuracy of findings by adhering to orthopedic implant testing standards to guarantee accurate and consistent testing. Examine the scaffolds' additional mechanical qualities and their potential for hard tissue engineering.

vi. To assure their strength after implantation, it is important to look at the fatigue behaviours of porous structures and their internal design, which achieved strength and load-sharing capability under static loading condition.

vii. For this study, internal unit architectures and porous structures were designed and characterized. In diverse designs of laser-melted graded cellular structures, the parameter requirements for the characteristics of bone osseointegration and functions remain unknown. In vivo bone osseointegration of these porous structures requires more research to be fully understood.

REFERENCES

1. Abbasi N, Hamlet S, Love RM, Nguyen NT. Porous scaffolds for bone regeneration. Journal of science: advanced materials and devices. 2020 Mar 1;5(1):1-9.

2. Abe F, Costa Santos E, Kitamura Y, Osakada K, Shiomi M. Influence of forming conditions on the titanium model in rapid prototyping with the selective laser melting process. Proceedings of the Institution of Mechanical Engineers, Part C: Journal of Mechanical Engineering Science. 2003 Jan 1;217(1):119-26.

3. Ahmadi SM, Campoli G, Yavari SA, Sajadi B, Wauthlé R, Schrooten J, Weinans H, Zadpoor AA. Mechanical behavior of regular open-cell porous biomaterials made of diamond lattice unit cells. Journal of the mechanical behavior of biomedical materials. 2014 Jun 1;34:106-15.

4. Ahmadi SM, Hedayati R, Jain RA, Li Y, Leeflang S, Zadpoor AA. Effects of laser processing parameters on the mechanical properties, topology, and microstructure of additively manufactured porous metallic biomaterials: A vector-based approach. Materials & Design. 2017 Nov 15;134:234-43.

5. Akbarzadeh R, Minton JA, Janney CS, Smith TA, James PF, Yousefi AM. Hierarchical polymeric scaffolds support the growth of MC3T3-E1 cells. Journal of Materials Science: Materials in Medicine. 2015 Feb;26:1-2.

6. Al Muderis M, Bohling U, Grittner U, Gerdesmeyer L, Scholz J. Cementless total hip arthroplasty using the Spongiosa-I fully coated cancellous metal surface: a minimum twenty-year follow-up. JBJS. 2011 Jun 1;93(11):1039-44.

7. Albrektsson T, Johansson C. Osteoinduction, osteoconduction and osseointegration. European spine journal. 2001 Oct;10(Suppl 2):S96-101.

8. Alishiri M, Shojaei A, Abdekhodaie MJ. Biodegradable polyurethane acrylate/HEMA-grafted nanodiamond composites with bone regenerative potential applications: structure, mechanical properties and biocompatibility. RSC advances. 2016;6(11):8743-55.

9. Amado A, Schmid M, Levy G, Wegener K. Advances in SLS powder

characterization.

10. Arabnejad Khanoki S, Pasini D. Multiscale design and multiobjective optimization of orthopedic hip implants with functionally graded cellular material.

11. Asaoka K, Kuwayama N, Okuno O, Miura I. Mechanical properties and biomechanical compatibility of porous titanium for dental implants. Journal of biomedical materials research. 1985 Jul;19(6):699-713.

12. Ascenzi A, Bonucci E, BENVENUTI MA. Relationship between ultrastructure and "pin test" in osteons. Clinical Orthopaedics and Related Research®. 1976 Nov 1(121):275-94.

13. Ashraf Imam M, Froes FS. Low cost titanium and developing applications. Jom. 2010 May;62:17-20.

14. Attar H, Bermingham MJ, Ehtemam-Haghighi S, Dehghan-Manshadi A, Kent D, Dargusch MS. Evaluation of the mechanical and wear properties of titanium produced by three different additive manufacturing methods for biomedical application. Materials Science and Engineering: A. 2019 Jul 8;760:339-45.

15. Attar H, Calin M, Zhang LC, Scudino S, Eckert J. Manufacture by selective laser melting and mechanical behavior of commercially pure titanium. Materials Science and Engineering: A. 2014 Jan 21;593:170-7.

16. Attar H, Prashanth KG, Chaubey AK, Calin M, Zhang LC, Scudino S, Eckert J. Comparison of wear properties of commercially pure titanium prepared by selective laser melting and casting processes. Materials Letters. 2015 Mar 1;142:38-41.

17. Ayers RA, Wolford LM, Bateman TA, Ferguson VL, Simske SJ. Quantification of bone ingrowth into porous block hydroxyapatite in humans. Journal of Biomedical Materials Research: An Official Journal of The Society for Biomaterials, The Japanese Society for Biomaterials, and The Australian Society for Biomaterials and the Korean Society for Biomaterials. 1999 Oct;47(1):54-9.

18. Bagheri ZS, Melancon D, Liu L, Johnston RB, Pasini D. Compensation strategy to reduce geometry and mechanics mismatches in porous biomaterials built with Selective Laser Melting. Journal of the mechanical behavior of biomedical materials.

2017 Jun 1;70:17-27.

19. Bahrami M, Fathi MH, Ahmadian M. The effect of nanobioceramic reinforcement on mechanical and biological properties of Co-base alloy/hydroxyapatite nanocomposite. Materials Science and Engineering: C. 2015 Mar 1;48:572-8.

20. Bai Y, Gai X, Li S, Zhang LC, Liu Y, Hao Y, Zhang X, Yang R, Gao Y. Improved corrosion behaviour of electron beam melted Ti-6Al–4V alloy in phosphate buffered saline. Corrosion Science. 2017 Jul 15;123:289-96.

21. Bandyopadhyay A, Espana F, Balla VK, Bose S, Ohgami Y, Davies NM. Influence of porosity on mechanical properties and in vivo response of Ti6Al4V implants. Acta biomaterialia. 2010 Apr 1;6(4):1640-8.

22. Bank NB. Aging of bobe tissue: Mechanical properties. vol. 8. 1960.

23. Barbas A, Bonnet AS, Lipinski P, Pesci R, Dubois G. Development and mechanical characterization of porous titanium bone substitutes. Journal of the mechanical behavior of biomedical materials. 2012 May 1;9:34-44.

24. Barui S, Chatterjee S, Mandal S, Kumar A, Basu B. Microstructure and compression properties of 3D powder printed Ti-6Al-4V scaffolds with designed porosity: Experimental and computational analysis. Materials Science and Engineering: C. 2017 Jan 1;70:812-23.

25. Bayraktar HH, Morgan EF, Niebur GL, Morris GE, Wong EK, Keaveny TM. Comparison of the elastic and yield properties of human femoral trabecular and cortical bone tissue. Journal of biomechanics. 2004 Jan 1;37(1):27-35.

26. Bidan CM, Kommareddy KP, Rumpler M, Kollmannsberger P, Fratzl P, Dunlop JW. Geometry as a factor for tissue growth: towards shape optimization of tissue engineering scaffolds. Advanced healthcare materials. 2013 Jan;2(1):186-94.

27. Biemond JE, Hannink G, Verdonschot N, Buma P. Bone ingrowth potential of electron beam and selective laser melting produced trabecular-like implant surfaces with and without a biomimetic coating. Journal of Materials Science: Materials in Medicine. 2013 Mar;24:745-53.

28. Bobbert FS, Lietaert K, Eftekhari AA, Pouran B, Ahmadi SM, Weinans H, Zadpoor

AA. Additively manufactured metallic porous biomaterials based on minimal surfaces: A unique combination of topological, mechanical, and mass transport properties. Acta biomaterialia. 2017 Apr 15;53:572-84.

29. Bobyn JD, Pilliar RM, Cameron HU, Weatherly GC. The optimum pore size for the fixation of porous-surfaced metal implants by the ingrowth of bone. Clinical Orthopaedics and Related Research®. 1980 Jul 1;150:263-70.

30. Bordjih K, Jouzeau JY, Mainard D, Payan E, Delagoutte JP, Netter P. Evaluation of the effect of three surface treatments on the biocompatibility of 316L stainless steel using human differentiated cells. Biomaterials. 1996 Jan 1;17(5):491-500.

31. Bose S, Ke D, Sahasrabudhe H, Bandyopadhyay A. Additive manufacturing of biomaterials. Progress in materials science. 2018 Apr 1;93:45-111.

32. Bowen PK, Drelich J, Goldman J. Zinc exhibits ideal physiological corrosion behavior for bioabsorbable stents.

33. Bram M, Schiefer H, Bogdanski D, Köller M, Buchkremer HP, Stöver D. Implant surgery: How bone bonds to PM titanium. Metal Powder Report. 2006 Feb 1;61(2):26-31.

34. Bram M, Stiller C, Buchkremer HP, Stöver D, Baur H. High-porosity titanium, stainless steel, and superalloy parts. Advanced engineering materials. 2000 Apr;2(4):196-9.

35. Breme HJ, Helsen JA. Selection of materials. Metals as biomaterials. 1998 Sep 1:1-35.

36. Breme J, Eisenbarth E, Biehl V. Titanium and its Alloys for Medical Applications, Titanium and Titanium Alloys.

37. Brenne F, Niendorf T, Maier HJ. Additively manufactured cellular structures: Impact of microstructure and local strains on the monotonic and cyclic behavior under uniaxial and bending load. Journal of Materials Processing Technology. 2013 Sep 1;213(9):1558-64.

38. Brunski J. Are oral implants stronger than natural teeth?. The International Journal of Oral & Maxillofacial Implants. 2004 Nov 1;19(6):801-2.

39. Burr DB, Martin RB. Errors in bone remodeling: toward a unified theory of metabolic bone disease. American Journal of Anatomy. 1989 Oct;186(2):186-216.

40. Campanelli SL, Contuzzi N, Ludovico AD, Caiazzo F, Cardaropoli F, Sergi V. Manufacturing and characterization of Ti6Al4V lattice components manufactured by selective laser melting. Materials. 2014 Jun 23;7(6):4803-22.

41. Cansizoglu O, Harrysson OL, Cormier D, West H, Mahale T. Properties of Ti–6Al–4V non-stochastic lattice structures fabricated via electron beam melting. Materials Science and Engineering: A. 2008 Sep 25;492(1-2):468-74.

42. Carter DR. Mechanical loading histories and cortical bone remodeling. Calcified tissue international. 1984 Mar;36(1):S19-24.

43. Challis VJ, Roberts AP, Grotowski JF, Zhang LC, Sercombe TB. Prototypes for bone implant scaffolds designed via topology optimization and manufactured by solid freeform fabrication. Advanced Engineering Materials. 2010 Nov;12(11):1106-10.

44. Challis VJ, Xu X, Zhang LC, Roberts AP, Grotowski JF, Sercombe TB. High specific strength and stiffness structures produced using selective laser melting. Materials & Design. 2014 Nov 1;63:783-8.

45. Cheah CM, Chua CK, Leong KF, Cheong CH, Naing MW. Automatic algorithm for generating complex polyhedral scaffold structures for tissue engineering. Tissue engineering. 2004 Mar 1;10(3-4):595-610.

46. Chen Q, Thouas GA. Metallic implant biomaterials. Materials Science and Engineering: R: Reports. 2015 Jan 1;87:1-57.

47. Chen Y, Zhang J, Dai N, Qin P, Attar H, Zhang LC. Corrosion behaviour of selective laser melted Ti-TiB biocomposite in simulated body fluid. Electrochimica Acta. 2017 Apr 1;232:89-97.

48. Chen Z, Yan X, Yin S, Liu L, Liu X, Zhao G, Ma W, Qi W, Ren Z, Liao H, Liu M. Influence of the pore size and porosity of selective laser melted Ti6Al4V ELI porous scaffold on cell proliferation, osteogenesis and bone ingrowth. Materials Science and Engineering: C. 2020 Jan 1;106:110289.

49. Cheng XY, Li SJ, Murr LE, Zhang ZB, Hao YL, Yang R, Medina F, Wicker RB. Compression deformation behavior of Ti–6Al–4V alloy with cellular structures fabricated by electron beam melting. Journal of the mechanical behavior of biomedical materials. 2012 Dec 1;16:153-62.

50. Chlebus E, Kuźnicka B, Kurzynowski T, Dybała B. Microstructure and mechanical behaviour of Ti—6Al—7Nb alloy produced by selective laser melting. Materials Characterization. 2011 May 1;62(5):488-95.

51. Choi K, Kuhn JL, Ciarelli MJ, Goldstein SA. The elastic moduli of human subchondral, trabecular, and cortical bone tissue and the size-dependency of cortical bone modulus. Journal of biomechanics. 1990 Jan 1;23(11):1103-13.

52. Chua CK, Chow KY. Generation of Three-dimensional Shapes in CAD/CAM Systems Using Art-to-part Technique. InComputer Aided and Integrated Manufacturing Systems: Volume 4: Computer Aided Design/Computer Aided Manufacturing (CAD/CAM) 2003 (pp. 1-33).

53. Chua CK, Leong KF, Sudarmadji N, Liu MJ, Chou SM. Selective laser sintering of functionally graded tissue scaffolds. MRS bulletin. 2011 Dec;36(12):1006-14.

54. Clemow R, Seah J. Collaborative working to improve the return of patients to their usual place of residence following fractured neck of femur. Journal of Orthopaedic Nursing. 2006 Feb 1;10(1):33-7.

55. Cools P, Declercq H, Ghobeira R, Morent R, De Geyter N. Acrylic acid plasma coatings for enhanced cell migration in PCL 3D additive manufactured scaffolds. Surface and Coatings Technology. 2018 Sep 25;350:925-35.

56. Cromwell PR, Field JV. BIBLIOGRAPHIE CRITIQUE-Mahtematiques-Polyhedra. One of the Most Charming Chapters of Geometry. Archives Internationales d'Histoire des Sciences. 1997;47(139):56-.

57. Currey JD. The design of mineralised hard tissues for their mechanical functions. Journal of Experimental Biology. 1999 Dec 1;202(23):3285-94.

58. Currey JD. The structure and mechanics of bone. Journal of Materials Science. 2012 Jan;47:41-54.

59. Dallago M, Fontanari V, Torresani E, Leoni M, Pederzolli C, Potrich C, Benedetti M. Fatigue and biological properties of Ti-6Al-4V ELI cellular structures with variously arranged cubic cells made by selective laser melting. Journal of the mechanical behavior of biomedical materials. 2018 Feb 1;78:381-94.

60. de Krijger J, Rans C, Van Hooreweder B, Lietaert K, Pouran B, Zadpoor AA. Effects of applied stress ratio on the fatigue behavior of additively manufactured porous biomaterials under compressive loading. Journal of the mechanical behavior of biomedical materials. 2017 Jun 1;70:7-16.

61. Despois JF, Mortensen A. Permeability of open-pore microcellular materials. Acta materialia. 2005 Mar 1;53(5):1381-8.

62. Deuerling JM, Yue W, Orías AA, Roeder RK. Specimen-specific multi-scale model for the anisotropic elastic constants of human cortical bone. Journal of biomechanics. 2009 Sep 18;42(13):2061-7.

63. Ding M, Odgaard A, Danielsen CC, Hvid I. Mutual associations among microstructural, physical and mechanical properties of human cancellous bone. The Journal of Bone & Joint Surgery British Volume. 2002 Aug 1;84(6):900-7.

64. Douglas TE, Hempel U, Żydek J, Vladescu A, Pietryga K, Kaeswurm JA, Buchweitz M, Surmenev RA, Surmeneva MA, Cotrut CM, Koptyug AV. Pectin coatings on titanium alloy scaffolds produced by additive manufacturing: Promotion of human bone marrow stromal cell proliferation. Materials Letters. 2018 Sep 15;227:225-8.

65. Egorova KS, Ananikov VP. Toxicity of metal compounds: knowledge and myths. Organometallics. 2017 Nov 13;36(21):4071-90.

66. Eisenmann MR. *Factors Influencing Dutility and Fracture Strength in W-Ni-Fe Alloys* (Doctoral dissertation, Rensselaer Polytechnic Institute, May).

67. Elema H, De Groot JH, Nijenhuis AJ, Pennings AJ, Veth RP, Klompmaker J, Jansen HW. Use of porous biodegradable polymer implants in meniscus reconstruction. 2) Biological evaluation of porous biodegradable polymer implants in menisci. Colloid and polymer science. 1990 Dec;268:1082-8.

68. Elias CN, Lima JH, Valiev R, Meyers MA. Biomedical applications of titanium and its alloys. Jom. 2008 Mar;60:46-9.

69. Engh CA, O'connor D, Jasty M, McGovern TF, Bobyn JD, Harris WH. Quantification of implant micromotion, strain shielding, and bone resorption with porous-coated anatomic medullary locking femoral prostheses. Clinical Orthopaedics and Related Research (1976-2007). 1992 Dec 1;285:13-29.

70. Esen Z, Bor Ş. Processing of titanium foams using magnesium spacer particles. Scripta materialia. 2007 Mar 1;56(5):341-4.

71. Evans FG. Mechanical properties and histology of cortical bone from younger and older men. The Anatomical Record. 1976 May;185(1):1-1.

72. Farzadi A, Waran V, Solati-Hashjin M, Rahman ZA, Asadi M, Osman NA. Effect of layer printing delay on mechanical properties and dimensional accuracy of 3D printed porous prototypes in bone tissue engineering. Ceramics International. 2015 Aug 1;41(7):8320-30.

73. Frame JC, Rohan PY, Corté L, Allena R. Optimal bone structure is dependent on the interplay between mechanics and cellular activities. Mechanics Research Communications. 2018 Sep 1;92:43-8.

74. Frosch KH, Barvencik F, Lohmann CH, Viereck V, Siggelkow H, Breme JA, Dresing K, Stürmer KM. Migration, matrix production and lamellar bone formation of human osteoblast-like cells in porous titanium implants. Cells Tissues Organs. 2002 Jul 1;170(4):214-27.

75. Gao C, Peng S, Feng P, Shuai C. Bone biomaterials and interactions with stem cells. Bone research. 2017 Dec 21;5(1):1-33.

76. Geetha M, Singh AK, Asokamani R, Gogia AK. Ti based biomaterials, the ultimate choice for orthopaedic implants–a review. Progress in materials science. 2009 May 1;54(3):397-425.

77. Ghanbari J, Naghdabadi R. Nonlinear hierarchical multiscale modeling of cortical bone considering its nanoscale microstructure. Journal of biomechanics. 2009 Jul 22;42(10):1560-5.

78. Ghosh S, Sanghavi S, Sancheti P. Metallic biomaterial for bone support and replacement. InFundamental biomaterials: metals 2018 Jan 1 (pp. 139-165). Woodhead Publishing.

79. Giannitelli SM, Accoto D, Trombetta M, Rainer A. Current trends in the design of scaffolds for computer-aided tissue engineering. Acta biomaterialia. 2014 Feb 1;10(2):580-94.

80. Gibson I, Rosen DW, Stucker B, Gibson I, Rosen DW, Stucker B. Medical applications for additive manufacture. Additive Manufacturing Technologies: Rapid Prototyping to Direct Digital Manufacturing. 2010:400-14.

81. Gibson IJ, Ashby MF. The mechanics of three-dimensional cellular materials. Proceedings of the royal society of London. A. Mathematical and physical sciences. 1982 Jul 8;382(1782):43-59.

82. Gibson LJ. Biomechanics of cellular solids. Journal of biomechanics. 2005 Mar 1;38(3):377-99.

83. Gibson LJ. Modelling the mechanical behavior of cellular materials. Materials Science and Engineering: A. 1989 Mar 1;110:1-36.

84. Gibson LJ. The mechanical behaviour of cancellous bone. Journal of biomechanics. 1985 Jan 1;18(5):317-28.

85. Girardin E, Barucca G, Mengucci P, Fiori F, Bassoli E, Gatto A, Iuliano L, Rutkowski B. Biomedical Co-Cr-Mo components produced by direct metal laser sintering. Materials Today: Proceedings. 2016 Jan 1;3(3):889-97.

86. Gong H, Wu W, Fang J, Dong X, Zhao M, Guo T. Effects of materials of cementless femoral stem on the functional adaptation of bone. Journal of Bionic Engineering. 2012 Mar 1;9(1):66-74.

87. Goodman S, Toksvig-Larsen S, Aspenberg P. Ingrowth of bone into pores in titanium chambers implanted in rabbits: Effect of pore cross-sectional shape in the presence of dynamic shear. Journal of biomedical materials research. 1993 Feb;27(2):247-53.

88. Gorny B, Niendorf T, Lackmann J, Thoene M, Troester T, Maier HJ. In situ

characterization of the deformation and failure behavior of non-stochastic porous structures processed by selective laser melting. Materials Science and Engineering: A. 2011 Oct 15;528(27):7962-7.

89. Griss P, Heimke G, Krempien B, Jentschura G. Ceramic hip joint replacement—experimental results and early clinical experience. InEngineering in Medicine: Volume 2: Advances in Artificial Hip and Knee Joint Technology 1976 (pp. 446-455). Berlin, Heidelberg: Springer Berlin Heidelberg.

90. Guillén T, Zhang QH, Tozzi G, Ohrndorf A, Christ HJ, Tong J. Compressive behaviour of bovine cancellous bone and bone analogous materials, micro CT characterisation and FE analysis. Journal of the mechanical behavior of biomedical materials. 2011 Oct 1;4(7):1452-61.

91. Gümrük R, Mines RA, Karadeniz S. Static mechanical behaviours of stainless steel micro-lattice structures under different loading conditions. Materials Science and Engineering: A. 2013 Dec 1;586:392-406.

92. Guo N, Leu MC. Additive manufacturing: technology, applications and research needs. Frontiers of mechanical engineering. 2013 Sep;8(3):215-43.

93. Haghighi SE, Lu HB, Jian GY, et al. Effect of α ″martensite on the microstructure and mechanical properties of beta-type Ti–Fe–Ta alloys. Materials & Design. 2015 Jul 5;76:47-54.

94. Hamed E, Jasiuk I, Yoo A, Lee Y, Liszka T. Multi-scale modelling of elastic moduli of trabecular bone. Journal of The Royal Society Interface. 2012 Jul 7;9(72):1654-73.

95. Hansma AH, Van Hensbergen Y, Kuenen BC, van Diest PJ, Hanemaaijer R, Meijer S, Pinedo HM, Hoekman K. A patient with a VEGF and endostatin producing gastrointestinal autonomic nerve tumour. Journal of clinical pathology. 2004 May 1;57(5):536-8.

96. Hao YL, Li SJ, Sun SY, Zheng CY, Hu QM, Yang R. Super-elastic titanium alloy with unstable plastic deformation. Applied Physics Letters. 2005 Aug 29;87(9).

97. Harris RA, Hague RJ, Dickens PM. The structure of parts produced by

stereolithography injection mould tools and the effect on part shrinkage. International Journal of Machine Tools and Manufacture. 2004 Jan 1;44(1):59-64.

98. Hazlehurst KB, Wang CJ, Stanford M. A numerical investigation into the influence of the properties of cobalt chrome cellular structures on the load transfer to the periprosthetic femur following total hip arthroplasty. Medical engineering & physics. 2014 Apr 1;36(4):458-66.

99. Hazlehurst KB, Wang CJ, Stanford M. The potential application of a Cobalt Chrome Molybdenum femoral stem with functionally graded orthotropic structures manufactured using Laser Melting technologies. Medical Hypotheses. 2013 Dec 1;81(6):1096-9.

100. Helsen JA, Jürgen Breme H. Metals as biomaterials. 1998 Oct.

101. Heuijerjans A, Wilson W, Ito K, van Donkelaar CC. The critical size of focal articular cartilage defects is associated with strains in the collagen fibers. Clinical Biomechanics. 2017 Dec 1;50:40-6.

102. Hildebrand T, Laib A, Müller R, Dequeker J, Rüegsegger P. Direct three-dimensional morphometric analysis of human cancellous bone: microstructural data from spine, femur, iliac crest, and calcaneus. Journal of bone and mineral research. 1999 Jul 1;14(7):1167-74.

103. Hollister SJ. Porous scaffold design for tissue engineering. Nature materials. 2005 Jul; 4(7):518-24.

104. Hoover S, Tarafder S, Bandyopadhyay A, Bose S. Silver doped resorbable tricalcium phosphate scaffolds for bone graft applications. Materials Science and Engineering: C. 2017 Oct 1;79:763-9.

105. Huang T, Wang W, George D, Mao X, Graves S. What can we learn from Australian Orthopaedic Association National Joint Replacement Registry 2016 annual report?. Annals of Joint. 2017 Apr 22;2(4).

106. Hungerford DS, KENNA RV. Preliminary experience with a total knee prosthesis with porous coating used without cement. Clinical Orthopaedics and Related Research®. 1983 Jun 1;176:95-107.

107. Hussaini S, Vaidyanathan TK, Wadkar AP, Quran FA, Ehrenberg D, Weiner S. Peri-implant strain in an in vitro model. Journal of Oral Implantology. 2015 Oct 1;41(5):532-7.

108. Hutmacher DW, Sittinger M, Risbud MV. Scaffold-based tissue engineering: rationale for computer-aided design and solid free-form fabrication systems. TRENDS in Biotechnology. 2004 Jul 1;22(7):354-62.

109. Inglam S, Chantarapanich N, Suebnukarn S, Vatanapatimakul N, Sucharitpwatskul S, Sitthiseripratip K. Biomechanical evaluation of a novel porous-structure implant: finite element study. International Journal of Oral & Maxillofacial Implants. 2013 Apr 1;28(2).

110. Jardini AL, Larosa MA, de Carvalho Zavaglia CA, Bernardes LF, Lambert CS, Kharmandayan P, Calderoni D, Maciel Filho R. Customised titanium implant fabricated in additive manufacturing for craniomaxillofacial surgery: Virtual and physical prototyping. 2014 Apr 3;9(2):115-25.

111. Jasty M, Anderson MJ, Harris WH. Total hip replacement for developmental dysplasia of the hip. Clinical Orthopaedics and Related Research (1976-2007). 1995 Feb 1;311:40-5.

112. Johannesdottir F, Bouxsein ML. Overview of bone structure and strength. InGenetics of Bone Biology and Skeletal Disease 2018 Jan 1 (pp. 197-208). Academic Press.

113. Junfeng L, Zhengying W. Process optimization and microstructure characterization of Ti6Al4V manufactured by selective laser melting. In IOP Conference Series. Materials Science and Engineering (Online) 2017 (Vol. 269, No. 1).

114. Kadkhodapour J, Montazerian H, Darabi AC, Anaraki AP, Ahmadi SM, Zadpoor AA, Schmauder S. Failure mechanisms of additively manufactured porous biomaterials: Effects of porosity and type of unit cell. Journal of the mechanical behavior of biomedical materials. 2015 Oct 1;50:180-91.

115. Karageorgiou V, Kaplan D. Porosity of 3D biomaterial scaffolds and osteogenesis. Biomaterials. 2005 Sep 1;26(27):5474-91.

116. Katarivas Levy G, Leon A, Kafri A, Ventura Y, Drelich JW, Goldman J, Vago R, Aghion E. Evaluation of biodegradable Zn-1% Mg and Zn-1% Mg-0.5% Ca alloys for biomedical applications. Journal of Materials Science: Materials in Medicine. 2017 Nov;28:1-1.

117. Keaveny TM, Morgan EF, Niebur GL, Yeh OC. Biomechanics of trabecular bone. Annual review of biomedical engineering. 2001 Aug;3(1):307-33.

118. Keaveny TM, Yeh OC. Architecture and trabecular bone-toward an improved understanding of the biomechanical effects of age, sex and osteoporosis. Journal of Musculoskeletal and Neuronal Interactions. 2002 Mar 1;2(3):205-8.

119. Khanuja HS, Vakil JJ, Goddard MS, Mont MA. Cementless femoral fixation in total hip arthroplasty. Jbjs. 2011 Mar 2;93(5):500-9.

120. Koppolu P, Mishra A, Swapna LA, Butchibabu K, Bagalkokar A, Baroudi K. Comparison of efficacy among various topical anesthetics: An approach towards painless injections in periodontal surgery. Saudi Journal of Anaesthesia. 2016 Jan 1;10(1):55-7.

121. Krishna BV, Bose S, Bandyopadhyay A. Low stiffness porous Ti structures for load-bearing implants. Acta biomaterialia. 2007 Nov 1;3(6):997-1006.

122. Kriszt B, Martin U, Mosler U, Maire E, Degischer HP, Kottar A. Characterization of cellular metals. Handbook of cellular metals: production, processing, applications. 2002 Mar 26:127-78.

123. Kühne JH, Bartl R, Frisch B, Hammer C, Jansson V, Zimmer M. Bone formation in coralline hydroxyapatite: effects of pore size studied in rabbits. Acta Orthopaedica Scandinavica. 1994 Jan 1;65(3):246-52.

124. Kuiper JH, Huiskes R. Mathematical optimization of elastic properties: application to cementless hip stem design.

125. Kumar P, Prakash O, Ramamurty U. Micro-and meso-structures and their influence on mechanical properties of selectively laser melted Ti-6Al-4V. Acta Materialia. 2018 Aug 1;154:246-60.

126. Laptev A, Bram M, Buchkremer HP, Stöver D. Study of production route for

titanium parts combining very high porosity and complex shape. Powder metallurgy. 2004 Jan 1;47(1):85-92.

127. Le Guehennec L, Lopez-Heredia MA, Enkel B, Weiss P, Amouriq Y, Layrolle P. Osteoblastic cell behaviour on different titanium implant surfaces. Acta biomaterialia. 2008 May 1;4(3):535-43.

128. Le Guéhennec L, Soueidan A, Layrolle P, Amouriq Y. Surface treatments of titanium dental implants for rapid osseointegration. Dental materials. 2007 Jul 1;23(7):844-54.

129. Leong KF, Cheah CM, Chua CK. Solid freeform fabrication of three-dimensional scaffolds for engineering replacement tissues and organs. Biomaterials. 2003 Jun 1;24(13):2363-78.

130. Leong KF, Chua SC, Sudarmadji N, Yeong WY. Engineering functionally graded tissue engineering scaffolds. Journal of the mechanical behavior of biomedical materials. 2008 Apr 1;1(2):140-52.

131. Li F, Li J, Xu G, Liu G, Kou H, Zhou L. Fabrication, pore structure and compressive behavior of anisotropic porous titanium for human trabecular bone implant applications. Journal of the mechanical behavior of biomedical materials. 2015 Jun 1;46:104-14.

132. Li SJ, Cui TC, Hao YL, Yang R. Fatigue properties of a metastable β-type titanium alloy with reversible phase transformation. Acta biomaterialia. 2008 Mar 1;4(2):305-17.

133. Li W, Liou F, Newkirk J, Taminger KM, Seufzer WJ. Investigation on Ti6Al4V-V-Cr-Fe-SS316 multi-layers metallic structure fabricated by laser 3D printing. Scientific reports. 2017 Aug 11;7(1):7977.

134. Li Y, Munir KS, Lin J, Wen C. Titanium-niobium pentoxide composites for biomedical applications. Bioactive Materials. 2016 Dec 1;1(2):127-31.

135. Li Y, Yang C, Zhao H, Qu S, Li X, Li Y. New developments of Ti-based alloys for biomedical applications. Materials. 2014 Mar 4;7(3):1709-800.

136. Li YU. *Topological design of porous titanium alloy scaffolds for additive*

manufacturing of orthopaedic implant applications (Doctoral dissertation, RMIT University).

137. Li YY, Zou LM, Yang C, Li YH, Li LJ. Ultrafine-grained Ti-based composites with high strength and low modulus fabricated by spark plasma sintering. Materials Science and Engineering: A. 2013 Jan 10;560:857-61.

138. Li Z, Kucukkoc I, Zhang DZ, Liu F. Optimising the process parameters of selective laser melting for the fabrication of Ti6Al4V alloy. Rapid Prototyping Journal. 2018 Jan 2;24(1):150-9.

139. Lin X, Xiao X, Wang Y, Gu C, Wang C, Chen J, Liu H, Luo J, Li T, Wang D, Fan S. Biocompatibility of bespoke 3D-printed titanium alloy plates for treating acetabular fractures. BioMed research international. 2018 Feb 22;2018.

140. Little CJ, Bawolin NK, Chen X. Mechanical properties of natural cartilage and tissue-engineered constructs. Tissue Engineering Part B: Reviews. 2011 Aug 1;17(4):213-27.

141. Liu X, Chu PK, Ding C. Surface modification of titanium, titanium alloys, and related materials for biomedical applications. Materials Science and Engineering: R: Reports. 2004 Dec 24;47(3-4):49-121.

142. Liu YJ, Li SJ, Wang HL, Hou WT, Hao YL, Yang R, Sercombe TB, Zhang LC. Microstructure, defects and mechanical behavior of beta-type titanium porous structures manufactured by electron beam melting and selective laser melting. Acta materialia. 2016 Jul 1;113:56-67.

143. Liu YJ, Wang HL, Li SJ, Wang SG, Wang WJ, Hou WT, Hao YL, Yang R, Zhang LC. Compressive and fatigue behavior of beta-type titanium porous structures fabricated by electron beam melting. Acta Materialia. 2017 Mar 1;126:58-66.

144. Liulan L, Qingxi H, Xianxu H, Gaochun X. Design and fabrication of bone tissue engineering scaffolds via rapid prototyping and CAD. Journal of Rare Earths. 2007 Jun 1;25:379-83.

145. Loh QL, Choong C. Three-dimensional scaffolds for tissue engineering applications: role of porosity and pore size.

146. Long M, Rack HJ. Titanium alloys in total joint replacement—a materials science perspective. Biomaterials. 1998 Sep 1;19(18):1621-39.

147. Lu JX, Flautre B, Anselme K, Hardouin P, Gallur A, Descamps M, Thierry B. Role of interconnections in porous bioceramics on bone recolonization in vitro and in vivo. Journal of Materials Science: Materials in Medicine. 1999 Feb;10:111-20.

148. Lütjering G, Williams JC. Alpha+ beta alloys. Titanium. 2007:203-58.

149. Lütjering G, Williams JC. Fundamental Aspects. InTitanium 2003 (pp. 13-50). Springer, Berlin, Heidelberg.

150. Lütjering G, Williams JC. Fundamental aspects. Titanium. 2007:15-52.

151. Marin E, Pressacco M, Fusi S, Lanzutti A, Turchet S, Fedrizzi L. Characterization of grade 2 commercially pure Trabecular Titanium structures. Materials Science and Engineering: C. 2013 Jul 1;33(5):2648-56.

152. Martens MV, Van Audekercke R, Delport P, De Meester P, Mulier JC. The mechanical characteristics of cancellous bone at the upper femoral region. Journal of biomechanics. 1983 Jan 1;16(12):971-83.

153. Melchels FP, Feijen J, Grijpma DW. A review on stereolithography and its applications in biomedical engineering. Biomaterials. 2010 Aug 1;31(24):6121-30.

154. Mengucci P, Barucca G, Gatto A, Bassoli E, Denti L, Fiori F, Girardin E, Bastianoni P, Rutkowski B, Czyrska-Filemonowicz A. Effects of thermal treatments on microstructure and mechanical properties of a Co–Cr–Mo–W biomedical alloy produced by laser sintering. Journal of the mechanical behavior of biomedical materials. 2016 Jul 1;60:106-17.

155. Metel AS, Stebulyanin MM, Fedorov SV, Okunkova AA. Power density distribution for laser additive manufacturing (SLM): potential, fundamentals and advanced applications. Technologies. 2018 Dec 30;7(1):5.

156. Moravej M, Mantovani D. Biodegradable metals for cardiovascular stent application: interests and new opportunities. International journal of molecular sciences. 2011 Jun 29;12(7):4250-70.

157. Mullen L, Stamp RC, Brooks WK, Jones E, Sutcliffe CJ. Selective Laser Melting: A regular unit cell approach for the manufacture of porous, titanium, bone in-growth constructs, suitable for orthopedic applications. Journal of Biomedical Materials Research Part B: Applied Biomaterials: The Japanese Society for Biomaterials, and The Australian Society for Biomaterials and the Korean Society for Biomaterials. 2009 May;89(2):325-34.

158. Mullen L, Stamp RC, Fox P, Jones E, Ngo C, Sutcliffe CJ. Selective laser melting: A unit cell approach for the manufacture of porous, titanium, bone in-growth constructs, suitable for orthopedic applications. II. Randomized structures. Journal of Biomedical Materials Research Part B: Applied Biomaterials: The Japanese Society for Biomaterials, and The Australian Society for Biomaterials and the Korean Society for Biomaterials. 2010 Jan;92(1):178-88.

159. Naing MW, Chua CK, Leong KF, Wang Y. Fabrication of customised scaffolds using computer-aided design and rapid prototyping techniques. Rapid Prototyping Journal. 2005 Sep 1;11(4):249-59.

160. Nakajima H. Fabrication, properties and application of porous metals with directional pores. Progress in Materials Science. 2007 Sep 1;52(7):1091-173.

161. Ni M, Wu B, Liu H, Ren P, Peng H, Zheng Q, Sun J, Chai W, Zhang G, Wang Y. Hip Replacement in Patients with Ankylosing Spondylitis. Surgical Treatment of Ankylosing Spondylitis Deformity. 2019:195-200.

162. Niinomi M, Nakai M, Hieda J. Development of new metallic alloys for biomedical applications. Acta biomaterialia. 2012 Nov 1;8(11):3888-903.

163. Niinomi M. Biologically and mechanically biocompatible titanium alloys. Materials transactions. 2008 Oct 1;49(10):2170-8.

164. Niinomi M. Fatigue performance and cyto-toxicity of low rigidity titanium alloy, Ti–29Nb–13Ta–4.6 Zr. Biomaterials. 2003 Jul 1;24(16):2673-83.

165. Niinomi M. Mechanical biocompatibilities of titanium alloys for biomedical applications. Journal of the mechanical behavior of biomedical materials. 2008 Jan 1;1(1):30-42.

166. Niinomi M. Recent applications, research and development in titanium and its alloys. Tetsu-to-hagane. 2004 Jul 1;90(7):462-71.

167. Niinomi M. Recent research and development in titanium alloys for biomedical applications and healthcare goods. Science and technology of advanced Materials. 2003 Sep 30;4(5):445.

168. Nishiyama KK, Agarwal S, Kepley A, Rosete F, Hu Y, Guo XE, Keating CL, DiMango EA, Shane E. Adults with cystic fibrosis have deficits in bone structure and strength at the distal tibia despite similar size and measuring standard and relative sites. Bone. 2018 Feb 1;107:181-7.

169. Nouri A, Hodgson PD, Wen CE. Biomimetic porous titanium scaffolds for orthopaedic and dental applications. InTech; 2010 Jan 1.

170. O'brien FJ. Biomaterials & scaffolds for tissue engineering. Materials today. 2011 Mar 1;14(3):88-95.

171. Oh IH, Nomura N, Masahashi N, Hanada S. Mechanical properties of porous titanium compacts prepared by powder sintering. Scripta Materialia. 2003 Dec 1;49(12):1197-202.

172. Oldani C, Dominguez A. Titanium as a biomaterial for implants, recent advances in arthroplasty, SamoFokter. IntechOpen. 2012.

173. Oshkour AA, A Abu Osman N, Davoodi MM, Yau YH, Tarlochan F, B Wan Abas WA, Bayat M. Finite element analysis on longitudinal and radial functionally graded femoral prosthesis. International journal for numerical methods in biomedical engineering. 2013 Dec;29(12):1412-27.

174. Oshkour AA, Abu Osman NA, Yau YH, Tarlochan F, Wan Abas WA. Design of new generation femoral prostheses using functionally graded materials: a finite element analysis. Proceedings of the Institution of Mechanical Engineers, Part H: Journal of Engineering in Medicine. 2013 Jan;227(1):3-17.

175. Oxnard CE. Thoughts on bone biomechanics. Folia Primatologica. 2004 Feb 8;75(4):189-201.

176. Parthasarathy J, Starly B, Raman S, Christensen A. Mechanical evaluation of porous

titanium (Ti6Al4V) structures with electron beam melting (EBM). Journal of the mechanical behavior of biomedical materials. 2010 Apr 1;3(3):249-59.

177. Parthasarathy J, Starly B, Raman S. A design for the additive manufacture of functionally graded porous structures with tailored mechanical properties for biomedical applications. Journal of Manufacturing Processes. 2011 Aug 1;13(2):160-70.

178. Pattanayak DK, Fukuda A, Matsushita T, Takemoto M, Fujibayashi S, Sasaki K, Nishida N, Nakamura T, Kokubo T. Bioactive Ti metal analogous to human cancellous bone: Fabrication by selective laser melting and chemical treatments. Acta biomaterialia. 2011 Mar 1;7(3):1398-406.

179. Paul BK, Baskaran S. Issues in fabricating manufacturing tooling using powder-based additive freeform fabrication. Journal of materials processing technology. 1996 Aug 1;61(1-2):168-72.

180. Peltola SM, Melchels FP, Grijpma DW, Kellomäki M. A review of rapid prototyping techniques for tissue engineering purposes. Annals of medicine. 2008 Jan 1;40(4):268-80.

181. Petrovic V, Vicente Haro Gonzalez J, Jordá Ferrando O, Delgado Gordillo J, Ramón Blasco Puchades J, Portolés Griñan L. Additive layered manufacturing: sectors of industrial application shown through case studies. International Journal of Production Research. 2011 Feb 15;49(4):1061-79.

182. Pilliar RM. Porous-surfaced metallic implants for orthopedic applications. Journal of biomedical materials research. 1987 Apr 1;21(A1 Suppl):1-33.

183. Pitto RP, Hayward A, Walker C, Shim VB. Femoral bone density changes after total hip arthroplasty with uncemented taper-design stem: a five year follow-up study. International orthopaedics. 2010 Aug;34:783-7.

184. Plum LM, Rink L, Haase H. The essential toxin: impact of zinc on human health. International journal of environmental research and public health. 2010 Apr;7(4):1342-65.

185. Podshivalov L, Fischer A, Bar-Yoseph PZ. On the road to personalized medicine:

multiscale computational modeling of bone tissue. Archives of Computational Methods in Engineering. 2014 Dec;21(4):399-479.

186. Polmear I. Light alloys: from traditional alloys to nanocrystals. Elsevier; 2005 Nov 11.

187. Ponader S, Vairaktaris E, Heinl P, Wilmowsky CV, Rottmair A, Körner C, Singer RF, Holst S, Schlegel KA, Neukam FW, Nkenke E. Effects of topographical surface modifications of electron beam melted Ti-6Al-4V titanium on human fetal osteoblasts. Journal of Biomedical Materials Research Part A: The Japanese Society for Biomaterials, and The Australian Society for Biomaterials and the Korean Society for Biomaterials. 2008 Mar 15;84(4):1111-9.

188. Pyka G, Burakowski A, Kerckhofs G, Moesen M, Van Bael S, Schrooten J, Wevers M. Surface modification of Ti6Al4V open porous structures produced by additive manufacturing. Advanced Engineering Materials. 2012 Jun;14(6):363-70.

189. Ralston SH. Bone structure and metabolism. Medicine. 2013 Oct 1;41(10):581-5.

190. Ralston SH. Bone structure and metabolism. Medicine. 2017 Sep 1;45(9):560-4.

191. Rho JY, Hobatho MC, Ashman RB. Relations of density and CT numbers to mechanical properties for human cortical and cancellous bone. Med Eng Phys. 1995;17:347-55.

192. Ritchie RO, Kinney JH, Kruzic JJ, Nalla RK. A fracture mechanics and mechanistic approach to the failure of cortical bone. Fatigue & Fracture of Engineering Materials & Structures. 2005 Apr;28(4):345-71.

193. Robertson DM, St. Pierre L, Chahal R. Preliminary observations of bone ingrowth into porous materials. Journal of biomedical materials research. 1976 May;10(3):335-44.

194. Rush SM. Bone graft substitutes: osteobiologics. Clinics in Podiatric Medicine and Surgery. 2005 Oct 1;22(4):619-30.

195. Ryan G, Pandit A, Apatsidis DP. Fabrication methods of porous metals for use in orthopaedic applications. Biomaterials. 2006 May 1;27(13):2651-70.

196. Schmidt R, Mueller L, Nowak TE, Pitto RP. Clinical outcome and periprosthetic bone remodelling of an uncemented femoral component with taper design. International orthopaedics. 2003 Aug;27:204-7.

197. Silva MJ, Gibson LJ. The effects of non-periodic microstructure and defects on the compressive strength of two-dimensional cellular solids. International Journal of Mechanical Sciences. 1997 May 1;39(5):549-63.

198. Singh A, Dutta MK, Jennane R, Lespessailles E. Classification of the trabecular bone structure of osteoporotic patients using machine vision. Computers in biology and medicine. 2017 Dec 1;91:148-58.

199. Smith M, Guan Z, Cantwell WJ. Finite element modelling of the compressive response of lattice structures manufactured using the selective laser melting technique. International Journal of Mechanical Sciences. 2013 Feb 1;67:28-41.

200. Sola A, Nouri A. Microstructural porosity in additive manufacturing: The formation and detection of pores in metal parts fabricated by powder bed fusion. Journal of Advanced Manufacturing and Processing. 2019 Jul;1(3):e10021.

201. Su XB, YANG YQ, Peng YU, SUN JF. Development of porous medical implant scaffolds via laser additive manufacturing. Transactions of Nonferrous Metals Society of China. 2012 Oct 1;22:s181-7.

202. Sudarmadji N, Chua CK, Leong KF. The development of computer-aided system for tissue scaffolds (CASTS) system for functionally graded tissue-engineering scaffolds. InComputer-Aided Tissue Engineering 2012 (pp. 111-123). Humana Press, Totowa, NJ.

203. Takaichi A, Nakamoto T, Joko N, Nomura N, Tsutsumi Y, Migita S, Doi H, Kurosu S, Chiba A, Wakabayashi N, Igarashi Y. Microstructures and mechanical properties of Co–29Cr–6Mo alloy fabricated by selective laser melting process for dental applications. Journal of the mechanical behavior of biomedical materials. 2013 May 1;21:67-76.

204. Taniguchi N, Fujibayashi S, Takemoto M, Sasaki K, Otsuki B, Nakamura T, Matsushita T, Kokubo T, Matsuda S. Effect of pore size on bone ingrowth into

porous titanium implants fabricated by additive manufacturing: An in vivo experiment. Materials Science and Engineering: C. 2016 Feb 1;59:690-701.

205. Tarala M, Janssen D, Verdonschot N. Balancing incompatible endoprosthetic design goals: a combined ingrowth and bone remodeling simulation. Medical engineering & physics. 2011 Apr 1;33(3):374-80.

206. Tarawneh AM, Wettergreen M, Liebschner MA. Computer-aided tissue engineering: benefiting from the control over scaffold micro-architecture. InComputer-Aided Tissue Engineering 2012 (pp. 1-25). Humana Press, Totowa, NJ.

207. Terrier JE, Paparel P, Gadegbeku B, Ruffion A, Jenkins LC, N'Diaye A. Genitourinary injuries after traffic accidents: analysis of a registry of 162,690 victims. Journal of trauma and acute care surgery. 2017 Jun 1;82(6):1087-93.

208. Thieme M, Wieters KP, Bergner F, Scharnweber D, Worch H, Ndop J, Kim TJ, Grill W. Titanium powder sintering for preparation of a porous functionally graded material destined for orthopaedic implants. Journal of materials science: materials in medicine. 2001 Mar;12:225-31.

209. Trevisan F, Calignano F, Aversa A, Marchese G, Lombardi M, Biamino S, Ugues D, Manfredi D. Additive manufacturing of titanium alloys in the biomedical field: processes, properties and applications. Journal of applied biomaterials & functional materials. 2018 Apr;16(2):57-67.

210. Tuchinskiy L, Loutfy R. Titanium Foams for Medical Applications. Materials & Processes for Medical Devices.

211. Turner TM, Sumner DR, Urban RM, Rivero DP, Galante JO. A comparative study of porous coatings in a weight-bearing total hip-arthroplasty model. JBJS. 1986 Dec 1;68(9):1396-409.

212. Ullah I, Elambasseril J, Brandt M, Feih S. Performance of bio-inspired Kagome truss core structures under compression and shear loading. Composite Structures. 2014 Dec 1;118:294-302.

213. Van Cleynenbreugel T, Van Oosterwyck H, Vander Sloten J, Schrooten J. Trabecular bone scaffolding using a biomimetic approach. Journal of Materials

Science: Materials in Medicine. 2002 Dec;13:1245-9.

214. Veiseh M, Edmondson D. Bone as an Open Cell Porous Material. ME 599K: Special Topics in Cellular Solids. 2003.

215. Wang X, Xu S, Zhou S, Xu W, Leary M, Choong P, Qian M, Brandt M, Xie YM. Topological design and additive manufacturing of porous metals for bone scaffolds and orthopaedic implants: A review. Biomaterials. 2016 Mar 1;83:127-41.

216. Wang XH, Li JS, Rui HU, Kou HC, Lian ZH. Mechanical properties of porous titanium with different distributions of pore size. Transactions of Nonferrous Metals Society of China. 2013 Aug 1;23(8):2317-22.

217. Wang XJ, Chen XB, Hodgson PD, Wen CE. Elastic modulus and hardness of cortical and trabecular bovine bone measured by nanoindentation. Transactions of nonferrous metals society of china. 2006 Jun 1;16:s744-8.

218. Weinmann M, Schnitter C, Stenzel M, Markhoff J, Schulze C, Bader R. Development of bio-compatible refractory Ti/Nb (/Ta) alloys for application in patient-specific orthopaedic implants. International Journal of Refractory Metals and Hard Materials. 2018 Sep 1;75:126-36.

219. Wen CE, Mabuchi M, Yamada Y, Shimojima K, Chino Y, Asahina T. Processing of biocompatible porous Ti and Mg. Scripta materialia. 2001 Nov 19;45(10):1147-53.

220. Wettergreen MA, Bucklen BS, Starly B, Yuksel E, Sun W, Liebschner MA. Creation of a unit block library of architectures for use in assembled scaffold engineering. Computer-Aided Design. 2005 Sep 15;37(11):1141-9.

221. Wieding J, Souffrant R, Mittelmeier W, Bader R. Finite element analysis on the biomechanical stability of open porous titanium scaffolds for large segmental bone defects under physiological load conditions. Medical engineering & physics. 2013 Apr 1;35(4):422-32.

222. Williams DF. There is no such thing as a biocompatible material. Biomaterials. 2014 Dec 1;35(38):10009-14.

223. Williams JM, Adewunmi A, Schek RM, Flanagan CL, Krebsbach PH, Feinberg SE, Hollister SJ, Das S. Bone tissue engineering using polycaprolactone scaffolds

fabricated via selective laser sintering. Biomaterials. 2005 Aug 1;26(23):4817-27.

224. Wu S, Liu X, Yeung KW, Liu C, Yang X. Biomimetic porous scaffolds for bone tissue engineering. Materials Science and Engineering: R: Reports. 2014 Jun 1;80:1-36.

225. Yamada H, Yoshihara Y, Henmi O, Morita M, Shiromoto Y, Kawano T, Kanaji A, Ando K, Nakagawa M, Kosaki N, Fukaya E. Cementless total hip replacement: past, present, and future. Journal of Orthopaedic Science. 2009 Mar;14:228-41.

226. Yavari SA, Ahmadi SM, van der Stok J, Wauthlé R, Riemslag AC, Janssen M, Schrooten J, Weinans H, Zadpoor AA. Effects of bio-functionalizing surface treatments on the mechanical behavior of open porous titanium biomaterials. Journal of the mechanical behavior of biomedical materials. 2014 Aug 1;36:109-19.

227. Yavari SA, Ahmadi SM, Wauthle R, Pouran B, Schrooten J, Weinans H, Zadpoor AA. Relationship between unit cell type and porosity and the fatigue behavior of selective laser melted meta-biomaterials. Journal of the mechanical behavior of biomedical materials. 2015 Mar 1;43:91-100.

228. Yavari SA, van der Stok J, Chai YC, Wauthle R, Birgani ZT, Habibovic P, Mulier M, Schrooten J, Weinans H, Zadpoor AA. Bone regeneration performance of surface-treated porous titanium. Biomaterials. 2014 Aug 1;35(24):6172-81.

229. Yavari SA, Wauthlé R, van der Stok J, Riemslag AC, Janssen M, Mulier M, Kruth JP, Schrooten J, Weinans H, Zadpoor AA. Fatigue behavior of porous biomaterials manufactured using selective laser melting. Materials Science and Engineering: C. 2013 Dec 1;33(8):4849-58.

230. Yu G, Li Z, Li S, Zhang Q, Hua Y, Liu H, Zhao X, Dhaidhai DT, Li W, Wang X. The select of internal architecture for porous Ti alloy scaffold: A compromise between mechanical properties and permeability. Materials & Design. 2020 Jul 1;192:108754.

231. Zhang LC, Lu HB, Mickel C, Eckert J. Ductile ultrafine-grained Ti-based alloys with high yield strength. Applied Physics Letters. 2007 Jul 30;91(5).

232. Zilberman M, editor. Active implants and scaffolds for tissue regeneration. Berlin,

Germany:: Springer; 2011 May 5.